PROCESS OPTIMIZATION OF DRYERS/TENTERS IN THE TEXTILE INDUSTRY

A Thesis

Presented to

The Academic Faculty

By

Li Xue

In Partial Fulfillment

of the Requirements for the Degree

Master of Science in Chemical Engineering in the

School of Chemical & Biomolecular Engineering

Georgia Institute of Technology

July 2004

PROCESS OPTIMIZATION OF DRYERS/TENTERS
IN THE TEXTILE INDUSTRY

Approved by:

Dr. Pradeep Agrawal, Chairman

Dr. Larry Forney

Dr. Wallace Carr

Date Approved: 07/08/2004

ACKNOWLEDGEMENTS

I would like to express my great appreciation to my advisor Dr. Pradeep K. Agrawal for encouraging me to undertake this thesis project and providing guidance and insight throughout the course of the work. His support, inspiration, and patience were vital to the completion of this thesis. His countless revisions of my manuscripts showed me the rigorous altitude of doing science, from which I will benefit for my professional growth. I would also like to thank Drs. Wallace W. Carr and Larry Forney for serving as my advisory committee members and careful review of my thesis. I am grateful to Dr. Limin He for his friendship and his assistance in the laboratory set-up and the experimental measurements at Milliken & Company. At this time, I would also like to thank Milliken & Company for providing background and support for this project.

Additionally, many thanks go to my brothers and sisters in Christ for their sincere friendship and support. Also deep thanks to God who has always been present throughout my research in this project.

Finally, I would like to thank my parents for their constant love and encouragement. Last but not least, I would like to give my deepest appreciation to my husband Dr. Gong Zhang for his infinite source of love, strength, and inspiration. Without his unconditional support it is hard to imagine the work can be completed.

This research was supported by the Consortium on Competitiveness for the Apparel, Carpet, and Textile Industry (CCACTI).

TABLE OF CONTENTS

LIST OF TABLES

LIST OF FIGURES

LIST OF SYMBOLS

Bi	Biot number
C	Concentration
Cp	Specific heat capacity
D	Diffusion coefficient
h	Heat transfer coefficient
H_v	Latent heat for evaporating water
k	Thermal conductivity
k_y	Mass transfer coefficient
L	Height of Nylon fiber
m	Weight
M_w	Molecular weight of water
N	Rate of moisture evaporation
Nu	Nusselt number
P	Pressure
Pr	Prandtl number
Q	Energy
R	Universal gas constant
Re	Reynolds number

Sc	Schmidt number
t	Time
T	Temperature
w	Moisture content (dry basis)
U	Internal energy
W	Work
x	Perpendicular distance from the carpet surface
y	Humidity ratio
ρ	Density

Subscripts

a	Air
c	Critical point
e	Equilibrium point
f	Fabric/carpet
i	Initial point
ref	Reference state
w	Water

Superscripts

*	Saturation point

LIST OF ABBREVIATIONS

GC	Gas Chromatography
RR	Carpet Roadrunner
MS	Carpet Midnight Sparkle
GP	Carpet Grand Plaza
WPU	Wet pick-up
SEM	Scanning electron microscopy

SUMMARY

Carpet manufacturing is an energy-intensive process, therefore it is vital that the resource gets used efficiently in order to reduce costs and keep the carpet industry competitive. Drying is an intermediate step in the dyeing and finishing operations in the textile industry and uses a substantial amount of energy. About one half of the energy used in a typical textile finishing mill is used in the drying processes, due to the increasing fuel cost, it is imperative that the dryers be operated as efficiently as possible.

The use of excess air is a major source of energy losses in a dryer operation. Air enters into a dryer at several points: (i) primary air to burn the natural gas or other fuel, (ii) secondary air to mix with the combustion products to obtain the desired temperature (set point), and (iii) entrance and exit slots of the dryer through which the fabric moves. Most dryers have a fan in the exhaust line to draw the flue gases from the dryer. This creates a differential pressure inside the dryer which allows air to move in through the entry/exit slots. One of the benefits of using excess air is to reduce the gas-phase moisture content, thereby presumably increase the driving force for the drying operation. On the other hand, this large amount of excess air requires extra energy to heat it from ambient temperature 70 F to 300-350 F. Most of this sensible heat associated with excess air leaves largely unrecovered in the exhaust (300-350 F). Another factor compounding this efficiency problem is the fact that oftentimes several types of fabric (varying in weight, moisture content, and range speed) are processed on the same dyeing and finishing range.

Due to a lack of quantitative understanding of drying rates, it is often customary to set the dryer operating parameters for the most demanding application (greatest moisture removal, for example). This inevitably would lead to significant losses for less demanding applications. Preliminary estimates have shown that as much as 60-80% of the total energy used in a dryer operation is wasted in exhaust. These estimates were derived from exhaust gas composition and energy balance analyses.

The primary cause of the energy loss is a lack of fundamental understanding of the drying characteristics and their relationship with key operating parameters. Therefore, one of the goals of this research is to obtain a better understanding of the mechanisms that govern the drying process. This understanding would not only help remove dryer as a bottleneck in many textile operations, but would also allow the design of control systems to accommodate a variety of textile products and thus reduce energy waste. Specific objectives of present study include: (i) real-time measurement of the excess air and energy consumption, (ii) a quantitative understanding of the drying process, and (iii) development of protocols for improving drying operation.

A data acquisition system for analyzing gas composition of the dryer exhaust was built, which provided quantitative information on the excess air and energy use during the dryer operation. Data were collected from several types of dryer/tenter applications in the textile dyeing/finishing operations.

A mathematical model was developed to simulate the drying of carpet tiles. Experiments were carried out in the laboratory to identify the drying characteristics of the

carpet tile drying. The model incorporates the physical features observed from both laboratory oven tests and industrial continuous dryer processes. The model was first validated by the laboratory results. In addition, the laboratory measurements allowed the evaluation of model parameters including the heat and mass transfer coefficients, diffusivity, and the critical moisture content. With adjustment in a single parameter (heat transfer coefficient h), this model accurately described the performance of industrial tile dryer. Once the model had been validated, it allowed for a parametric study. It predicted that the temperature has a significant effect on the drying rate of the constant drying rate period. The temperature should be set as high as the sensitive temperature that the carpet permits. It was also found that the reduction of initial moisture content of the carpet tile can lead to a significant increase in drying rates.

The model was then applied to optimize the carpet tile drying process. Variables included the initial moisture content, the temperature settings in each of the ten heating zones. The model predicted that the last few heating zones of the dryer should be set at a higher temperature than the current settings in general, which would improve the drying rate. This prediction was verified in the industrial dryer operation. The initial moisture content of the carpet tile, which was identified as another critical parameter, was reduced through improved vacuum slot operation. Optimized temperature profiles and reduction in the initial moisture content increased the dryer speed from 14 ft/min to 20.9 ft/min (~49% increase). A similar approach with other carpet tile products would lead to dryer optimization and increased speeds for those products as well. This study has thus set the

foundation for improving the dryer performance both in terms of debottlenecking as well as reducing energy losses.

CHAPTER I

INTRODUCTION

1.1 Background of the Research and Problem Identification

Approximately 45% of the world's carpet is supplied by the United States, and 80% of the U. S. carpet market is supplied by manufacturers located in Georgia. Therefore, carpet manufacturing plays a very important role in Georgia's economy. Carpet manufacturing incurs very big expenditures in terms of energy use, therefore it is vital that this resource gets used as efficiently as possible in order to reduce costs and maximize operating profits. Drying is an essential part of the dyeing and finishing operations in the textile industry and uses a substantial amount of energy. About one half of the energy used in a typical textile finishing mill is for drying processes with 25% of this amount being consumed by tenter frame dryers[1]. Figure 1.1 shows a schematic of the tenter frame dryers used in carpet industry. The dryer is composed of multiple drying zones with different temperature settings. Each zone has separate natural gas burners and temperature control systems. Due to the increasing fuel costs, it is imperative that these dryers be operated as efficiently as possible.

Figure 1.2 shows a simplified schematic of the dryer operation. Although most of the air enters the dryer through the burner, a large amount of air may also enter through the fabric entry and exit slots into the tenter frame dryer. This secondary air inflow usually results from the pressure differential caused by the exhaust fan. High exhaust

(a)

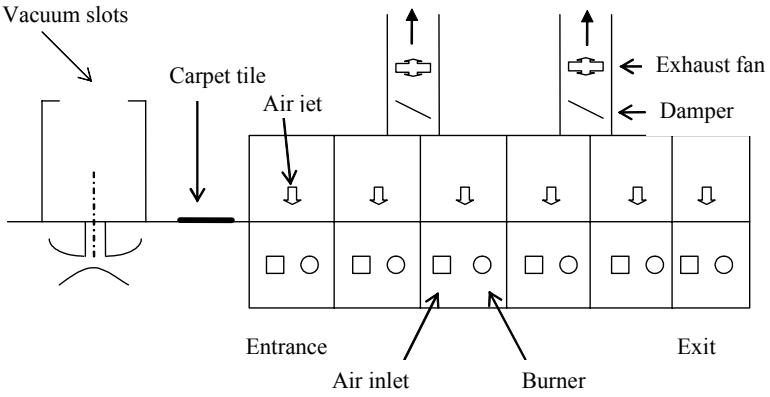

(b)

Figure 1.1 (a) Commercial tenter frame dryers used for carpet industry; (b) Schematic of the tenter frame dryer structure.

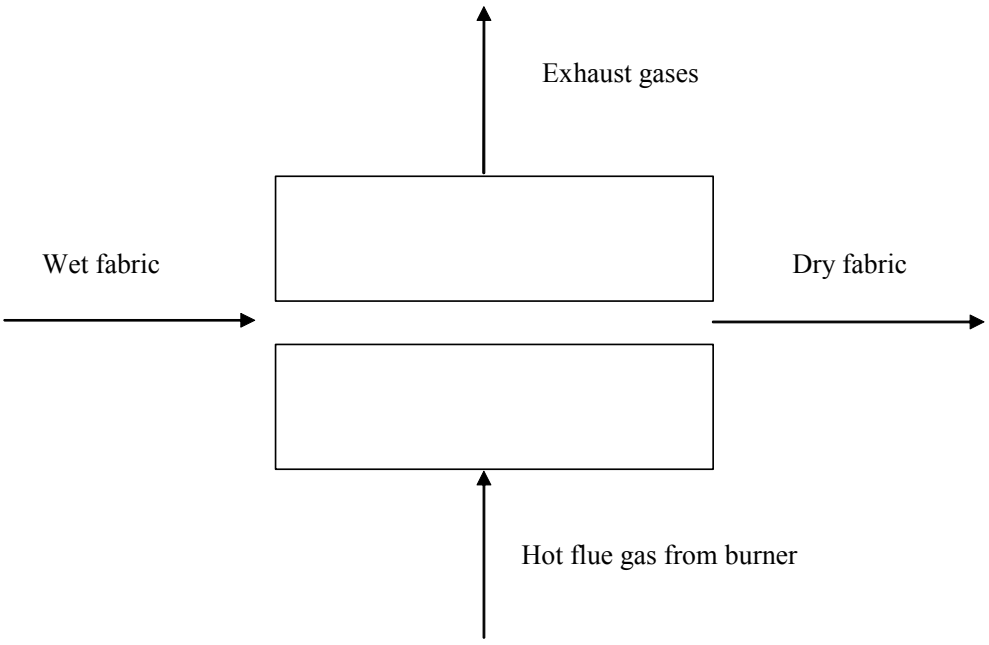

Figure 1.2 Schematic of a typical dryer operation showing the gas flow and carpet feeding direction

fan speed leads to excess air being brought in through the entry and exit slots in the dryer, which has two effects: (a) increase gas velocity leading to higher transport rates; and (b) presumably increase the driving force for mass transfer by keeping the gas-phase moisture content low.

However, excess air usage is also a major cause for energy inefficiency in the dryer operation. Even in a well-insulated dryer excess air is a primary source of energy loss due to the large amount of unrecovered energy carried by the exhaust of flue gases (250-350F). A very large fraction of the heating value of the fuel consumed in the burner ends up as waste in the dryer exhaust. The quantitative relationship between the energy loss and the excess air consumed can be determined through energy balance on the flue gas combustion analysis as demonstrated in Figure 1.3[2]. This figure shows the relationship between the energy loss, exhaust moisture content and the excess air. With increasing air/fuel ratio (increasing amount of excess air), the moisture content in flue gas decreases; while the energy loss increases. For demanding applications like carpet tile drying in this research, the excess air appears necessary to keep the relative humidity of the drying air low. But quantitative treatment and calculation are still required for justifying as well as minimizing the excessive air use.

Figure 1.4 shows a typical temperature profile of the fabric under constant drying air temperature during the drying process. Zone I represents the initial heating of the carpet. Zone II represents the removing of the free moisture of the carpet tile. During this period, the temperature of the carpet tile usually remains constant.

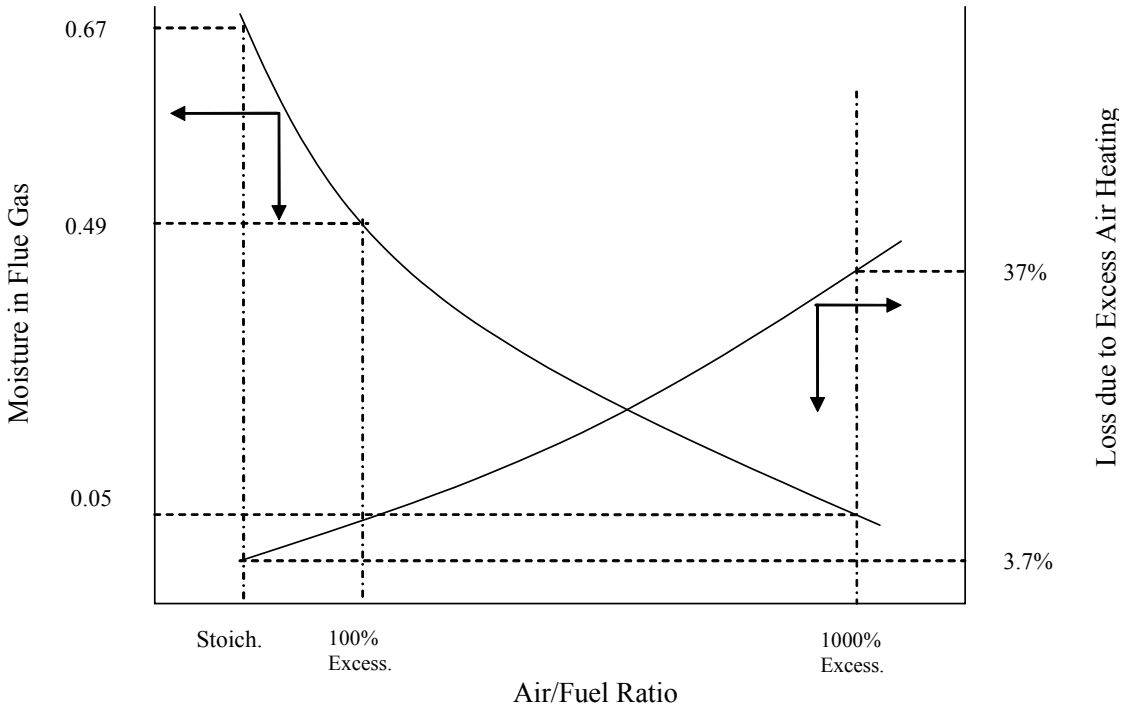

Figure 1.3 The relationship between the energy loss, exhaust moisture content, and the excess air

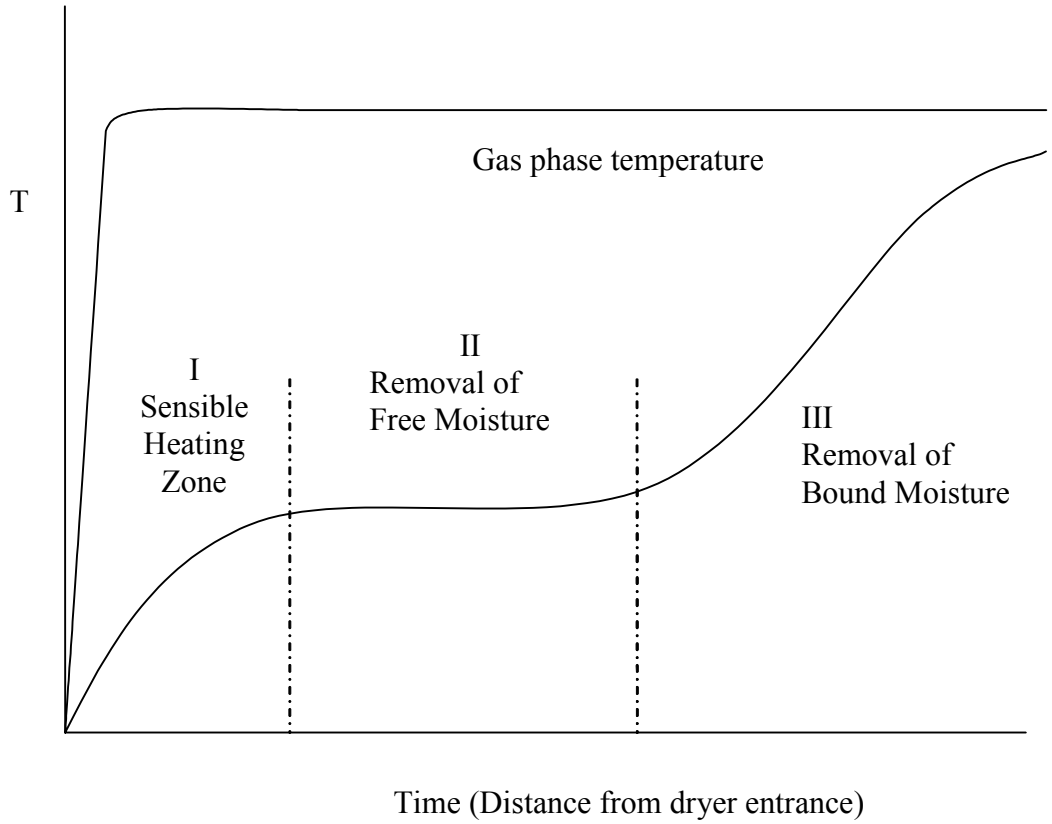

Figure 1.4 Carpet temperature profile in the drying process

This period is called the constant drying rate period. Zone III is for removing the rest of the moisture from the carpet. The temperature of the carpet tile increases rapidly. The drying rate decreases as the moisture content of the carpet deceases, defined as the falling drying rate period. For low demanding applications, such as heat-setting the fabric, the heating process is mainly represented by Zone I; For medium demanding applications, such as removing free moisture off low pile or no pile fabrics, the heating process includes Zone I and Zone II; For high demanding applications such as carpets and tile drying, the heating process includes all the three zones.

Another factor compounding the energy efficiency problem is that often times several grades of fabric may be processed on the same dyeing and finishing range. Due to the lack of quantitative understanding, the temperature inside the dryer is usually set for the most demanding application. This leads to an even higher energy loss during less demanding applications.

The high energy loss is a direct consequence of not having a knowledge of the drying rate curves in general and roles of various operating parameters in particular. Besides, the complex relationships among these factors exacerbate the problem and result in difficulty of controlling the drying operation in a timely and precise fashion. Thus, quantifying the energy waste and understanding the drying process will be of great importance for the carpet drying process. The role of each parameter that affects the drying rate as well as their correlations needs to be clarified. Only by obtaining a

deep understanding of the drying process and its characteristics, can one provide meaningful suggestions on how to improve the drying efficiency.

1.2 Research Objectives

A thorough understanding of the mechanisms that govern the drying process can not only facilitate the design of faster and more efficient industrial dryers, but also allow for the proper control of high energy efficient dryers. Research on the drying of tufted carpet should lead to improved production rates and lower operational cost. One way of solving the problem is by developing mathematical models, which incorporates a higher level of understanding of the dryer and tenter. In this study, an extensive model simulating the drying process was built as a powerful tool. Upon validation the model eventually led to optimize the process and improve the drying efficiency for real time manufacturing.

The following goals should be achieved at the successful conclusion of this project: (1) Develop a portable off-line measurement system for dryer exhaust composition - % excess air; (2) Perform energy balance calculations for minimum energy needs and compare these to the actual energy used; (3) Measure drying rate curves and define transition points from constant drying rate region to the falling rate region; (4) Build mathematical model to predict system behavior in the two regions; (5) Develop optimum dryer operation strategy protocols based on input variables and mathematical model.

1.3 Outline of Research Work

To achieve these goals, initial efforts were focused on building and testing a portable off-line gas chromatography based measurement system for the dryer exhaust gas composition. This allows determination of the excess air amount in the dryer/tenter and serve as one of the parameters in the control strategy. Theoretical fuel consumption needs were determined to quantify the energy waste and evaluate the dryer efficiency. In low-demanding applications, e.g. heat-setting and flat/low pile fabric, quick energy savings would be realized based on the excess air measurement and the energy consumption.

For high demanding situations, e.g. high pile fabrics like carpets, a significant portion of the drying occurs in the falling rate region and diffusion of moisture through the porous fiber controls the drying rate. Thus the drying rate curves for such demanding situations are needed before the task of optimizing dryer performance can be undertaken. Experiments were carried out in a laboratory set-up to identify the drying characteristics of the carpet tile drying, which included the constant drying rate period and the falling drying rate period. Based on the preliminary drying results, analytical model was developed to describe the simultaneous mass and heat transfer for the carpet drying. Transport properties were determined from the laboratory drying experiments. This transient, one-dimensional model is shown to predict important drying characteristics for the industrial carpet drying process and evaluate the role of the

different operating parameters on the carpet drying. This can provide guidance for the industrial drying operation settings.

In summary, this research includes the following specific steps:

1) Build a measurement system to analyze the dryer exhaust composition and excess air use.

2) Quantify the energy waste.

3) Obtain the drying characteristics in the laboratory that can be easily applied to the industrial conditions.

4) Develop mathematical models for describing the drying process

5) Determine the key parameters in the drying model from laboratory experiments as well as industrial data.

6) Validate the model for industrial dryer and then apply it to develop new approaches for dryer operation optimization.

1.4 Organization of the Thesis

This thesis begins with this introductory chapter, laying the ground for the carpet drying project and outlining critical drying problems in the carpet industry. It also outlines the goals that the research needs to achieve. Chapter II gives a technical background of the carpet drying process, which includes an overview of carpet

manufacturing process, identification of critical industrial drying problems, introduction to the drying principles, and a review of drying models in the literature. Chapter III details the development of a portable off-line gas chromatography system to measure the excess air usage, compares the theoretical and actual energy consumption, and evaluates the tenter/dryer efficiency, and finally proposes strategies for energy saving for the low-demanding situations. Chapter IV describes the equipment set-up and methods used to obtain the drying rate curves under laboratory conditions. Chapter V builds the model that is consistent with the observed characteristics of the carpet drying; these include simultaneous heat and mass transfer for both the constant drying rate period and falling drying rate period. Chapter VI analyzes the drying results from the laboratory experiments by using the model, and transport properties such as the heat transfer coefficient, mass transfer coefficient, diffusion coefficient, and the critical moisture content are obtained by fitting experimental data to the model. Chapter VII applies this mathematical model to simulate the industrial drying process. The value of the heat transfer coefficient during the industrial drying process is first determined. The effects of the dryer zone temperature settings and the percent wet pickup on the total drying time are studied. Based on the model simulation results, improvements in the carpet drying rate are identified and suggested to the industrial partner. Finally, Chapter VIII concludes by summarizing the main results from this study and presents a set of recommendations for the industrial drying process.

CHAPTER II

BACKGROUND AND LITERATURE REVIEW

2.1 Drying Principles

The term drying refers to removal of water or other liquids from the solid or semi-solid material to reduce the liquid content to an acceptable value. Liquids may be removed either mechanically by press or thermally by moisture vaporization, which is the focus of this research.

2.1.1 Bound and Unbound Moisture in a Solid

Two types of moistures exist in a solid: bound and unbound moisture[3,4]. The drying process is governed by the equilibrium relationship between the moisture content of the solid and the relative humidity of the drying air, as shown in Figure 2.1. Point A in Figure 2.1 represents the transition between unbound moisture and bound moisture. At solid moisture content levels higher than point A, the equilibrium curve is flat. This shows that the solid moisture content can be reduced without lowering the relative humidity of air. In some references, it is also referred to as "free moisture". Below Point A, the solid moisture is considered "bound moisture". Removal of this bound moisture may be

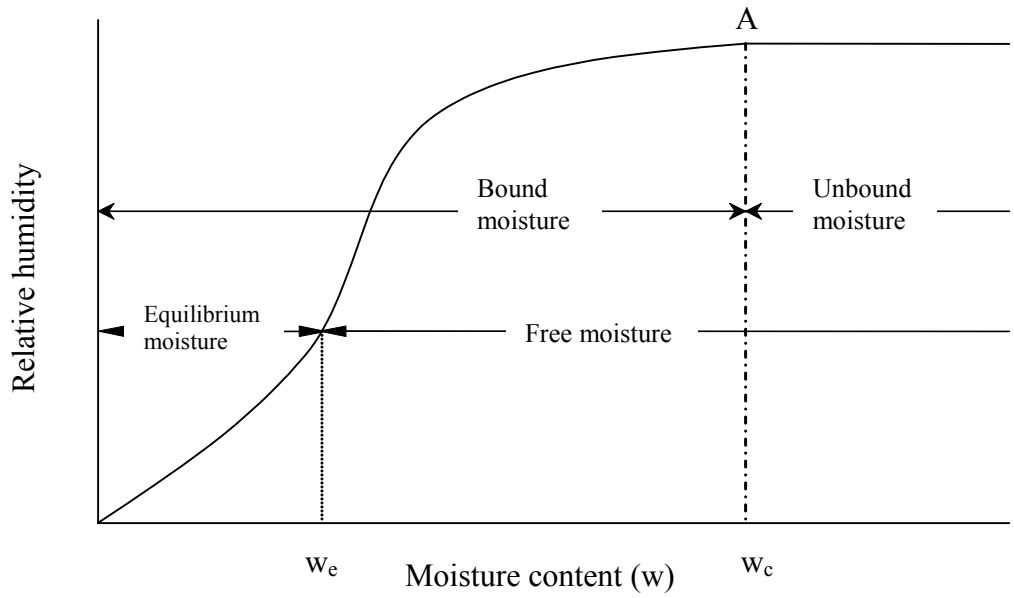

Figure 2.1 Types of moisture involved in the drying of porous solid materials based on the relative humidity of the drying gas and the moisture content of the material

governed by the diffusion of moisture through the porous solid. Another interpretation of the unbound (free) and bound moisture can be offered in terns of vapor pressure exerted by the liquid (or water) present in the solid. At solid moisture at or above point A, the vapor pressure exhibited by the moisture present in the solid equals the vapor pressure of the liquid water at a given temperature. At solid moisture contents below point A, the vapor pressure exerted by the wet solid is less than the vapor pressure of the liquid water at the same temperature. The difference between the initial moisture content and the equilibrium moisture content, $w_{e,}$ is the moisture that can be removed.

2.1.2 Typical Drying Characteristics

The general drying behavior under constant external conditions can be represented by a moisture content versus time curve and temperature versus time curve shown in Figure 2.2, all of which exhibit a constant-rate period and falling-rate period.

At the beginning of the drying, the solid temperature adjusts itself until reaching a steady state where the temperature of the wet solid surface is the same as the wet-bulb temperature of the drying air, and the drying rate is constant. From this point onwards it is called the constant rate drying period. The drying rate is determined by the movement of water vapor through the stationary film of air surrounding the material, which is proportional to the difference between the partial pressure of the water vapor at the surface of the material and that in the dry air. The constant rate

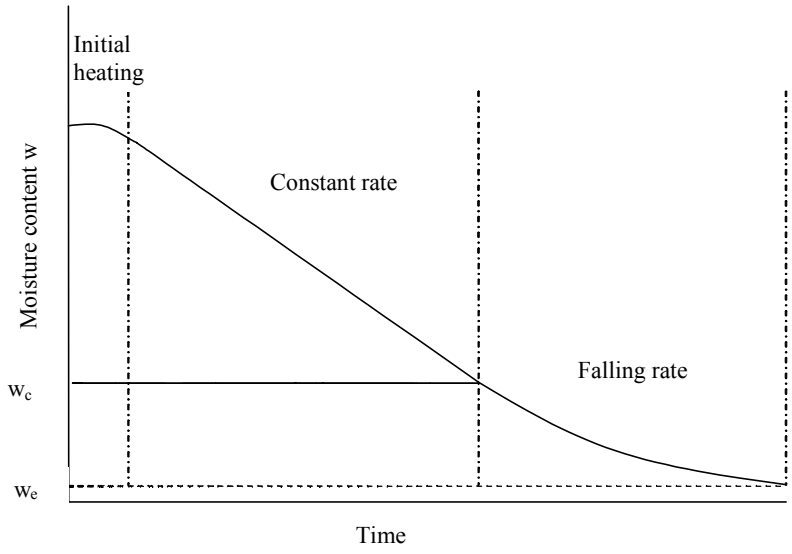

(a)

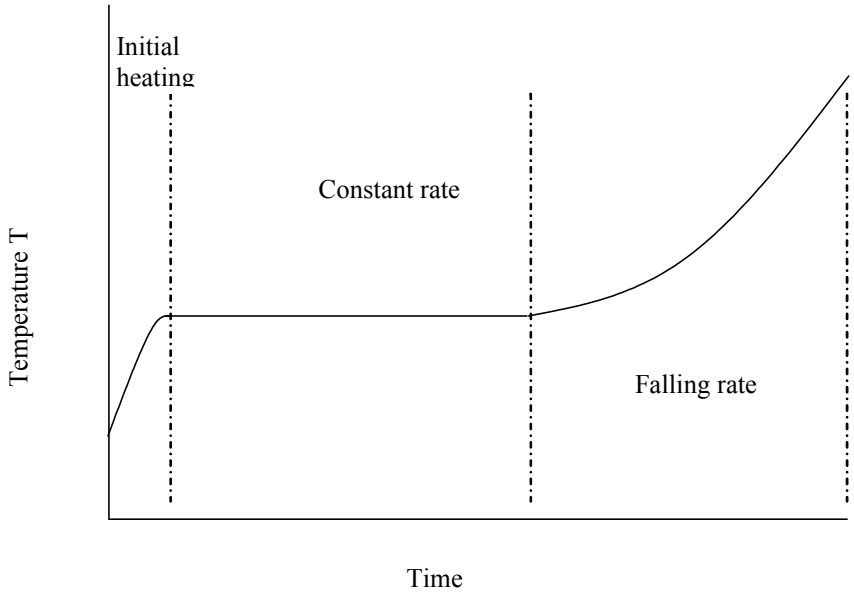

(b)

Figure 2.2 Typical drying curves showing: (a) the change of moisture content in a solid as a function of time (b) the change of temperature in a solid under constant drying conditions

drying period continues as the water removed from the surface is replenished by the unbound (free) water from interior of the solid.

As moisture content decreases, the constant-rate drying period ends at a certain moisture content (point A in Figure 2.1), and the falling-rate period starts. This transition point is defined as the critical point, w_c. Beyond this point, the surface temperature rises, and the vapor pressure of moisture at the solid surface falls below the saturation point causing the drying rate to decrease. Figure 2.3 shows a typical drying curve on a drying rate versus moisture content basis. Depending on the materials and their physical characteristics, the falling-rate period may be further divided into the following two zones:

1. The unsaturated surface zone also known as the first falling rate period. During this period, the surface becomes depleted in liquid because the rate of liquid transfer to the surface is slower than the rate of mass transfer of moisture away from the surface. With the decreased fraction of saturated region, the total surface evaporation rate decreases.

2. The internal moisture control zone. In this second falling-rate period, all evaporation occurs from the interior of the solid, and the plain of vaporization moves into the solid. As a result, the drying rate is governed by the rate of internal moisture vapor movement. As the moisture content continues to fall, the diffusion path of mass grows longer. When the moisture content in the solid decreases to an equilibrium w_e, the whole drying process stops.

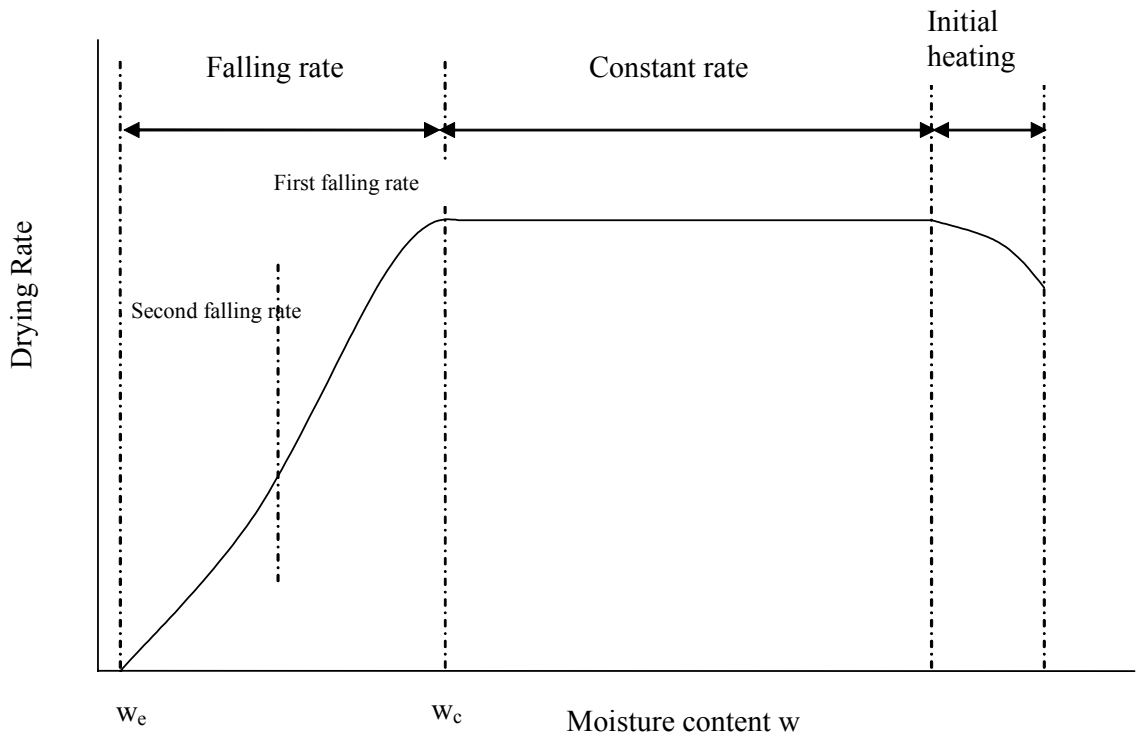

Figure 2.3 A typical drying rate curve: drying rate as a function of moisture content for constant drying condition.

2.1.3 Drying Models /Mechanism

During the constant drying rate period, the molar flux N can be estimated using correlations developed for drying rate of a free liquid surface. Either the mass transfer or the heat transfer equation may be used. In terms of the mass transfer, the drying rate may be written as follows :

$$N=k_y(y_i-y_a) \qquad (2.1)$$

Where k_y is the mass transfer coefficient, y_i is the mole fraction of water vapor at interface (the interface temperature can be considered equal to the wet bulb temperature T_{wb}), and y_a is the mole fraction of water vapor in the air.

For the falling drying rate periods, two different mechanisms have been proposed: (i) Diffusion model, and (ii) Capillary model. Below is a brief description of each of the two mechanisms.

(i) Diffusion Model for drying of heterogeneous solids such as nonporous media or some porous media when dried below the critical moisture content. The moisture is either trapped within the material or held as an integral part of the solid. Moisture movement is slow and occurs by diffusion. A typical concave drying curve in Figure 2.2(a) represents the diffusion mechanism. Figure 2.4 shows a schematic of the moisture distribution and movement. The resistance to mass transfer of vapor from the solid surface to the air is

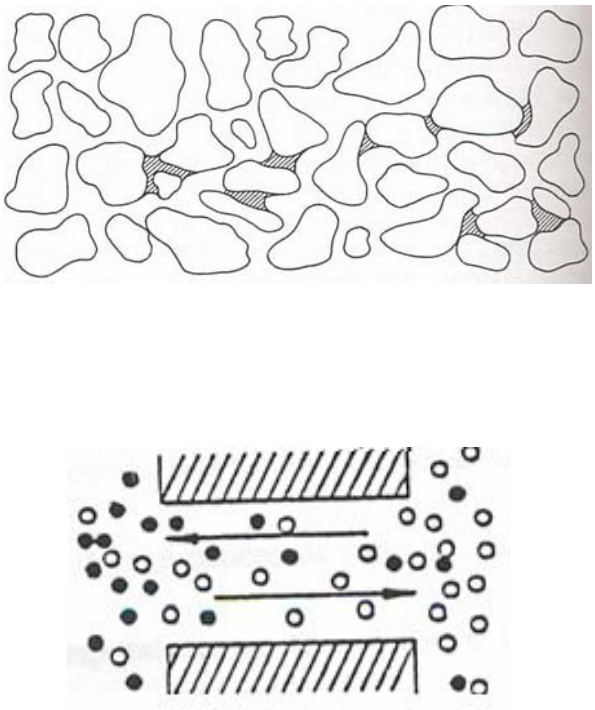

Figure 2.4 Schematics showing the moisture distribution and movement by diffusion mechanism

(ref [6,5])

usually negligible, and diffusion of water vapor within the solid controls the overall drying rate. Therefore, the moisture content at the solid surface is nearly in equilibrium with the air humidity. Since diffusivity increases with temperature, the drying rate increases with the temperature of the solid. The rate of moisture movement is expressed by Fick's law described as follows[6],

$$\frac{\partial w}{\partial t} = D\frac{\partial^2 w}{\partial x^2} \qquad (2.2)$$

where D is the diffusion coefficient; w is the moisture content (lb mole water/lb mole solid).

Although the actual mechanism is probably more complicated than simple diffusion, the above equation has long been used for quantitative description of the drying rate of nonporous solids. Even if diffusion does control the moisture movement through the solid, the equation does not usually provide a quantitative fit to the measured drying rates curves well. Many solids change their pore characteristics during drying, and the moisture distribution at the critical moisture content is generally nonuniform. However, diffusion provides an acceptable interpretation for materials with concave-shape drying curves.

(ii) Capillary model. This type of drying usually occurs in materials with a large open-pore structure and a complicated network of pores and channels, which is shown in Figure 2.5. The length and the cross section of these pores and channels vary greatly. Moisture movement is due to surface tension or capillary forces. As water is removed by vaporization, a meniscus across each pore is formed, which sets up capillary forces by the interfacial tension between the water and the solid. The capillary forces provide the driving force for the movement of moisture through the pores toward the surface. The capillary force at a given point in a pore depends on the curvature of the meniscus, which is described by the following equation:

$$\Delta P = 2\gamma / r \qquad (2.3)$$

where ΔP represents the driving force for liquid movement in capillary due to surface tension, γ is the surface tension, and r is radius of curvature of the capillary.

Some other drying theories have appeared to account for the drying behaviors of other solids. For highly porous solids, the influence of gravity is far more than that from the capillary forces. For this type of material, it may show two linear falling rate periods. For hygroscopic porous solid, the bound water is removed by progressive vaporization below the surface of the solid, which is accompanied by diffusion of the water vapor through the solid. Usually only one critical point is found.

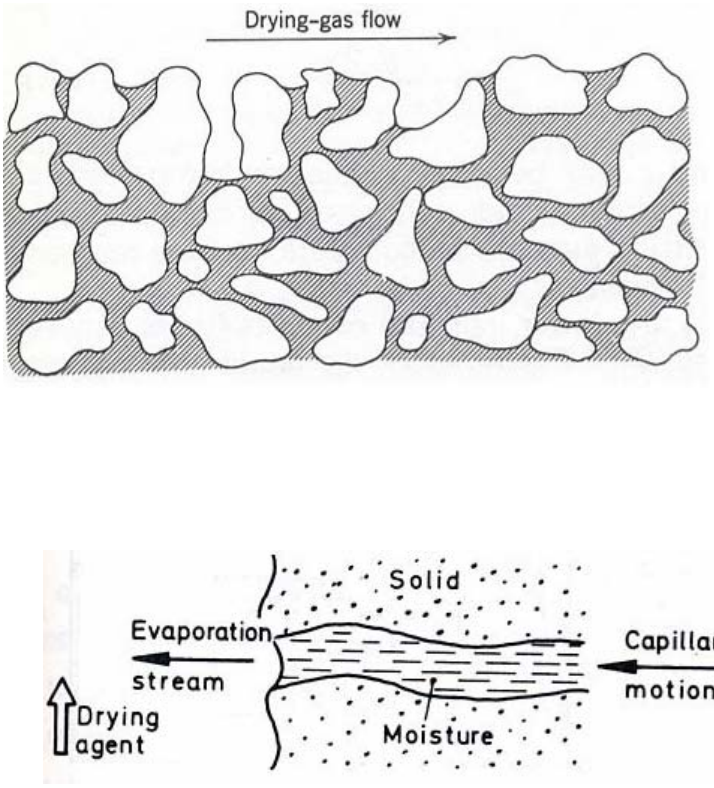

Figure 2.5 Schematics showing the moisture distribution and movement by capillary mechanism

(ref [6,7])

2.2 Review on Textile Drying

2.2.1 Typical Drying Processes and Methods Used in Textile Industry

Drying is essential to dyeing and finishing operations in the textile industry. With complex simultaneous heat and mass transfer processes involved, the drying operation remains a primary factor in setting the production rate.

Convection dryers are still the drying equipment most commonly used in the carpet industry. Under drying operation, water in the textile fabric is evaporated with the latent heat for the moisture evaporation provided by the drying air through convection to the surface of the carpet. There are two drying methods used in the textile industry, flow though drying and impingement drying. Figure 2.6 shows a schematic of the two methods. The flow through method is the preferred production method for permeable carpet products such as unbacked broadloom carpet. In this case, the air flows through the carpet and around the individual carpet yarn. This minimizes the shielding, in turn increasing the evaporation rate. Impingement drying is a more effective drying method for impermeable carpet (e.g. carpet tiles). Impingement dryers may consist of a gas jet or an array of gas jets impinging perpendicular to a drying surface. In impingement flow, the direction of gas flow is perpendicular to the carpet feeding direction. Air is forced through ducts above and below the carpet and hit the carpet at high velocity. Typically, the jet velocity and temperature in impingement drying may range from 10 m/s to 100m/s and 100°C to 350°C, respectively, depending on the product[8].

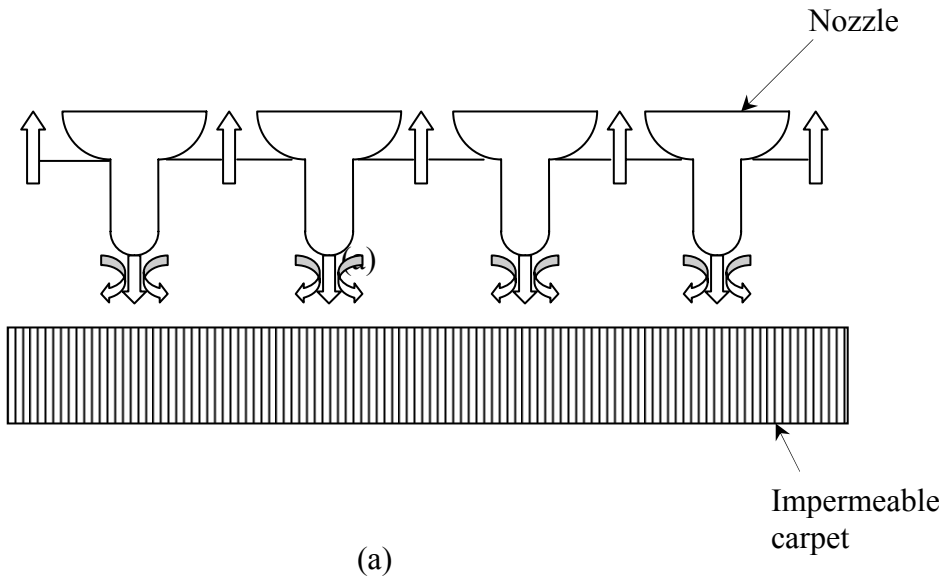

(a)

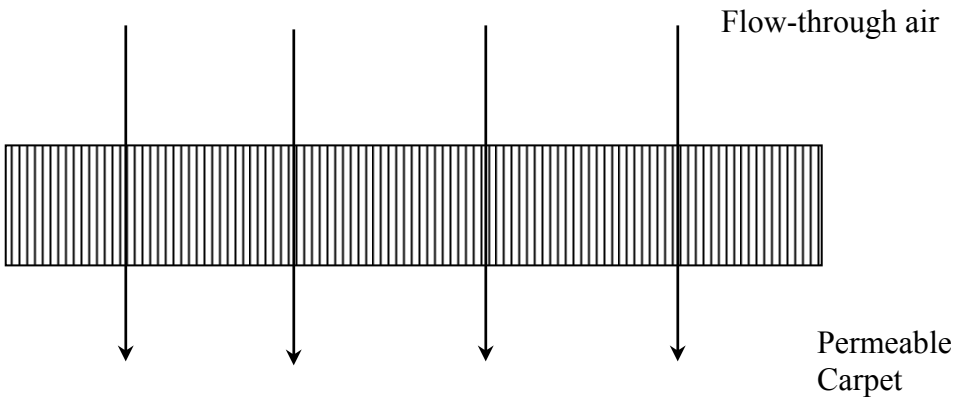

(b)

Figure 2.6 Schematics of the drying systems for carpet: (a) impingement drying; (b) flow through drying

This kind of design reduces the dead air space surrounding the evaporation surfaces. In addition, it also yields very high heat and mass transfer rates, greatly reducing the drying time.

In recent years, new techniques have been considered as an add-on improvement to the convection dryers. These include infrared and microwave drying. The unique heating mechanisms associated with these methods are proven to be efficient for removing moisture for both natural and synthetic textiles. In addition, these methods also offer many other advantages. They offer the potential for reduced energy consumption (lower exhaust losses) and improved product quality by minimizing dye migration and accurately controlling the final moisture content. However, these methods are usually prohibitively expensive (both capital and operating costs) for use as a stand-alone unit. Instead, they are better suited as a supplement to the convection dryers. Combined drying mode, such as infrared plus air jets or microwave with impingement drying, is commercially feasible.

As stated before, the drying operation is a bottleneck in many carpet dyeing and finishing operations. Even with many advances in this area, the drying operation is still the main factor limiting the production rate. Optimization of the drying process should involve an improvement in product quality and production rate at a reduced cost. By increasing the production rate, one can achieve reduced variable costs (labor and utilities) per unit of production. In order to increase the production rate, higher temperature and higher air flow rate are normally needed to enhance the heat and mass transport rates for

the drying process. However, precautions should be taken to increase the temperature. If the temperature exceeds the carpet sensitive temperature, it may result in product degradation. Higher air flow rates would improve the mass transfer process. However, the needed excess air may carry a lot of energy unrecovered and is a major cause for energy inefficiency in the drying operations. Before any optimization of dryer performance can be undertaken, quantitative understanding of the drying characteristics e.g., the effects of the operating parameters on the drying process as well as on the product quality, should be understood. In the next section, a brief review of mathematical drying models as applied to the textile industry will be presented.

2.2.2 General Experimental Observations in Textile Drying

As stated before, the shape of drying curves depends on not only the external drying conditions but also the type of the carpet being dried. Carpet materials have been classified as the hygroscopic porous material[9,10,11,12,13,14]. This type of material is characterized by: (1) clearly recognizable pore space between nylon fibers, which is of the same magnitude as the diameter of the fiber; (2) a large amount of bound moisture trapped in the solid-backing layer. The material classification is important for studying the drying mechanism, especially in the last stages of drying, because the moisture transport mechanism is highly dependent on the microstructure and transport properties of the carpet. The carpet tiles studied in this investigation contain a saturated porous nylon fiber layer attached to a solid impermeable backing layer. Figure 2.7 shows a schematic of the tufted carpet cross section.

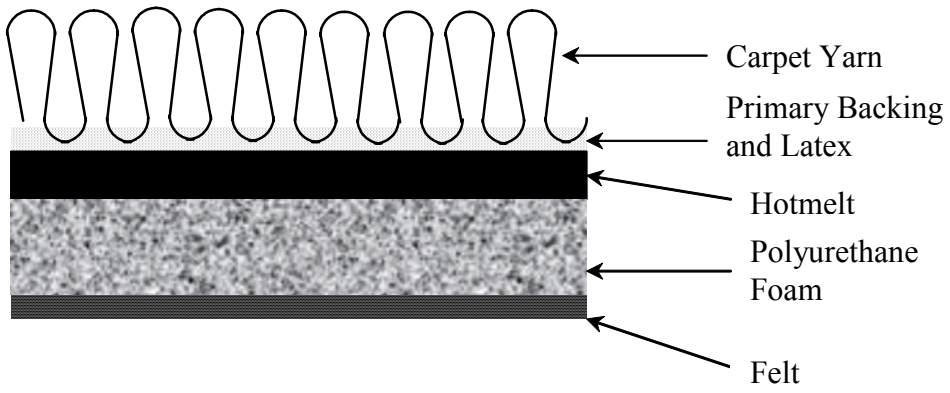

Figure 2.7 Schematic of the tufted carpet cross section

The physical quantification of the drying process has been performed by various authors and verified by the experimental data[15,16,17,18]. A typical carpet drying process consists of two drying periods: a constant drying rate period and a falling drying rate period. During the constant drying stage, the evaporation takes place at the carpet surface. The moisture movement is in a continuous phase. The drying rate at this stage is constant, provided that enough moisture can be transported to the carpet surface from the interior of the carpet material. As the moisture content continues to decrease and approaches the critical moisture content, enough moisture is no longer available at the carpet surface and evaporation front begins to recede into the interior of the carpet. In this period, the moisture transport is controlled only by diffusion. With more moisture evaporating and the evaporation front receding further into the carpet, the diffusion path grows longer and the drying rate continually decreases. As a result, the second drying period is characterized by a decrease in the drying rate, and the properties of the carpet material, such as diffusion resistance, have far more impact on the drying rate than the external drying conditions (e.g. air velocity and air humidity etc.). In order to simulate the drying process, theoretical models often consider not only the external conditions but also their dependence on the processes governing the internal moisture transport. Different models are summarized based on these two drying periods in the following sections.

2.2.3 Mathematical Drying Models on Textile Drying

Brock and Gorton[19,20] pioneered the work in flow through drying of tufted carpets. They studied effects of the different operating variables on the drying rate and the drying time for different carpet materials. It was found that the carpet exhibited both the constant drying rate period and the falling drying rate period in the drying rate curves. The pressure drop and the flow rates were correlated by Reynolds number and drag coefficient. The drag coefficient was used to analytically predict the drying rate of the constant drying period. An empirical equation was used to predict the drying rate and time in the falling drying rate period. From experiments, it was found that the tufted carpet could be dried with the flow through drying in less than one-fifth the time required in the industrial dryers at that time. However, the results predicted from the mathematical model did not agree with the experimental data well.

Lee and Carr[21,22,23] studied the through-air drying of unbacked tufted carpets. First, a model was developed to predict the variation of the velocity with pressure drop across the unbacked tufted carpet including inertial and viscous effects. Second, they also proposed a two-dimensional drying model for the through-air drying of the unbacked tufted carpet considering simultaneous heat, mass, and momentum transports. To feed the model, moisture distribution in nylon pile unbacked tufted carpet was obtained from magnetic resonance imaging system (MRI). The two-region drying model being considered includes the wet region and sorption region. For the wet region, internal moisture transport is controlled by capillary flow, while for the sorption region

bound moisture migration and vapor diffusion dominate. As drying process went on, the evaporation front receded from the surface into the sorption region. As a result, the final form of this drying model consists of two sets of coupled differential equations with relevant initial and boundary conditions. While this model was able to explain the observed drying behavior, it had too many adjustable parameters to have predictive capabilities for various carpets. In order to solve this problem, a simplified drying model was developed including fewer physical and transport properties by considering only dominant transport mechanisms. It was found that, an increase in either air flow rate or air temperature increases the drying rate, but for the same energy input to heat the inlet air, increasing air temperature is more effective. The simplified drying model agreed with the experimental drying results, which is shown in Figure 2.8 .

Francis[24,25,26] developed a model to investigate the carpet drying under continuous industrial impingement drying conditions. The conservation of mass, energy, and momentum were used to describe the drying process. A constant drying rate period (wet region) and a falling drying rate period (sorption region) were considered. The mechanisms of the liquid mass transfer were capillary flow described by the Darcy's law for unbound moisture in the wet region, and liquid diffusion for bound moisture during the sorption region. Besides, the differential heat of sorption was reflected by the enthalpy of the bound liquid in the sorption region. The enhanced mass and heat transport coefficients at the drying surface for the multiple jet impingement flow were estimated using the Kolmogoroff theory of isotropic turbulence[27]. The one-dimensional transient conservation equations provided the temperature, volumetric

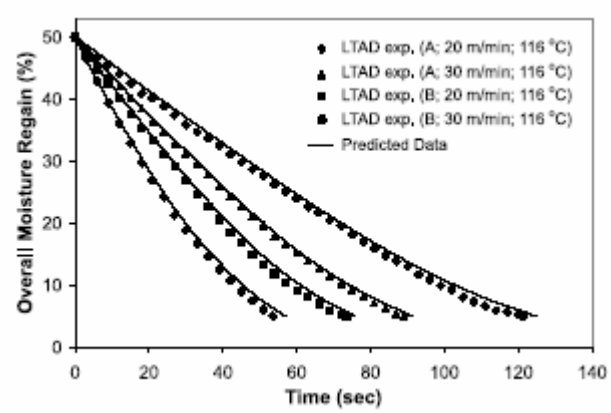

Figure 2.8 Comparison of experimental and predicted overall moisture regain with time for carpet samples A and B at different airflow rates (ref.[22])

saturation, and gas phase pressure distributions in the porous fiber layer. The model results were compared to independent experimental temperature and overall moisture content measurements taken in an operational industrial dryer. It was found that low heat transfer coefficient more accurately represented the internal transport occurring during the drying process. The transport properties for the impingement drying obtained from the Kolmogoroff theory were closer to experimental data than other correlations. The drying results from the model have shown a good fit to the experimental data by adjusting the surrounding fluid dissipation coefficient. However, it can also be seen that, because of the number of parameters, such as the variable fluid dissipation coefficient and thus the heat and mass transfer coefficient, and a number of other unknown thermodynamic and transport properties, uncertainties exist in this model's predictability. One noteworthy point which the author did not mention is that, it can be readily shown from the data on heat and mass transport coefficients that the principles of simultaneous heat and mass transfer hold. In other words, the Chilton-Colburn analogy applies in this part of the drying.

Francis[28,29] developed distributed parameter models for modular carpet drying in a tenter frame dryer. Two different models including conservation of mass and energy were proposed. The simplified model (two layer model) only consists of constant drying rate period. The three layer model includes both the constant drying rate period and the falling drying rate period. The driving force for the mass transfer of the unbound water is the moisture gradient. An empirical equation was used for the falling drying rate period which was similar to that used by Brock[19,20]. A lumped parameter approach was

used to assume that each layer's temperature was only a function of time. The governing equations in each case included mass and energy balances, as well as relative rates equations. However, due to the incomplete understanding of the moisture transport mechanism, the results from the model did not agree with the experimental well. Solis[30,31] performed similar studies with foam backed carpet instead of hot-melt backed carpet. The differential equations were derived in the same way. But four layers instead of three layers were included in this drying model. He also assumed that evaporation takes place only in the fiber layer of the carpet, and internal liquid movement was included. Internal resistance and the correlations between the mass transfer and heat transfer were modeled differently. Based on these modifications, the model showed an improvement in describing the general drying process compared to Francis's model. However, better understanding was needed for the model to predict the drying characteristics of the different layers of the modular carpet.

Moyne and Degiovanni[32] developed a model to describe a superheated steam drying process for a concrete slab. The major mechanisms for moisture transport considered were capillary moisture movement and vapor diffusion with bulk flow. O'Dell [33] investigated and compared the drying characteristics of carpet tiles in air, humidified air, and superheated drying conditions. He found that under the steam drying conditions, the existence of a more clearly defined constant drying rate period was observed, and the drying rate in the falling rate drying period is higher than that in the air drying conditions. But no fundamental study was reported of the mechanism of the

mass transfer, heat transfer, and moisture migration for carpet tile drying under superheated steam conditions.

A significant number of models in literature utilize the concept of evaporation front--the line (dividing the dry and wet region) retreats into the interior of the drying media as the drying process proceeds. Therefore, methods used to track the evaporation front will be reviewed here. The basic idea of the submerged front models is that the evaporation takes place inside porous materials from a clearly recognizable region. The evaporation front retreats into the porous media when the surface becomes dry, whereas the liquid concentration behind the evaporation front remains almost constant. Numerous studies have shown the existence of evaporation front when investigating the drying of clay and timber. Craptise et al.[34] modeled the drying of food products by considering the water flux transport within the cellular material and concluded that, the time variation in moisture profile within the material supports the assumption of the existence of a submerged evaporation front. Ratti and Craptiste[35] proposed the receding evaporation front model for the drying of food products such as potato, apple and carrot. The predictions showed good agreement with experimental results. Almubarak and Mumford[36] studied the receding velocity of the front of glass beads and activated alumina in correlation with the drying rate. They have demonstrated that it is possible to identify the position of the evaporation front. The point at which the temperature at any given depth just reaches the asymptotic temperature provides an indication of the position of the receding evaporation front.

Under certain assumptions, the distance of the evaporation front from the surface is proportional to the square root of drying time. Heertjes and Tuinder[37] have confirmed this by observing a linear relationship between the distance of the evaporation front and the square root of time with reasonable accuracy. Chou[38] investigated the evaporation front during the drying of food products by measuring the temperature distribution profile. The experimental work identified the existence of a receding evaporation front during drying. The relationship between the receding evaporation front and the square root of the drying time is linear. Figure 2.9 shows experimental data in describing this relationship. But no simple models have been proposed to account for this relationship.

2.3 Focus of This Research

Review of mathematical models on textile carpet drying mentioned above shows that most of the models suffer from either one of the two drawbacks: (1) The results from the mathematical models do not agree with the experimental data obtained from carpet drying operations, and/or (2) A set of differential equations with many unknown adjustable parameters makes it difficult to have predictive capabilities. Either one of the two drawbacks would render the mathematical model less useful for industrial applications.

As stated before, the impermeable carpet tiles studied in this research work have been classified as hygroscopic-porous media. Modeling the drying process of these

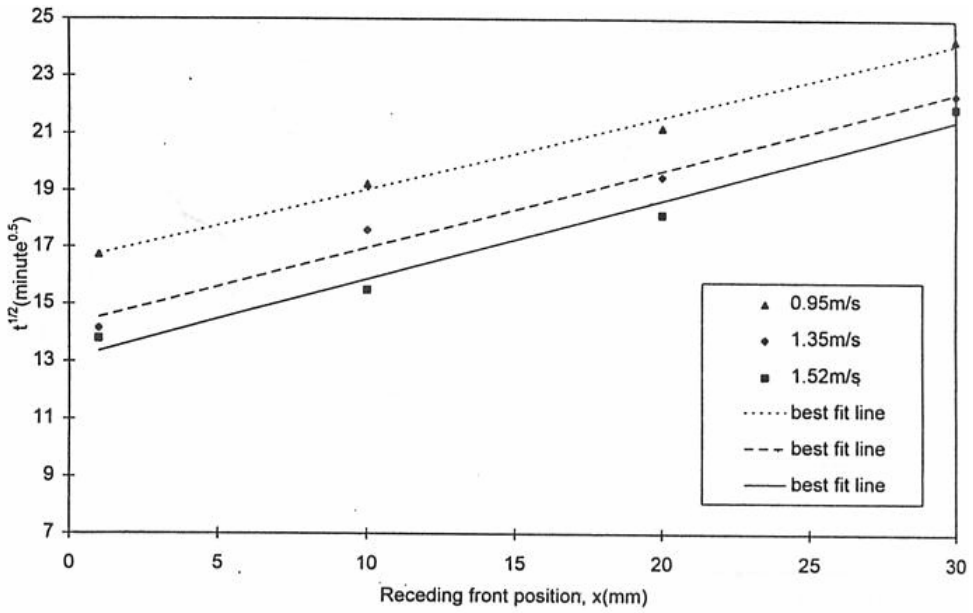

Figure 2.9 The relationship between the position of the evaporation front and time (ref.[38])

materials such as clay, wood, and food products, by using the submerged evaporation front model has been demonstrated and documented. However, most of these publications did not provide explicit expression for the relationship between the moving submerged evaporation front and the time. The empirical function is obtained only by curve-fitting the experimental data. Besides, little investigation has been done to use the receding evaporation front model on the drying of carpet tiles.

In this research work, the receding evaporation front model was applied to the drying of carpet tiles. Analytical equations were derived and explicit expressions for the position of the evaporation front with time were obtained. Independent study in the laboratory was conducted to obtain the adjustable parameters, and the model was validated by the industrial drying data. Upon validation, the model was used to solve the industrial drying problems stated in the first chapter. Specific goals for this research include: (1) Develop a portable off-line measurement system for dryer exhaust composition - % excess air; (2) Perform energy balance calculations for minimum energy needs and compare these to the actual energy used; (3) Measure drying rate curves and define transition points from constant drying rate region to the falling rate region; (4) Build mathematical model to predict system behavior in the two regions; (5) Develop optimum dryer operation strategy protocols based on input variables and mathematical model.

CHAPTER III

EXCESS AIR MEASUREMENT

3.1 Introduction

The project has twin goals: (i) Quantify the excess air usage in dryer operations, and (ii) Develop a mathematical model for the drying of carpet tiles. Most dryers/tenters employed in the textile industry lack adequate measurement and feedback control system to monitor the fabric drying and heat-setting process, resulting in a large amount of excess air and wasted energy in exhaust. Though a qualitative understanding of the role of many operating variables exists, quantitative knowledge about the effect of these parameters is sorely missing. Therefore, the first step of this project is to quantify the energy losses in the drying process before modeling and optimization work can be undertaken.

Two approaches can be used to reduce the energy losses in a dryer exhaust: (i) humidity or moisture measurement in the gas phase, and (ii) on-line fabric moisture content measurement. On-line fabric moisture monitoring is not an economically viable option with current state of the art. As described in the previous chapter, excess air usage is a major cause of energy loss in the operation of dryers. The amount of air coming in through the entry and exit slots in the dryer is directly related to the exhaust fan speed**.** Therefore, an analysis of the dryer exhaust composition can be used to

discern the excess air, and the energy losses can be quantified. In this chapter, the methodology and experimental set-up for exhaust samples collection and subsequent off-line analysis will be described.

3.2 Rationale

Analysis of exhaust gas composition can be used to investigate the total amount of excess air since accounting of air from each inlet is difficult. The air-fuel ratio in the burner is set by factory and is not easy to change. One generally does not know this ratio at the production site. Additional air is drawn into the burner to control the flue gas temperature. The secondary air, i.e., from the entry/exit slots is a major source of excess air as demonstrated in the simplified schematic Figure 3.1, and it is not easily defined. The flow of this secondary air depends on the pressure differential that exists across the ambient and the dryer entry/exit slots. This pressure differential, in turn, is governed by the exhaust fan speed. The only way to estimate the total air in the dryer is by analyzing the exhaust. The N_2/CO_2 ratio would be an accurate indicator of the total air being brought into the dryer. Some amount of excess air is purposely used in the burner to ensure complete fuel combustion, so that no CO is present in the exhaust. The fuel consumption may be represented by the following reaction:

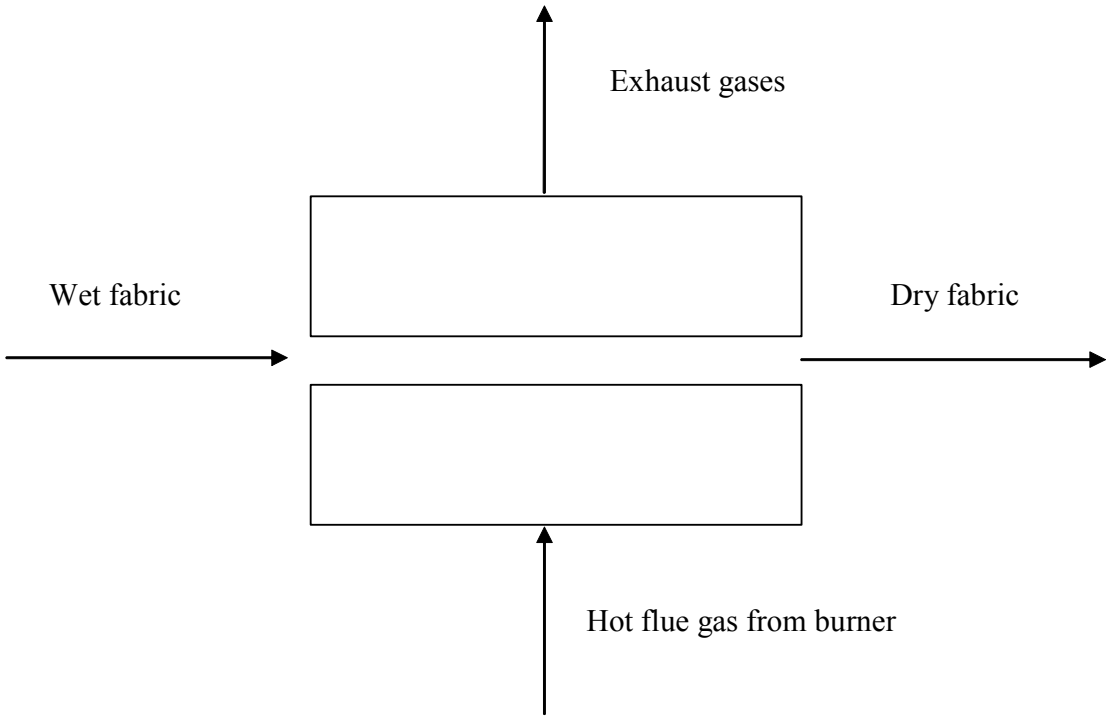

Figure 3.1 Schematic of a typical dryer operation showing the gas flow and carpet feeding direction

$$CH_4 + 2O_2 \rightarrow CO_2 + 2H_2O, \qquad \Delta H_r = -802.3 \text{ KJ/mol} \qquad (3.1)$$

Theoretically, for each mole of methane, 9.52 moles of air (2 moles of oxygen and 7.52 moles of nitrogen) are required. Thus, a N_2/CO_2 ratio of 7.52 is a threshold value and represents stoichiometric air use (no excess). A ratio of 22.56, for example, would indicate 200% excess air being used and so on.

The amount of energy needed to dry the fabric can be calculated from the following energy balance equation:

$$Q_{total} = m_c . Cp_c (T_{out} - T_{in}) + m_w . Cp_w(T_{out} - T_{in}) + m_w . H_v \qquad (3.2)$$

The first term on the right hand side represents the sensible heat associated with heating the fabric from its inlet temperature to the outlet temperature value. The second term is the sensible heat needed to heat the water associated with wet fabric to its exit temperature. The third and last term in the above equation represents the latent heat associated with evaporating the water into the gas phase. The parameters in Equation 3.2 are discussed below. m_c is the weight of the carpet tile passing through the dryer in a unit time. In order to evaluate m_c, we need to know the operating speed as well as the width of fabric. Also, the areal density of the fabric in oz/yd^2 is needed. Knowing m_c and the moisture content of the wet fabric w, we can calculate m_w. H_v represents the

latent heat of evaporation of water. The third term in the above equation represents 80-90 percent of the total heat requirements in most drying situations. In heat-setting processes, only the first term is present and it should be possible to operate a heat-setting tenter very close to the theoretical needs. The total energy requirements calculated from the above equation can be compared to the actual energy being used in the dryer burner. A ratio of actual energy used to the theoretical energy needs can be used as benchmark to compare the operation of various dryers. The above energy balance equation can be readily used for a variety of textile fabrics, provided one can estimate the variables listed herein. For many low demanding dryer/tenter operations that involve either (1) heat-setting of fabric, or (2) drying of low-pile or flat fabric, we can move quickly to realize energy savings by reducing excess air.

3.3 Experimental Set-up

In order to determine the N_2/CO_2 ratio in dryer exhaust, one may consider using some solid state sensors for real time on-line analysis. Presently, on-line solid state sensor technology does not allow one to measure the nitrogen content in the dryer exhaust. Zirconia-based dual sensor technology would allow one to get on-line real time measurement of O_2, H_2O, and CO_2. There are four major constituents in the dryer exhaust: N_2, O_2, H_2O, and CO_2. Knowing three of these should enable one to determine the fourth constituent. While that would be a desirable operating/control strategy in an industrial dryer, it would also force us to focus all our efforts on a single dryer. One of

the goals of present study was to collect gas samples from many different dryer exhausts. Hence we decided to develop a portable gas-sampling device. A portable gas-sampling module draws in a sample of the dryer exhaust. This sampling module would allow us to condense the moisture by cooling, and this dry sample of the exhaust stream would be directed to Gas Chromatography (GC) for accurate measurement of the other three constituents: N_2, O_2, and CO_2. The advantages of developing this portable off-line analyzer are: (1) it permits the calibration of on-line solid state sensors in future, (2) it allows direct determination of N_2/CO_2 ratio, thus minimizing the potential for error in solid state sensor, and (3) due to its portability, it can be easily used to check the performance of other dryers/tenters.

A GC measurement system for analysis of the gas composition of the industrial dryer exhausts was set up at a Milliken plant site (Live Oak Plant) in LaGrange, GA. The off-line measurement system mainly includes a gas sampling bulb and a gas chromatograph.

Figure 3.2 shows the schematic of 250 ml Pyrex sampling bulb that was used to trap the dryer exhaust gas for GC analysis. The samples were collected at the plant roof where a portion of the dryer exhaust was diverted to flow through this sampling bulb. After allowing sufficient time for the bulb to become equilibrated with the exhaust composition, the two stop cocks were closed. The pressure in the sampling bulb was near one atmosphere at this point, whereas the temperature was well above the ambient condition. The sampling bulb was transported to the laboratory area for GC analysis.

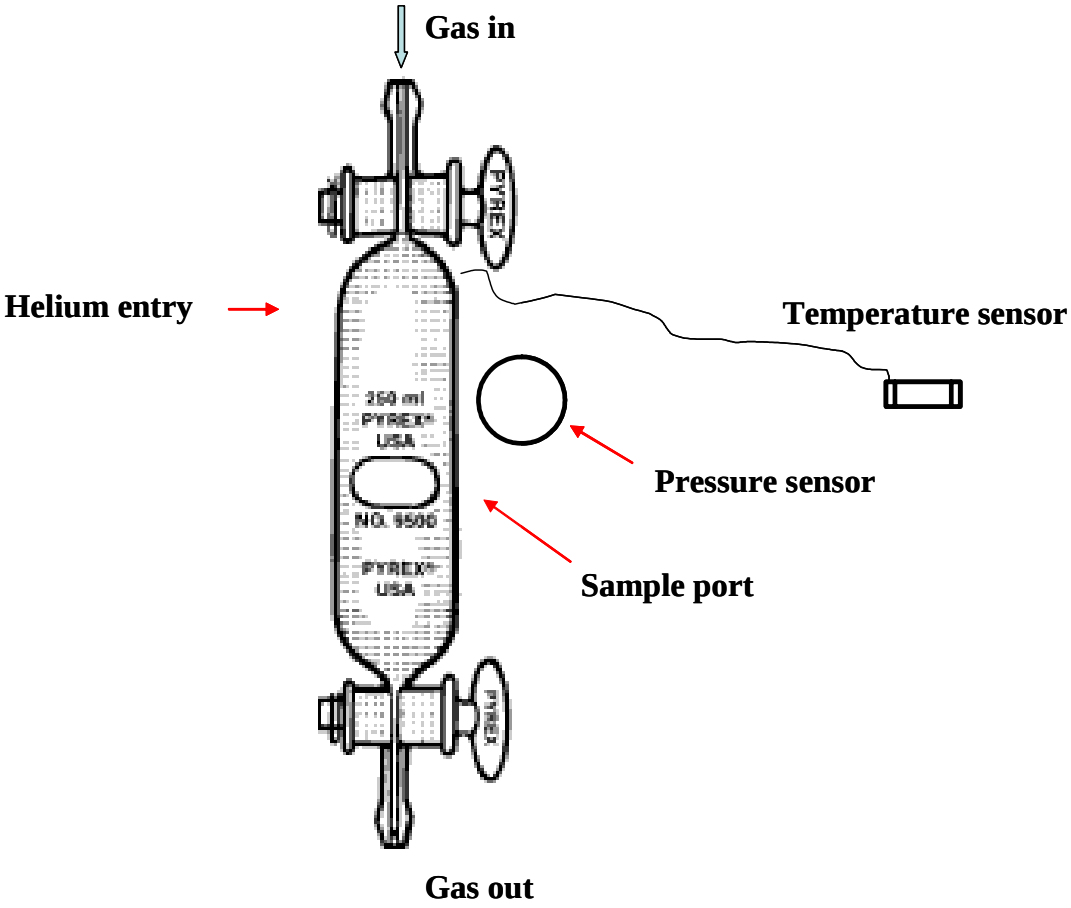

Figure 3.2 Schematic of the exhaust gas sampling bulb

During this interval, the pressure in the bulb decreased, as indicated by the pressure gauge. This was due to: (i) cooling of gases, and (ii) more importantly, condensation of water vapor present in the dryer exhaust. Since our goal was primarily to measure N_2/CO_2 ratio to quantify the excess air in use, no attempts were made to record the pressure (or partial vacuum). Helium gas was injected into the sampling bulb through a rubber septum to bring the pressure back to atmospheric condition. The sampling bulb was now set to collect a sample for injection into the gas chromatograph.

The gas chromatograph (Buck Scientific, Model 910) used for analysis employed a thermal conductivity (TC) detector. It employed dual columns to allow a flat base line, even in the event of a temperature-programmed operation. Helium was used as the carrier gas, at a flow rate of 30 ml/min. The gases CO_2, N_2, and O_2 were separated using a Carbosieve S II column (stainless steel 1/8" tubing, 6 ft long). CO could also be detected, but was never observed in any dryer exhaust samples, indicating complete combustion.

3.4 Results and Discussions

3.4.1 Live Oak/Milstar Plant

Table 3.1 lists the different dryers/tenters investigated at the Live Oak/Milstar Plant, in sequence from the least demanding applications to the most demanding applications. For example, Ranges L1 and L2 represent the least demanding applications, and the

Table 3.1 Characteristics of the different dryers/tenters investigated at the Live Oak/Milstar Plant

Ranges	Products	Comments
L1	Back coating of broadloom carpet	Curing of latex applied as carpet backing; Nylon pile dry
L2	Back coating of broadloom carpet	Curing of latex applied as carpet backing; Nylon pile dry
L3	Broadloom carpet	Flow through drying
L4	Broadloom carpet	Flow through drying
L5	Drying of carpet tile after dyeing/steaming	Nylon pile wet; non-flow through. Possibly most demanding applications
L6	Drying of carpet tile after dyeing/steaming	Nylon pile wet; non-flow through. Possibly most demanding applications

tenter is used for curing of the latex applied as the carpet backing with the Nylon Pile dry; While Ranges L5 and L6 represent the most demanding applications which utilize the impingement drying for impermeable carpet tiles, with the Nylon pile wet after dyeing and steaming. Ranges L3 and L4 represent the intermediate scenario.

With the methodology and the GC-based measurement set-up presented in the preceding section, an assessment of excess air usage and energy losses began at the Live Oak/Milstar Plant. Figure 3.3 shows a gas chromatograph spectrum for the analysis of exhaust gas composition of Range L4. As shown, only O_2, N_2 and CO_2 peaks were observed; no CH_4 and CO peaks showed up, indicating complete combustion. From the previous theoretical calculation, we know that for each mole of methane, the ratio of nitrogen to carbon dioxide equal to 7.52 reflects the stoichiometric value. As shown in Figure 3.3, N_2/CO_2 molar ratio of 75.34 suggests a 902% excess air being used for Range L4.

Figure 3.4 is a summary of the nitrogen to carbon dioxide ratio of all the dryers at the Live Oak/Milstar plant. From the low demanding dryer L1 to the heavy demanding dryer L6, the N_2/CO_2 molar ratio increases from 33 to 375. This trend is as expected because of the increasingly demanding applications. It should be noted that there are 3-5 data points for each dryer, and these points were measured on different days. Thus, Figure 3.4 can be thought of showing some day-to-day process variation. Nevertheless, some general trends are obvious and would be briefly discussed below. For the least demanding applications L1 and L2 used for back coating of the broadloom

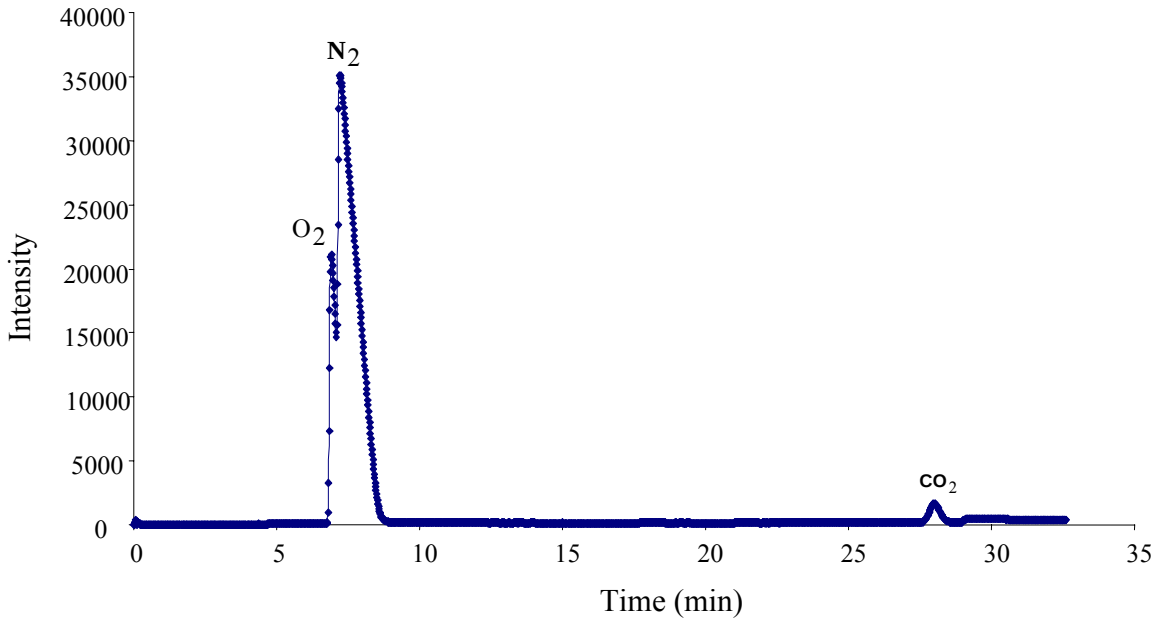

Notes: 1. Carrier gas (He) flows at 30ml/min;
2. GC oven temperature is initially set at 30°C for 3min and then ramps at 5 °C /min to 200 °C.

Figure 3.3 The gas Chromatography spectrum of the exhaust gas of range L4 at Live Oak/Milstar Plant

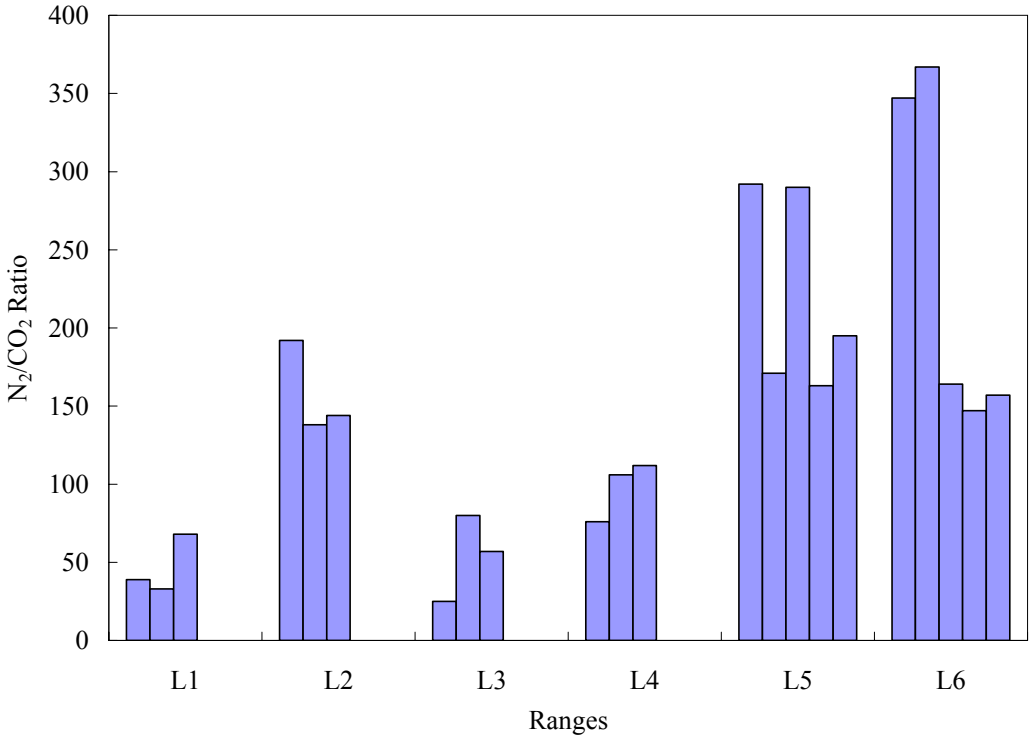

Figure 3.4 Ratios of nitrogen to carbon dioxide in the exhaust gas of dryers/tenters at Live Oak/Milstar Plant

carpet, the products go through the dryers just for curing the latex applied as the carpet backing. For this type of applications, the Nylon pile is dry; so the dryer operation can be considered to be low/medium demand, involving zone I & II (Figure 3.5). So there is not much need to use excess air. But, as seen in Figure 3.4, both ranges are using a large amount of excess air, especially L2. For the medium demanding applications, L3 and L4 represented the flow-through drying of broadloom carpet. For flow-through drying, the dryer operation would lie mostly in the constant drying rate region. The heating process mainly includes zone I and zone II in Figure 3.5. Due to the latent heat associated with water evaporation, the rate of drying is governed by the rate of heat transfer. As will be shown in Chapters VI-VII, zone II represents the case of simultaneous heat and mass transfer. However, the heat requirements are far more due to phase change (latent heat), and thus the limiting process here is heat transfer. Therefore, the drying rate can be enhanced significantly by increasing the gas velocity of circulating air instead of the total amount of air fed in the dryer. However, as shown in Figure 3.4, the amounts of excess air use in L3 and L4 are also very large. Whether the large N_2/CO_2 ratios observed for Range L2 are indicative of inefficient dryer operation or a merely represent an attempt to remove the bottleneck in the speed of Range L2, is not clearly defined. This should be investigated in detail by the production management (and it was not an objective of this study).

For the most demanding applications, dryers L5 and L6 presented the drying of carpet tiles after dyeing/steaming. In this case, the carpet tiles are impermeable and Nylon pile is wet. The drying process includes all the three zones shown in Figure 3.5.

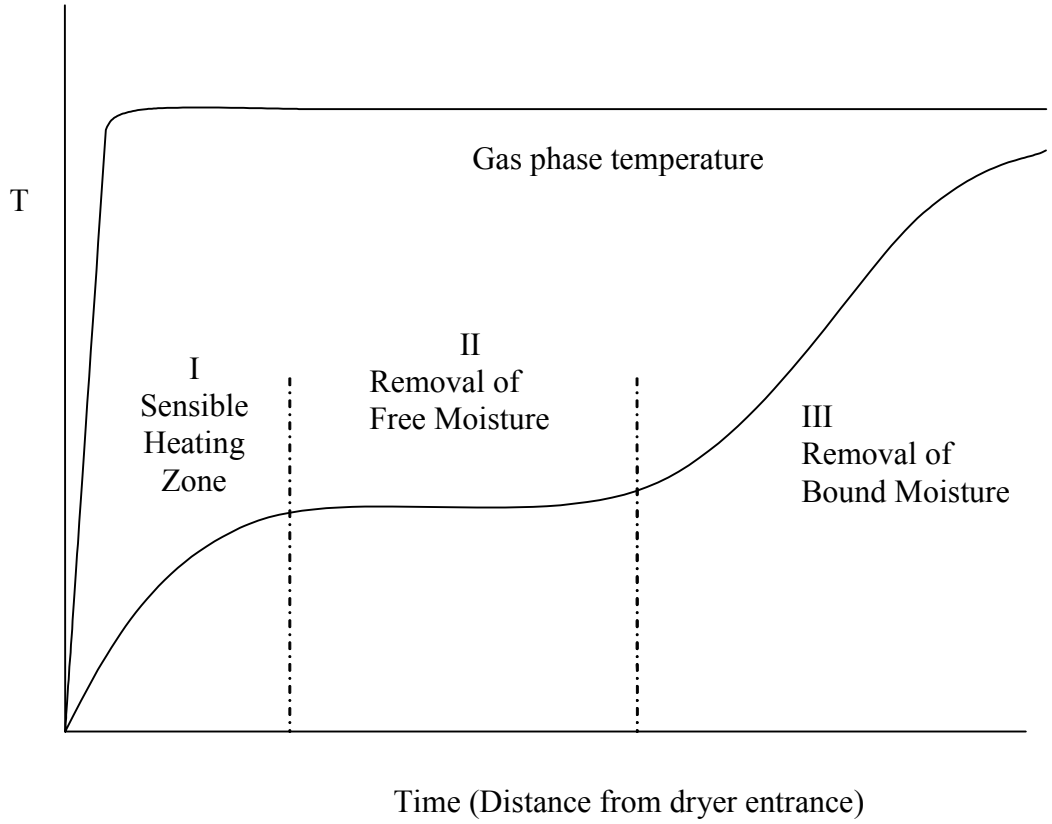

Figure 3.5 Carpet temperature profile in a dryer

Figure 3.4 shows that the amount of excess air used ranged from 1854% to 4890%. It seems that excess air is necessary to keep the moisture content low in order to increase the driving force for the carpet drying. The dryers in Ranges L5 and L6 represent the production bottlenecks and thus there is little interest in saving energy if it would potentially slow down the production. Even so, a quantitative understanding of the role of the moisture content in the dryer gas phase air is needed for justifying the large amount of excess air. This will be addressed in development of mathematical model for carpet tile drying in Chapter V and VII.

Figure 3.6 shows the fuel consumptions of all dryers/tenters. For range L5 and L6, the actual energy consumed is twice higher than theoretical needs. One of the primary causes for energy losses is the large amount of excess air usage, as shown in Figure 3.4. This large amount of excess air requires extra energy to heat it from ambient temperature 70 F to 300-350 F. Most of this sensible heat associated with excess air leaves largely unrecovered in the exhaust (300-350 F). Low/intermediate demanding situations such as L1 and L2 should not require a large amount of excess air, so a more detailed study should be undertaken by plant management. For the high demanding applications such as L5 and L6, large amount of excess air appears needed to accommodate the dryer operation. However, as stated earlier, a quantitative understanding of the drying rate curves is needed to justify the amount of excess air.

Figure 3.7 shows a plot of the concentration of carbon dioxide versus oxygen in the exhaust gas for all data collected at the Live Oak Plant. From theoretical calculation

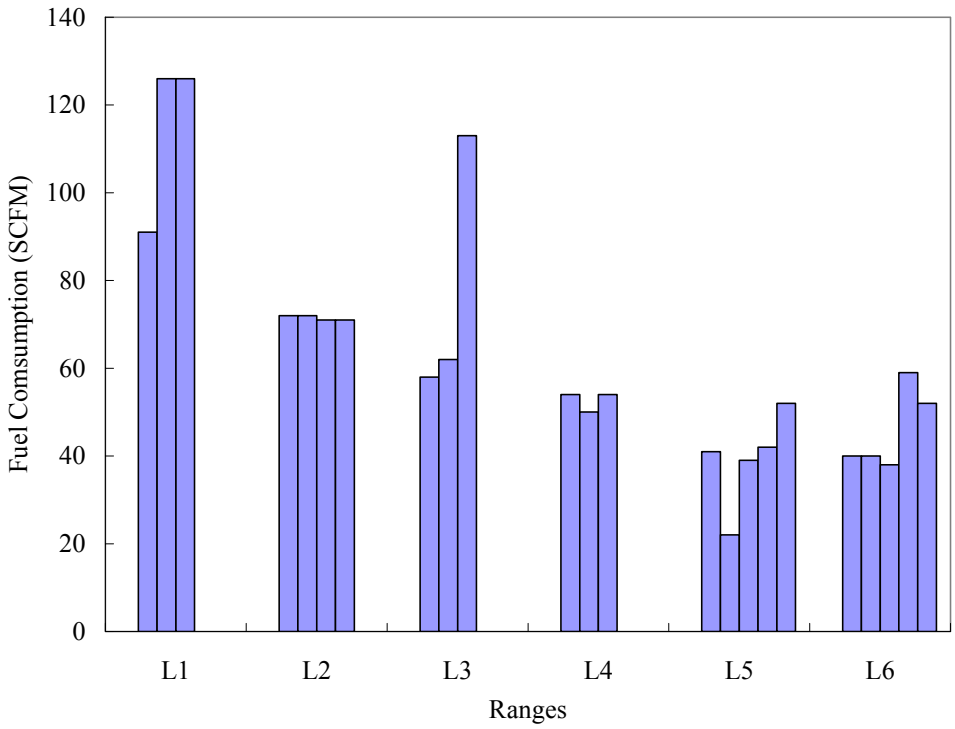

Figure 3.6 Fuel consumptions for different dryers/tenters at Live Oak/Milstar Plant

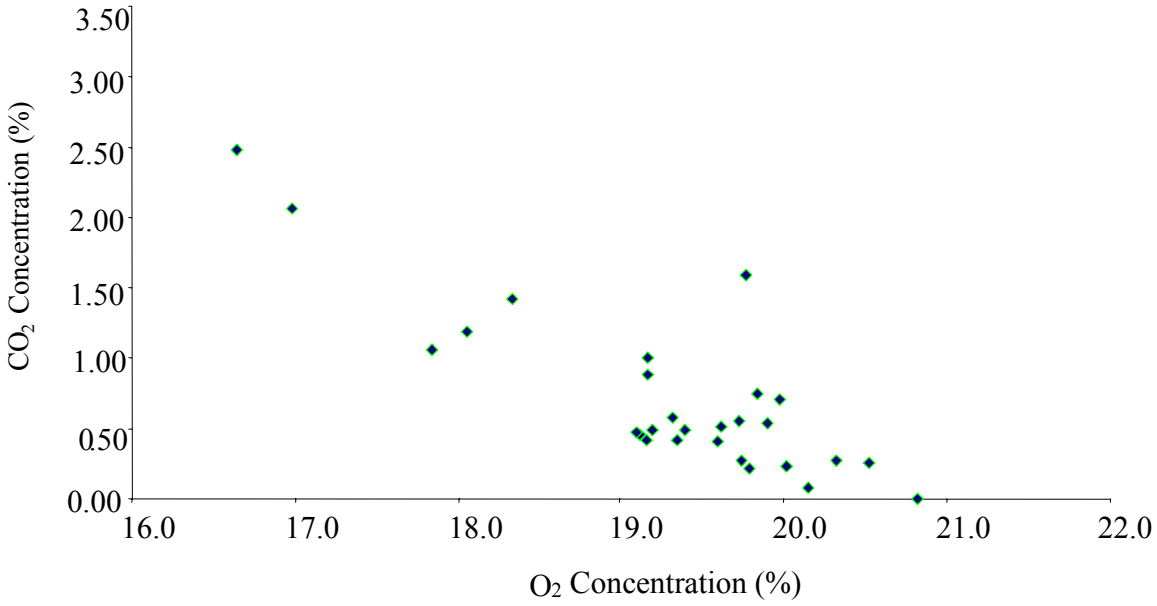

Figure 3.7 Results of carbon dioxide to oxygen ratio for exhaust gas from different ranges of dryers at Live Oak/Milstar Plant

we know that, for complete combustion of natural gas, with zero percent of excess air, the concentration of carbon dioxide would be 11.7%, while the oxygen concentration would be zero. When there is very large amount of excess air, the concentration of oxygen would be approximately 21%, and the concentration of carbon dioxide would be reduced. As seen in Figure 3.6, most of the points are around the lower part of the line (19-21% oxygen). It serves to corroborate that the amount of excess air used in the dryers was very large, which provided verification for the results of the excess air shown in Figure 3.4.

3.4.2 Duncan Stewart Plant

Table 3.2 lists the tenters investigated in Duncan Stewart Plant. For Range D1, the fabrics processed contain a single layer of polyester pile (used in upholstery). While for Range D2, the fabrics are sandwiched form of polyester. Both tenters at the Duncan Stewart plant are used for heat-setting of the fabric; This should represent a zone I operation. Figure 3.8 shows the ratio of N_2/CO_2 in the tenter exhaust gases. It demonstrated that excess air usage in Range D1 for heat-setting of single form polyurethane and Range D2 for heat-setting of sandwiched form of polyurethane are around 1600% and 2400%, respectively. Figure 3.9 represents the fuel consumption on each range. Fuel consumption values for D1 and D2 are around 15 and 30 times those of the theoretical values, respectively. Both ranges of tenters use far more excess air, and as a result, the energy losses are tremendous. It should be noted that heat-setting

Table 3.2 Characteristics of the different tenters investigated at the Duncan Stewart Plant

Ranges	Products	Comments
D1	Single form of Polyester	Heating setting of the fabric
D2	Sandwich form of Polyester	Heating setting of the fabric

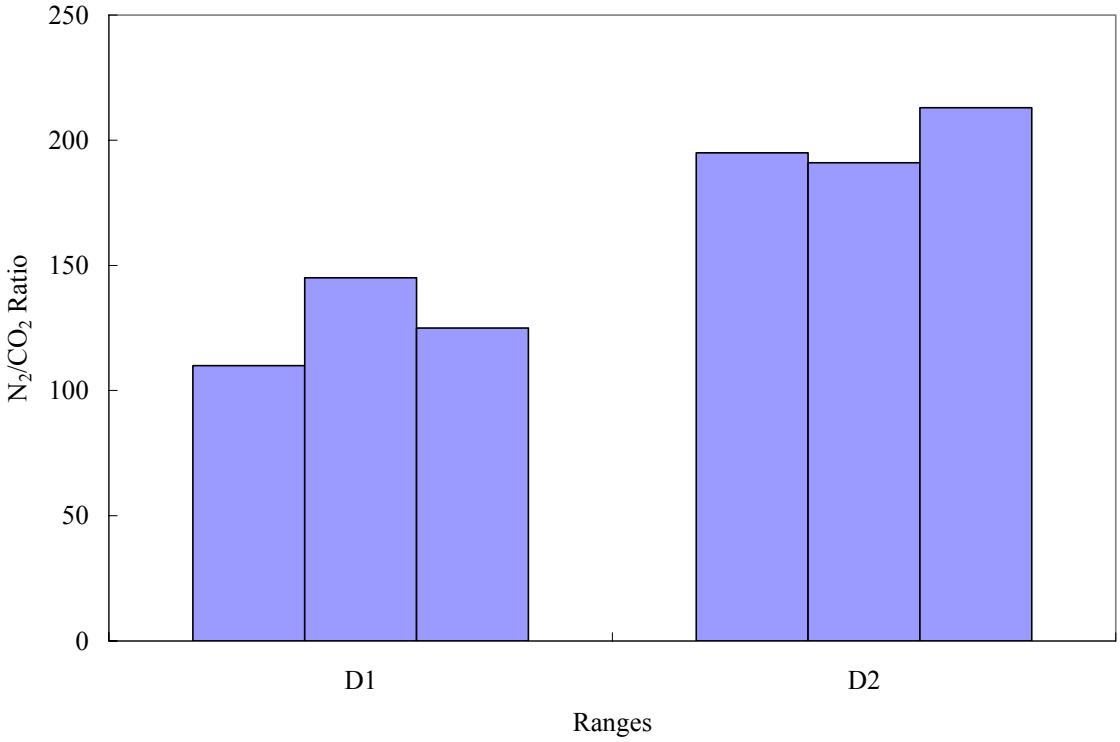

Figure 3.8 Results of nitrogen to carbon dioxide ratio of exhaust gas from different tenters at Duncan Stewart Plant

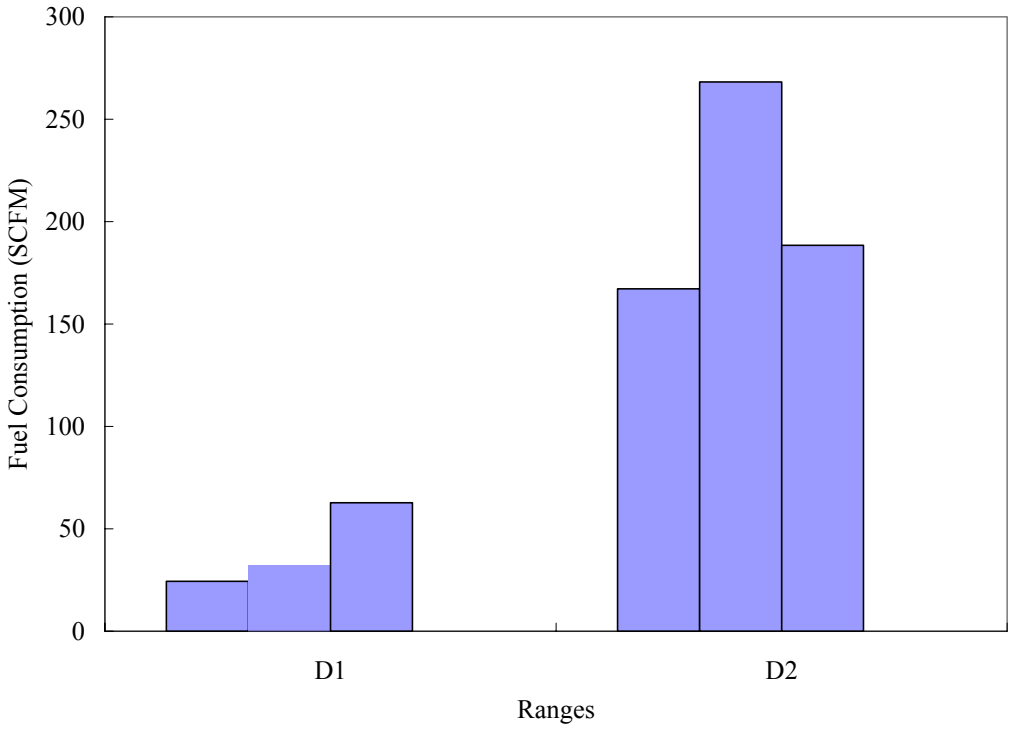

Figure 3.9 Fuel consumptions for different ranges of tenters at Duncan Stewart Plant

process is a zone I operation, and theoretically no excess air is needed. But actually, it utilizes even more excess air than the more demanding situations of carpet drying at Live Oak/Milstar Plant.

The large amount of excess air is apparently justified on the basis of smoke/volatiles being generated due to heat setting. To avoid the smoke/volatiles from coming out the entry/exit slots, a large exhaust fan speed is utilized. Further investigation into the tenter heat-setting system revealed some details explaining the usage of excess air and energy loss. The structure of the tenter exhaust system is shown in Figure 3.10. Air flow in the system is mainly controlled by the damper settings and the roof exhaust fans. Currently the exhaust fan runs at its greatest capacity which causes high pressure differential for the excess air to enter the tenter. The dampers are either fully open or half open, allowing more air to go into the tenter. In addition, for Range D1, excess air can also enter the tenters through the 15 open windows (14'×10') on both sides of the tenter. For tenter D2, at the exit of the tenter, a smoke fan was used to get rid of the smell from the fabrics coming out of the high temperature tenter, which was also a major source of excess air.

3.5 Conclusions

From the energy balance calculations and experimental measurements of exhaust gas, it has been shown that, for the heat setting of fabrics in Duncan Stewart Plant, the excess air usage is up to 2400% resulting in up to 95% of the energy being

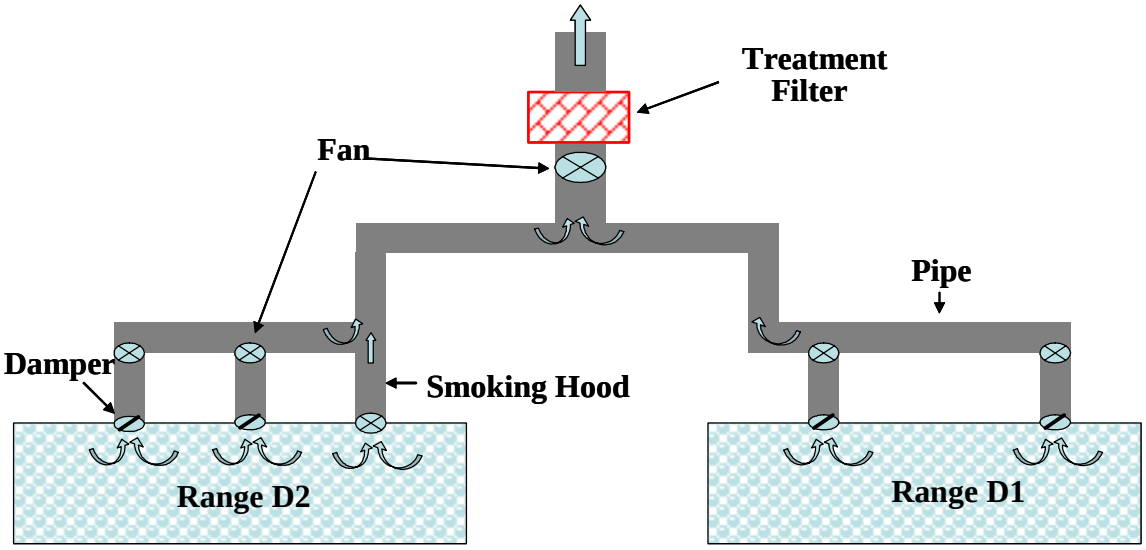

Figure 3.10 Schematic of the flow systems of the tenters

wasted. Analysis of the fabric heat-setting revealed that there are multiple unintended sources of excess air, such as the exhaust fan, the damper settings, cooling fan, and the smoking hood. The large amount of excess air is justified on the basis of the smoke/volatilization being generated due to heat setting. A more efficient flow system is needed. Energy savings could be realized by reducing the excess air.

For the demanding application in Live Oak/Milstar Plant, large amount of excess air appears needed to accommodate the dryer operation. Ranges L5 and L6 represent the most demanding applications, followed by Ranges L3 and L4, and finally, Ranges L1 and L2 represent relatively low demanding applications. For these demanding situations (L5 and L6), excess air seems necessary to keep low moisture level in the drying air in order to maintain a high driving force. However, better understanding of the drying rate curves is still needed to justify this. Quantitative understanding of the drying characteristics through mathematical drying model will be presented in the following chapters. Next chapter describes the experimental set-up for obtaining drying rate curves.

CHAPTER IV

EXPERIMENTAL SET-UP

As stated in the previous chapter, a large amount of excess air and energy are wasted in the dryer operations. Optimization of the operations requires a quantitative understanding of drying characteristics and the role of various operating parameters. Drying rate curves were defined previously in Figures 2.2 and 2.3 respectively. To obtain these curves, it is necessary to have a well-characterized gas-phase temperature and gas-phase moisture content. In addition, one needs to be able to follow in real time the carpet moisture content. It should be obvious that it is not possible to obtain these results in a production dryer. Firstly, there are ten zones in a typical industrial dryer, each zone having an independent fuel burner and temperature control system. Since different amounts of water will be removed in each zone, the gas-phase moisture level would also vary from zone to zone. Secondly, it is not possible to monitor the moisture content of the carpet as it moves through the dryer zones. Only the end result (last zone of the dryer) is a measurable quantity. Hence, an alternate approach is necessary.

A bench scale dryer simulating system was set up in the School of Chemical Engineering at Ga Tech in order to measure the drying rate curves for carpet tiles, and to use these data to determine the model parameters such as transport properties and critical moisture content. The experimental set-up was built in order to obtain drying

curves at several different temperatures. In this way, the dependence of model parameters on temperature would be well-defined, and then model could be applied to an industrial dryer where the temperature changes from one zone to the next. Three different types of carpets tiles were tested, each at three different temperatures, to determine the drying characteristics. Below is a description of the experimental set-up, instruments, and testing procedures.

4.1 Experimental Set-up

Experimental set-up consisted of three main components: an oven, an electronic balance, and a PC-based data acquisition software. A schematic of the set-up is illustrated in Figure 4.1. The oven is a Cole Parmer laboratory oven (model number G05053-10), which can be heated to a temperature of 220^{o}C (with an accuracy of 1^{o}C). A sample holder frame was constructed to hold the carpet tile sample (7"×4"). The electronics balance (Denver Instrument, Model number APX-4001) was placed on top of the oven. The sample holder was suspended into the oven through the two holes drilled in the top surface of the oven, such that the sample holder rested on top of the electronic balance. The electronic balance has a load capacity of 4000 g ± 0.1 g. The software used for data acquisition was Balance Talk XL Version 5.0 through RS232 connections (Labtronics Inc.). The air was supplied by Airgas Company. The gas flow was controlled by AALBORG mass flow controller with capacity up to 500 ml/min.

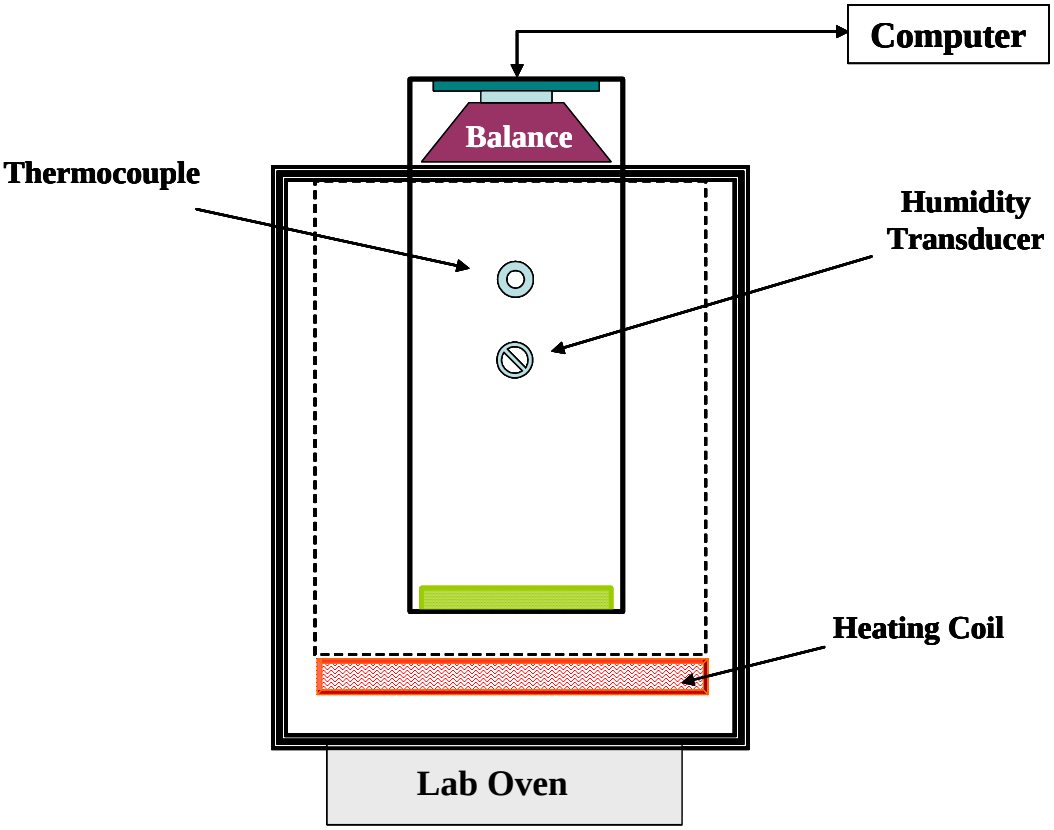

Figure 4.1 Experimental set-up for drying curve measurement under bench scale oven conditions

Extra precautions were taken to design the air flow configuration so that vibrations and fluctuations in the measurement of the carpet tile weight change were minimized. As a result, the air flow was diverted away from the sample. Oven conditions such as temperature and humidity are very important in the drying process. Both parameters were continuously monitored with time during the experiments. Oven chamber humidity was measured by a transducer (Ohmic Instruments Co., model AHT-200-01) with working temperature range up to 200^{o}C. The oven temperature was measured by a K-type thermocouple with an accuracy up to ±0.1^{o}C inserted close to the sample. The drying experiments were carried out at constant temperatures; three different temperatures were utilized 100 ^{o}C, 120 ^{o}C, 140 ^{o}C.

4.2 Sample Preparations

The carpet samples used in this study were tufted carpet tiles produced by the Milliken & Company in LaGrange, Georgia. Three different types of carpet tiles were investigated: Roadrunner (RR), Midnight Sparkle (MS), and Grand Plaza (GP). Among them, RR and MS are loop piles, and GP is cut pile. Prior to experiment, an 18"×18" tile was cut into 7"×4" pieces using a band saw. The moisture content is defined as the ratio of the weight of water to the weight of the dry nylon pile on top of the carpet surface. The initial moisture content was kept at about 200%, which is close to the conditions used at Milliken manufacturing site. After weighing dry sample, desired amount of moisture was sprayed, and the wet sample was weighed again. It was then

placed in the sample holder in the preheated oven to begin the drying rate curve measurements.

4.3 Experimental Method

Critical operating variables were strictly controlled and monitored in order to duplicate the same conditions in each laboratory test. These variables include the oven temperature, initial water moisture content of the carpet tile, and the oven humidity. The oven scale was tared to zero and calibrated before each series of experimental tests. The oven was set at a predetermined operating temperature and allowed at least 30 minutes for stabilization prior to each run. The oven temperature in this study ranged from 100 ^{o}C to 120 ^{o}C (212 F to 284 F) to obtain a reasonably wide drying range for each type of carpet. Besides, this temperature range was chosen to cover the temperatures used in various zones of the tile dryer. This would help in the model validation and parametric analysis later on. Each drying curve was generated at isothermal conditions. Air flows into the oven at the flow rate of 500 ml/min. The gas flow avoids direct impact on the sample in order to minimize vibrations. There were two other reasons for having a well-defined air flow rate and direction. First, to sweep the oven chamber at a uniform rate to maintain gas-phase moisture level. Second, more importantly, to have the same convective heat transfer coefficient at a given temperature. Meanwhile, the carpet tiles were sprayed with a specified amount of water on the surface of the carpet. Extra precaution was taken to ensure uniform distribution of water, intended to simulate the

industrial conditions. Then the wet sample was inserted into the oven, and the data collection program was initiated. Weight of the carpet tile, oven temperature and humidity were monitored and recorded during the experiment. When the weight of the carpet tile no longer changed for about three minutes, the experiment was stopped. The sample could be considered "dry" at this point.

Figure 4.2 shows a typical sample weight versus time plot for one of the tests. This data was analyzed using the Origin Lab spreadsheet to determine the moisture content and drying rates. Typically, plots of oven humidity versus time, moisture content evolution, drying rate versus moisture content, and drying rate versus time are generated. Critical parameters were also determined by model fitting, including the critical moisture content, the heat and mass transfer coefficients, and the diffusion coefficient. These details will be presented in Chapter VI.

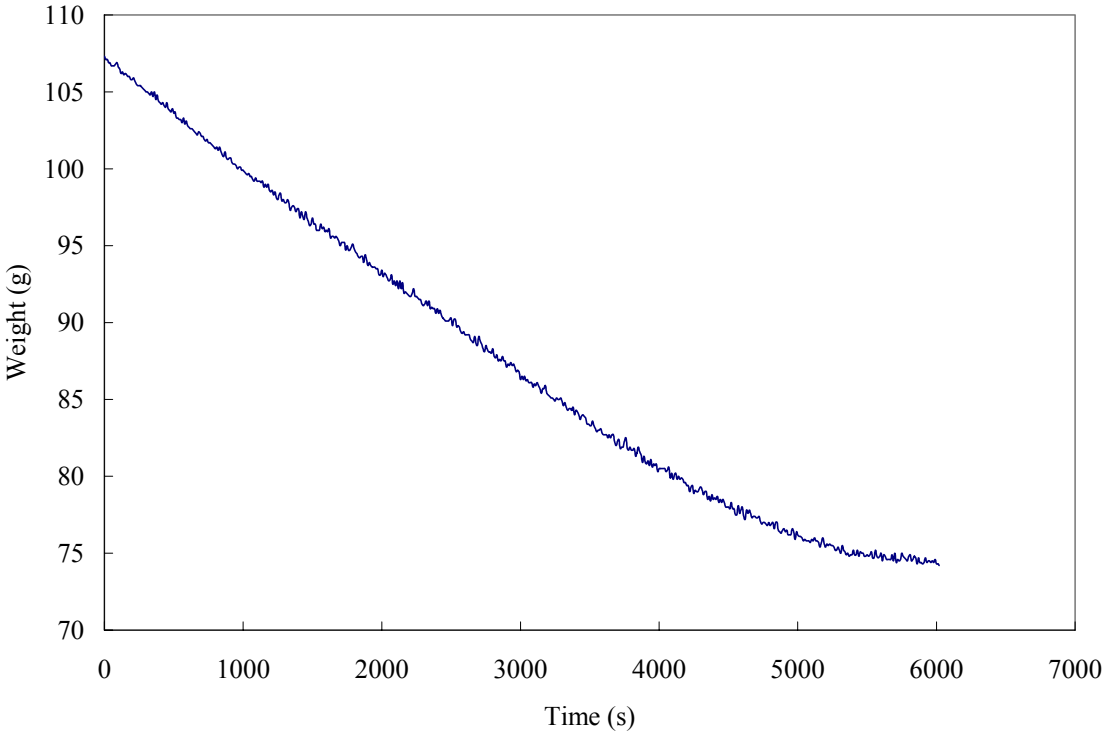

Figure 4.2 Weight change as a function of time for carpet Midnight Sparkle drying at 120^{o}C

CHAPTER V

MATHEMATICAL MODELLING

5.1 Introduction

As stated in Chapter III, carpet tile drying represents demanding situations where dryer operation is limiting the production rate, and a large amount of excess air is used. The primary cause of this is a lack of understanding the drying rate curves. The role of various operating parameters that affect the drying rate is not well quantified, and it leads one to choose far more conservative dryer operational parameters than would be needed. A significant portion of the drying may occur in the falling rate region, and diffusion of moisture through the porous fiber may control the drying rate. Excess air may be essential for providing the necessary driving force for moisture transport. Thus the drying rate curves for such demanding situations are needed before the task of optimizing dryer performance can be undertaken.

A mathematical model is developed below to simulate the mass and heat transfer processes that occur during carpet tile drying. A brief review of various mathematical models to describe the drying operations in general, and textile tenters in particular, was presented in Chapter II. The goal of present study is to develop a model that can quantitatively describe the evolution of transient temperature and moisture content profiles in a carpet tile. In order for a mathematical model to have predictive ability, it

should be based on the physical features observed in specific applications. Another desirable characteristic would be to have a model where all or most of the model parameters could be determined from independent experiments. Below, an initial attempt is made to examine the physical characteristics of the carpet tile drying. This shall include a time-temperature profile in an industrial dryer as well as scanning electron microscopy (SEM) results from the tile cross-section. Other pertinent features will also be discussed. This would then be followed by model development.

5.2 Tile Drying-Physical Characteristics

Figure 5.1 shows a schematic of the carpet tile cross-section. The moisture in a wet carpet tile resides in the nylon pile as well as in the region jointly occupied by the primary backing, latex coating, and the nylon fibers near the primary backing layer. The hot melt layer is known to be impermeable and does not retain any moisture. The polyurethane foam layer also does not contain any open cells. This has been experimentally confirmed to be the case. Figure 5.2 shows an SEM image of the cross-section of the tile layer. The thickness of hot melt layer is ~400 μm (16 mils). The thickness of the space that is occupied jointly by the primary backing and latex may be considered to be ~500 μm (20 mils). A clear boundary exists between the primary backing/Latex layer and the hot melt layer. The hot melt layer is impermeable to water preventing the moisture from diffusing into the inner layers. Moreover there is almost

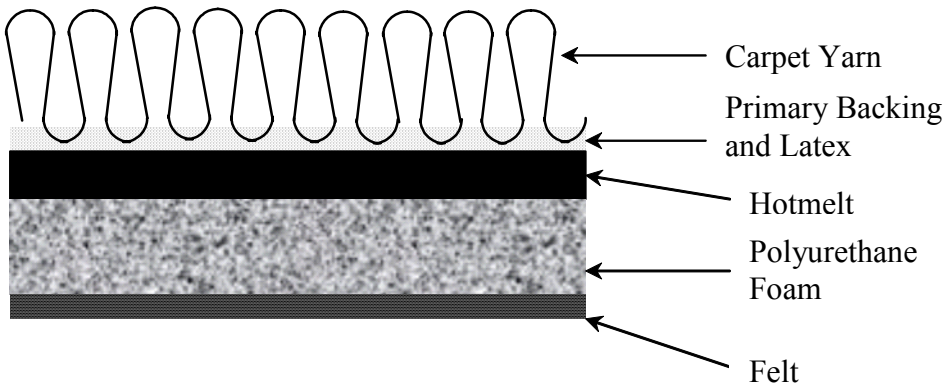

Figure 5.1 A schematic of the carpet tile cross section

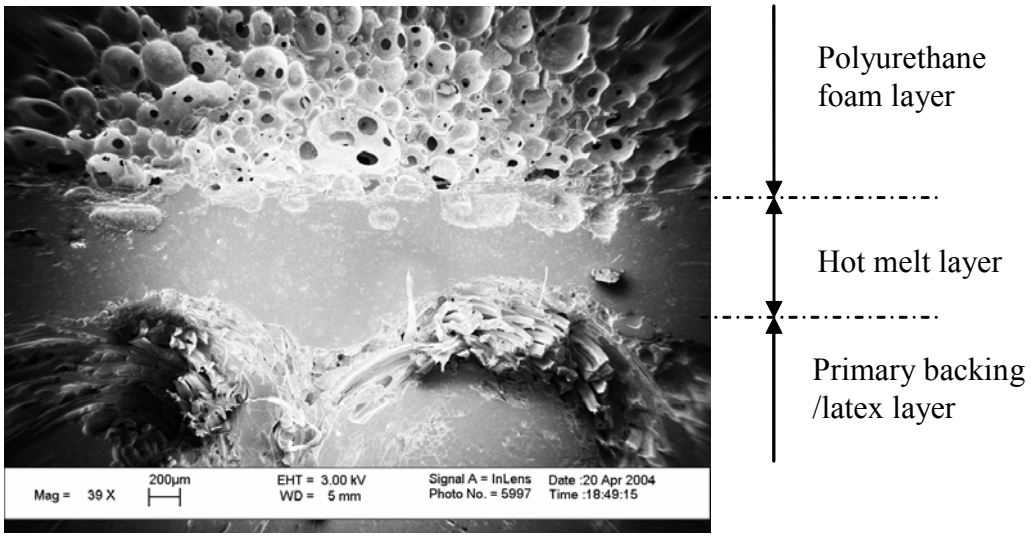

Figure 5.2 The SEM picture showing the cross sections of the different layers in a carpet tile

no nylon fiber below binder of the primary backing and, as a result, little or no moisture can be expected to reside beyond the primary backing layer. Besides microstructure analysis a series of water adsorption experiments were reported in the literature confirms this picture. Solis[39] conducted experiments on the moisture distribution in the different layers of carpet tiles. Samples with and without the nylon fiber layer were submerged in a known quantity of water for a period of time, after which the water was reweighed to estimate the amount adsorbed on the carpet. The results show that the carpet tile with the fiber layer adsorbed 3 to 4 times more water than the samples without the nylon fiber, which agrees well with the industrial carpet manufacturer's claims that nylon pile usually adsorbs seventy to eighty percent of the total moisture in the whole carpet tile. Given these results and the fact that the backing's exposed surface area is very small, it was concluded that the amount of moisture that could be absorbed into the inner layers was very small. Beckham and Carr[40] showed from MRI results, that the water resides nearly exclusively within the fiber loops of the pile, with little in the binder or backing region.

Three different carpet tile products were examined in present study: (i) Roadrunner (RR), (ii) Midnight Sparkle (MS), and (iii) Grand Plaza (GP). Table 5.1 summarizes the key distinguishing features of these three products (all manufactured by the Milliken & Co.).

Figure 5.3 shows the micrographs of the nylon filaments used in these three different products. In summary, trilobe Nylon filament is used in each product, but

Table 5.1 Pile type and Nylon pile weight of the three carpet tiles: Roadrunner, Midnight Sparkle, and Grand Plaza

Product	Pile type	Nylon pile weight (oz/yd^2)
Roadrunner (RR)	Loop pile	21
Midnight Sparkle (MS)	Loop pile	26
Grand Plaza (GP)	Cut-pile	40

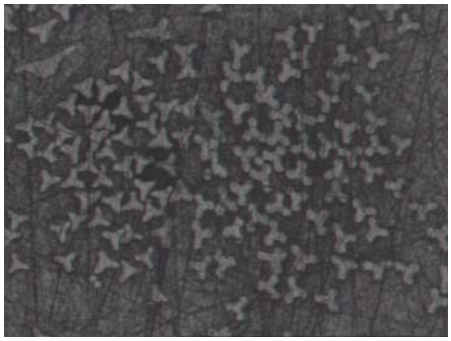

(a)

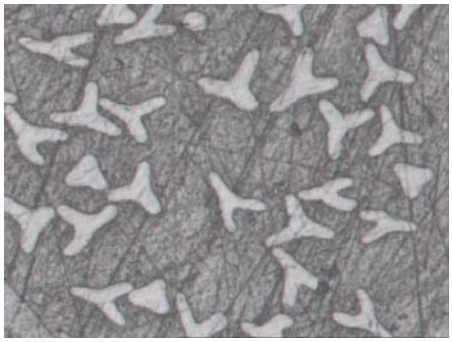

(b)

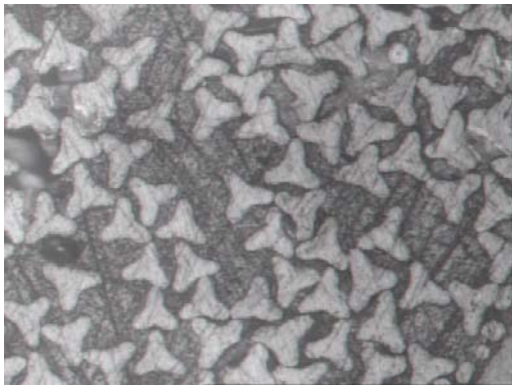

(c)

Figure 5.3 Cross-section of the Nylon fiber of three different carpet tiles: (a) Roadrunner; (b) Grand Plaza; (c) Midnight Sparkle

slight variations in the filament cross-sections exist. Even so, the effective diameter of the nylon filament may be taken as 40~50 μm. The space between these fibers is of the same magnitude. Both cut pile and loop pile products show dimensions of similar magnitude. Most of the work has been done with Roadrunner tile products, in terms of model validation. However, laboratories studies were conducted on all three tile products.

Figure 5.4 shows a typical temperature profile for tile drying as the tile moves through the dryer. Upper line in Figure 5.4 shows the gas-phase temperature, whereas the lower line shows the temperature as measured using a thermocouple inserted between the hot melt layer and the latex layer. The profile shown in Figure 5.4 is for the tile product RR, but qualitatively similar profiles are observed for the other products as well. Briefly, the Nylon pile temperature rises quickly as the tile enters the dryer. It quickly reaches a plateau (near 140 F) and stays at that temperature for about 2-3 zones. This period can be called the constant drying rate period, where the free moisture evaporates from the Nylon pile surface. As surface moisture evaporates, more moisture readily moves to the surface to replenish the evaporating moisture. The temperature of Nylon pile (~140 F) is said to represent the wet bulb temperature. Most of the heat supplied in the first three zones (~30 ft) is used up as latent heat for water evaporation. Near the end of the third zone, the Nylon pile temperature begins to rise. This is obvious because the evaporation rate has begun to decrease and some of the heat supplied is being used to provide sensible heating of the Nylon pile. The falling rate period may be described by diffusion of water vapor through the nylon pile or/and through the

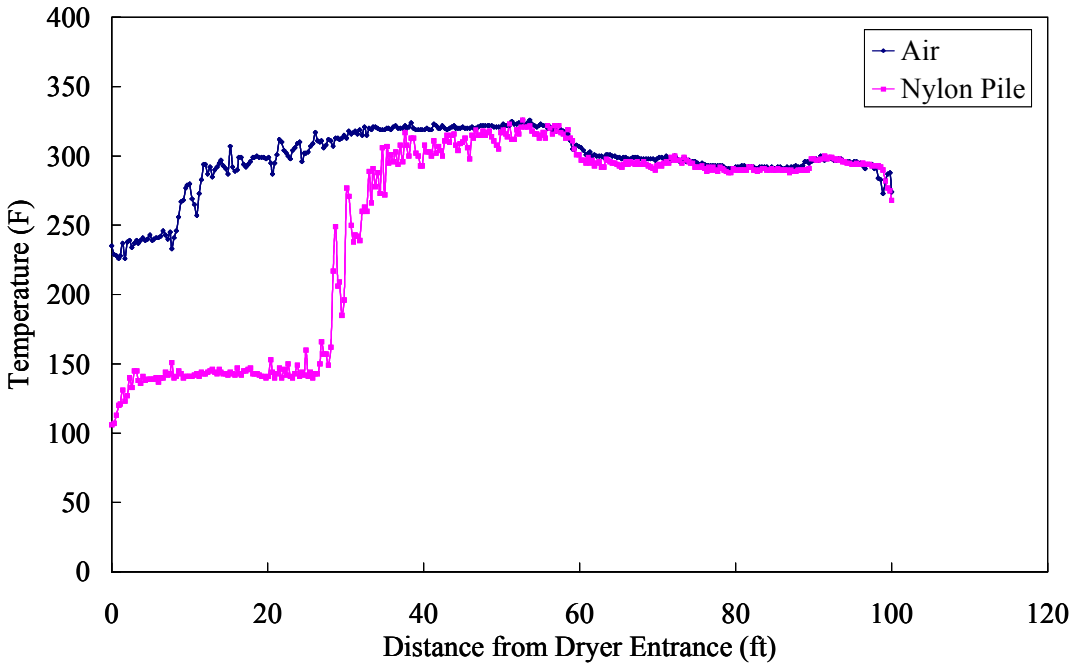

Figure 5.4 Temperature profile of carpet tile Roadrunner during industrial drying process

interface of latex and primary backing. Generally this is referred to as bound moisture removal. Therefore, the model developed in this study incorporates these two drying modes.

5.3 Model Development

A typical drying curve consists of a constant drying rate period and a falling drying rate period. During the constant drying rate period, the rate of moisture migration from the interior of the materials to surface is sufficiently high to keep the surface saturated. As a result, the surface water evaporation is the rate-limiting step. The constant drying rate is controlled by the simultaneous heat and mass transfer via convection mechanism on surface. The constant drying rate period ends when the moisture level in the nylon pile has dropped to a value referred to as the critical moisture content. This point indicates the start of the falling drying rate period. In this period, the drying rate is mainly determined by the moisture diffusion.

A one-dimensional model of mass and heat transfer within the nylon pile is developed in this section. Macroscopic equations governing conservation, simultaneous heat and mass transfer are developed for the constant and falling rate periods separately.

The following assumptions are made:

1) Mass and heat transfer are one dimensional processes.
2) The material is homogeneous along the moisture migration direction.

3) Temperature and humidity of the drying air are constant in time.
4) Carpet and moisture are at the same temperature at all times (lumped parameter approach).
5) The thermo-physical properties of the fiber are constant during the entire drying process.
6) The change in dimensions of the carpet tile during the drying process is neglected
7) Enthalpies of the liquid and carpet are a linear function of temperature
8) No chemical reactions occur during drying

5.4 Governing Equations for the Constant Drying Rate Period

The constant rate drying period is characterized by having the same evaporation rate throughout the period. It is physically characterized by a thin film or pool of unbound water at the solid's surface. When the porous solid is exposed to a drying stream such as air, evaporation will occur at a constant rate such that the heat transferred to the surface equals the latent heat of vaporization. Consequently, the temperature remains constant in this region. In this regime, the water within the nylon fibers moves readily to the surface to keep it wet.

5.4.1 Mass Balance

For the constant drying rate period, it is generally assumed that the resistance to the mass transfer is within the boundary layer between the air and the drying surface. The mass transfer rate is governed by the driving force for water vapor between the nylon-air interface (y) and the air (y_a):

$$N_c = k_y(y - y_a) \qquad (5.1)$$

where k_y is the convective mass transfer coefficient (lb moles water/ft^2-hr).

y is the water vapor mole fraction at the surface of the Nylon pile which remains constant in the constant drying rate period. It is only a function of Nylon temperature and can be calculated by the following equation:

$$y = \frac{P^*}{P_a} \qquad (5.2)$$

Where P_a is the atmospheric pressure; P* is the vapor pressure of water at the Nylon pile temperature. The correlation between the saturation pressure P* and the temperature T is given by Antoine equation[41] :

$$\log P^* = A - \frac{B}{(T + C)} \qquad (5.3)$$

P* is in mmHg; T in ^oC; A, B, C are constants.

y_a is the mole fraction of water vapor in the drying air.

From Equation (5.1), the evaporation rate for the constant drying rate period is derived as follows:

$$-m_f \frac{dw}{dt} = k_c C M_w (y - y_a) \qquad (5.4)$$

where m_f is Nylon pile weight (lb/ft^2); w is moisture content of Nylon pile or the wet pick-up (lb H_2O/lb Nylon); k_c is the convective mass transfer coefficient (ft/hr). C is gas phase concentration (lb moles/ft^3), defined by the following equation:

$$C = \frac{P}{RT} \qquad (5.5)$$

Where R is the universal gas constant; P and T denote the pressure and temperature, respectively.

For the mass and heat transfer coefficients, Treybal[42] has indicated that the coefficients are constant as long as the velocity and flow direction of the drying air are constant. The mass transfer coefficient can be correlated to convective heat transfer coefficient by Chilton-Colburn analogy, which is based on the thermal boundary layer and the concentration boundary layer analysis, and the heat and mass analogy[43]. The ratio of the convective heat transfer coefficient to the mass transfer coefficient may be expressed as,

$$\frac{k_c}{h} = \frac{1}{\rho C_p}\left(\frac{\mathrm{Pr}}{Sc}\right)^{2/3} \qquad (5.6)$$

Where ρ is the density (lb/ft3); C_p is the specific heat capacity (BTU/lb-F); Sc is the Schmidt number; Pr is the Prandtl number; and h is the convective heat transfer coefficient (BTU/hr-ft^2-F).

The moisture content of the carpet tile is defined as the ratio of the weight of water in the Nylon fiber to the dry weight of the Nylon fiber as follows:

$$w = \frac{m_w}{m_f} \qquad (5.7)$$

Where w is the moisture content (also called wet pick-up), m_w is the weight of water; and m_f is the weight of the dry Nylon fiber.

5.4.2 Energy Balance

The modeling work of heat balance takes the approach of a lumped parameter analysis. The heat transfer resistance to conduction within the carpet tiles is neglected, and all layers were assumed to be at the same temperature. This lumped parameter analysis yields a negligible error when the Biot number is small (Bi<0.1).

$$Bi = \frac{hl}{k} \qquad (5.8)$$

Parameters h, k, and l stand for the convection heat transfer coefficient, thermal conductivity, and characteristic length, respectively. The characteristic length turns out to be half of the thickness of the carpet tile. The Biot number is seen to be the ratio of *l/k*, the internal conductive resistance to heat transfer, to *1/h*, the external convective

resistance to heat transfer. Biot number is a good indicator of judging which resistance, convection or conduction, dominates. A large Biot number indicates that the conductive resistance controls, i.e., it is easier for heat to leave the surface by convection than to reach it by conduction. Under this condition, large temperature gradients within the solid exist. A small Biot number represents the case where conduction resistance is negligible and the temperature gradient within the solid is quite small. This forms the basic assumption for the lumped-parameter analysis. Biot numbers were calculated for the carpet tile to be 0.13, close enough to assume that all internal layers have the same temperature, and convection resistance dominates the drying process. The purpose of this assumption was to simplify the resulting heat transfer equations by leaving the derivatives of temperature only with respect to time.

The equation for energy balance is based on the first law of thermodynamics, with the following form,

$$Q - W = \frac{dE}{dt} \qquad (5.9)$$

Where the work, W, is zero. The energy balance is written as,

$$E = m_f U_f + m_w U_w \qquad (5.10)$$

Taking derivative of the internal energy with respect to time, the following equation is obtained,

$$\frac{dE}{dt} = m_f \frac{dU_f}{dt} + \frac{d(m_w U_w)}{dt} \qquad (5.11)$$

The internal energy U is a linear function of temperature, established by the well-known thermodynamic relation[44]. The temperature in the square bracket of the following equation is the temperature at which the properties are evaluated.

$$U_f[T_f] = Cp_f(T_f - T_{ref}) + U_f[T_{ref}] \qquad (5.12)$$

Where the specific heat capacity of the carpet tile, Cp_f, is assumed to be constant[45] (Cp_f= 0.35 BTU/lb-F).

From Equation (5.12), the derivative of energy with respect to time can be obtained as,

$$\frac{dU_f}{dt} = Cp_f \frac{dT_f}{dt} \qquad (5.13)$$

Similarly, the energy of the water present in the carpet tile is

$$U_w[T_w] = Cp_w(T_w - T_{ref}) + U_w[T_{ref}] \qquad (5.14)$$

Since the variation of the liquid water specific heat with temperature is small, it is assumed to be constant (Cp_w = 1 BTU/lb-F) in this study.

The derivative of the energy in water with time is,

$$\frac{d(m_w U_w)}{dt} = m_w \frac{dU_w}{dt} + U_w \frac{dm_w}{dt} \qquad (5.15)$$

The derivative of mass of water with respect to time t is expressed as following:

$$\frac{dm_w}{dt} = m_f \frac{dw}{dt} \qquad (5.16)$$

By substituting Equations (5.13), (5.15) and (5.16) into Equation (5.11), the following equation can be obtained,

$$\frac{dE}{dt} = m_f Cp_f \frac{dT_f}{dt} + m_f wCp_w \frac{dT_w}{dt} + m_f \frac{dw}{dt}\left(Cp_w\left(T_w - T_{ref}\right) + U_w\left[T_{ref}\right]\right) \quad (5.17)$$

It is assumed that the temperature distribution in carpet tile is uniform with time and that the water temperature is equal to the fiber temperature (i.e. $T_w = T_f$). This assumption allows the carpet tile to be represented by a single uniform temperature T. So Equation (5.17) can be simplified as

$$\frac{dE}{dt} = (m_f Cp_f + m_f wCp_w)\frac{dT}{dt} + m_f \frac{dw}{dt}\left(Cp_w\left(T_w - T_{ref}\right) + U_w\left[T_{ref}\right]\right) \quad (5.18)$$

The heat input to the carpet tile is written as follows:

$$Q = h(T_a - T) + N\left(H_v + Cp_w\left(T_w - T_{ref}\right) + H_w\left[T_{ref}\right]\right) \quad (5.19)$$

Where N is the water evaporate rate

$$N = m_f \frac{dw}{dt} \qquad (5.20)$$

The first term on the right hand side in Equation (5.19) contains convection heat transfer from the air. The latent heat term is included due to the water evaporation as the drying proceeds. The enthalpy and internal energy of water are based on a reference temperature of 32 F. Additionally, at this temperature, it is assumed that value of the following item is small and can be neglected:

$$H_w\lfloor T_{ref} \rfloor - U_w\lfloor T_{ref} \rfloor = PV \approx 0 \qquad (5.21)$$

Substitute Equations (5.18) and (5.19) into Equation (5.9), the governing differential equation for heat transport in the carpet tile becomes:

$$-H_v m_f \frac{dw}{dt} + \left(m_f Cp_f + m_f wCp_w\right)\frac{dT}{dt} = h\left(T_a - T\right) \qquad (5.22)$$

Where h is the convective heat transfer coefficient. The general relationship between the convective heat transfer coefficient h and the mass transfer coefficient k_c has been discussed earlier.

5.5 Governing Equations for the Falling Drying Rate Period

When the moisture content in the carpet reaches the critical moisture content, w_c, the drying process enters the so called falling rate regime. During this period, the rate of moisture movement from the interior of Nylon pile to the pile surface begins to decrease; dry spots begin to appear on the solid surface as the moisture evaporation front recedes into the carpet tile. As the evaporation front continues to retreat into the porous medium, the liquid concentration behind the evaporation front remains almost constant. The driving force for this moisture diffusion lies entirely between this evaporation front and the Nylon pile surface.

5.5.1 Mass Balance

Figure 5-5 is a schematic representation of the moving evaporation front during the carpet drying process. Above the evaporation front, there is no liquid. Mass transport takes place by vapor diffusion from the evaporation front, situated at x^*, to the pile surface (x=0). Below the evaporation front, the liquid phase is continuous. Thus the

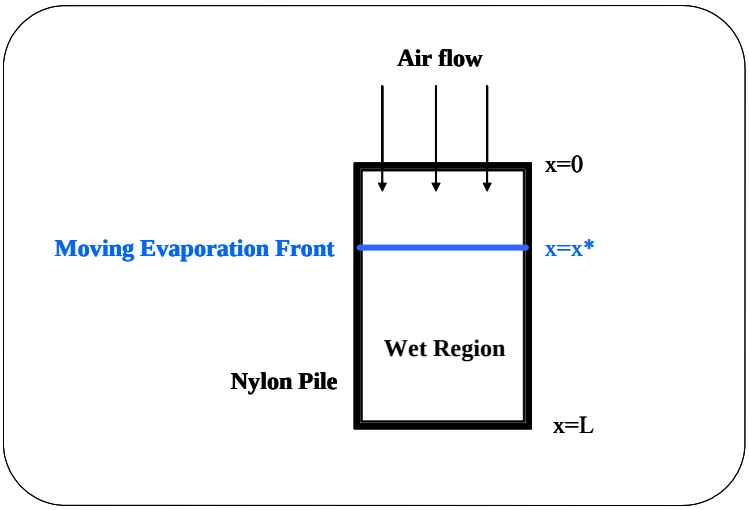

Figure 5.5 Schematic of the submerged evaporation front model

drying rate is determined by the resistance to vapor diffusion from the evaporation front to the pile surface. The length of this diffusion path (x*) increases with time.

It is assumed in our model that the total moisture content in the carpet (w) is related to the depth (x*) of the moving evaporation front. Their relationship can be represented by the following equation:

$$\frac{x^*}{L} = 1 - \frac{w}{w_c} \qquad (5.23)$$

Where L is the height of the carpet Nylon fiber; w_c is the critical moisture content; x^* is the position of the evaporation front. It is a good assumption that the thickness of the boundary layer above the Nylon surface is negligible as compared to the diffusion path (x*). The evaporation rate can be expressed by a pseudo-steady state Fickian expression for diffusion:

$$N = \frac{DC\left(y_{x^*} - y_a\right)}{x^*} \qquad (5.24)$$

Where N is the molar flux; D is the diffusion coefficient; C is the mole concentration.

The molar flux of water can also be represented by

$$N = -\frac{m_f}{M_w}\left(\frac{dw}{dt}\right) \qquad (5.25)$$

Insert Equation (5.25) into Equation (5.24), the following equation can be obtained,

$$-\frac{m_f}{M_w}\left(\frac{dw}{dt}\right) = \frac{DC\left(y_{x^*} - y_a\right)}{x^*} \qquad (5.26)$$

The effective diffusion coefficient, D, stands for the molecular diffusion coefficient for water vapor in air and may be written as[46],

$$D = 8.64 \times 10^{-1}\left(\frac{T}{273.15}\right)^{1.75} \qquad (5.27)$$

Where D is the diffusion coefficient (ft^2/hr); T is the temperature (K).

M_W is the molecular weight of water (18 lb/lbmol). C is the concentration of the gas-phase ($lbmol/ft^3$) and can be readily calculated using the Ideal Gas law.

C_a, the product of C and y_a, is the water vapor concentration in the gas phase in $lbmol/ft^3$, and y_a can be obtained from the gas-phase humidity data. C*, the product of C and y*, is water vapor concentration at the interphase of moving front:

$$C^* = \frac{P^*}{RT} \qquad (5.28)$$

Where T is the water vapor temperature the same as the carpet tile temperature; P* is the vapor pressure of water at temperature T; and R is the gas constant.

From Equation (5.23), the relationship of derivative of moisture content with respect to time and the evaporation front can be obtained,

$$\frac{dw}{dt} = -\left(\frac{w_c}{L}\right)\frac{dx^*}{dt} \qquad (5.29)$$

Combining Equation (5.26) with Equation (5.29), we find that

$$x^* = \sqrt{\frac{2DM_w CLt\left(y_{x^*} - y_a\right)}{w_c m_f}} \qquad (5.30)$$

Inserting Equation (5.30) into Equation (5.23), the moisture content as a function of time can be described as,

$$w = w_c\left(1 - \sqrt{\frac{2DM_w Ct\left(y_{x^*} - y_a\right)}{w_c m_f L}}\right) \qquad (5.31)$$

5.5.2 Energy Balance

The energy balance for the falling rate period is described in a fashion similar to that in the constant drying rate period,

$$NH_v + \left(m_f Cp_f + m_f wCp_w\right)\frac{dT}{dt} = h\left(T_a - T\right) \qquad (5.32)$$

$$\text{Where } N = \sqrt{\frac{Dm_f w_c C\left(y_{x^*} - y_a\right)}{2M_w Lt}} \qquad (5.33)$$

Insert Equation (5.33) into Equation (5.32), the final form of the energy balance during the falling rate period is

$$H_v\sqrt{\frac{Dm_f w_c C\left(y_{x^*}-y_a\right)}{2M_w Lt}}+\left(m_f Cp_f+m_f wCp_w\right)\frac{dT}{dt}=h\left(T_a-T\right) \tag{5.34}$$

CHAPTER VI

RESULTS AND DISCUSSION

The evaporation front model was developed in the previous chapter to simulate the carpet tile drying process in industry. In order for the model to predict the drying characteristics for industrial operations, variables including heat transfer and mass transfer coefficients, diffusivity, and critical moisture content need to be determined. Little information reported in the literature on these parameters is useful, since these parameters would be specific to the products studied in this research. Even so, literature contains very few studies in which an attempt is made to obtain model parameters from independent experiments. In this chapter, results on laboratory experiments carried out to determine the drying curves and key model parameters for three different carpet tile products supplied by the Milliken and Company are presented.

Due to the different characteristics of the two drying periods, the key model parameters are determined separately from the different parts of the experimental data. Convective heat and mass transfer coefficients were calculated from data obtained in the constant drying rate period. Since convective heat and mass transfer coefficients are correlated by the Chilton-Colburn analogy, there is only one independent parameter. On the other hand, the diffusion coefficient was determined from the data in the falling

drying rate period. The critical moisture content, w_c, was determined from the mass versus time plot where the transition occurs from a straight line to a curved line.

6.1 Comparison between the Model Results and the Experimental Data

Figures 6.1-6.3 show moisture content profiles of the three different types of carpet tiles RR, MS, and GP, at three different temperatures 212 F, 248 F, and 284 F. All the carpet tile samples were subjected to identical drying conditions; i.e., they were exposed to air at constant air humidity and velocity at each temperature. The scatter in data in these figures is due to the vibrations caused by the introduction of air flow. The scatter could be almost eliminated by shutting the air flow, but the ambient humidity value would then go up. The scatter in the data was hence a necessary diversion. Even so, attempts were made to minimize it by diverting the flow away from the tile surface.

All drying curves in this study displayed these two drying rate periods. As stated in the previous chapter, the constant rate drying is characterized by the drying of unbound moisture, and the falling rate drying is characterized by the drying of bound moisture. During the constant rate drying regime, the Nylon fiber temperature and the moisture evaporation rate remain constant. During the falling drying rate period, due to reduced moisture content in the carpet tile and an increase in the diffusion path length, the mass transport rate of moisture decreases. Detailed calculations for one such run (Roadrunner at 248 F) are shown in Appendix A. As can be seen, the model fits the

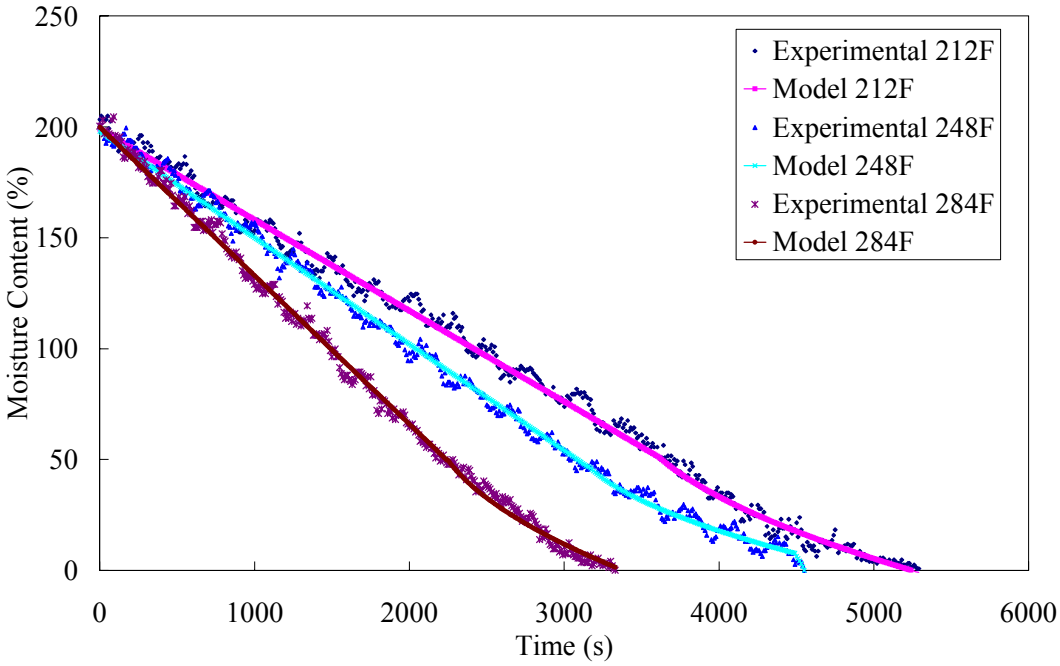

Figure 6.1 Comparison of the experimental and model results of moisture content evolution for RR at different temperatures

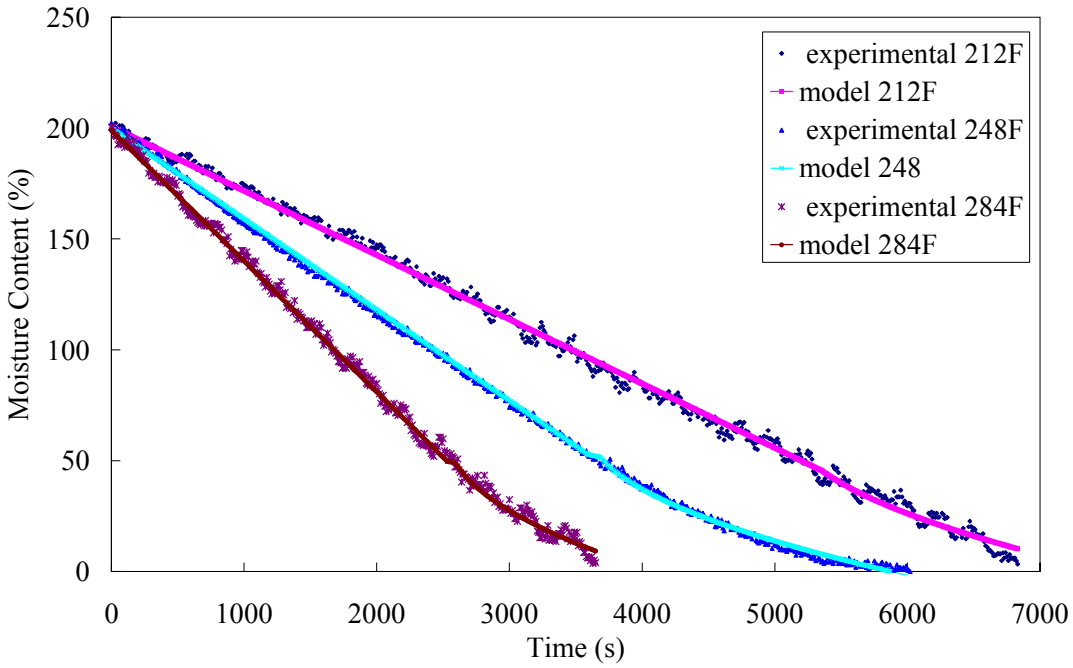

Figure 6.2 Comparison of the experimental and model results of moisture content evolution for MS at different temperatures

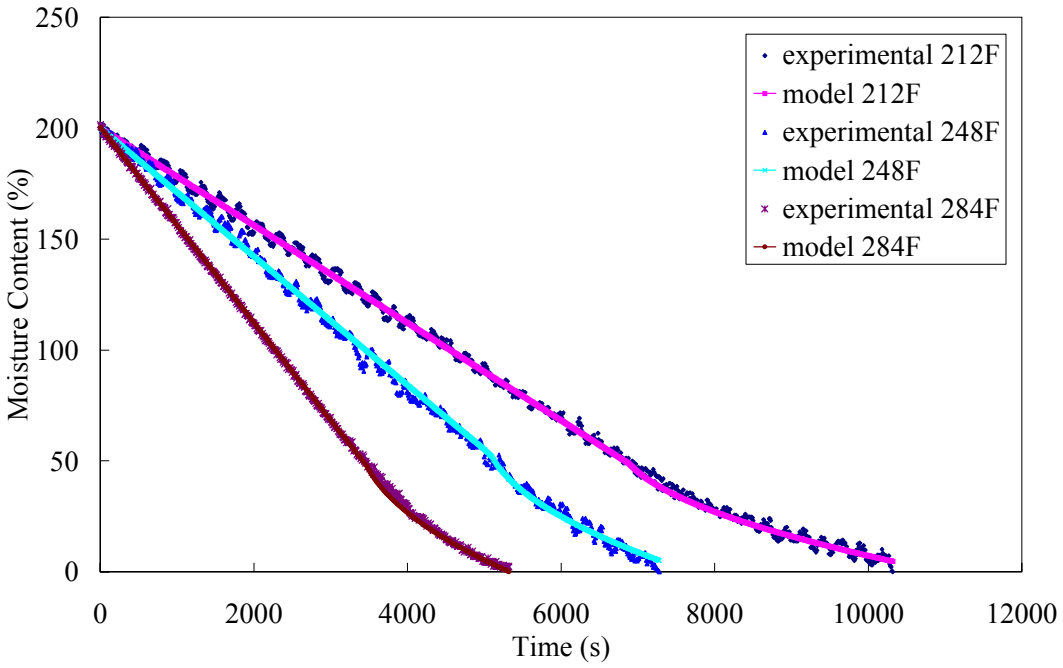

Figure 6.3 Comparison of the experimental and model results of moisture content evolution for GP at different temperatures

experimental data very well. It thus provides a good basis for the determination of the transport properties and the critical moisture content analysis.

6.2 Critical Moisture Content

The moisture content at the end of the constant drying rate period is called the critical moisture content. At this point, the moisture movement in the solid becomes insufficient to replenish the liquid being evaporated at the surface of the solid. Therefore, the critical moisture content depends upon the ease of moisture movement through the solid, which is determined by the pore structure of the Nylon pile, primary backing, and the type and the amount of latex used as a backing-coating layer. There is no theoretical basis for predicting the critical moisture content, and it is best obtained from experimental data. Some controversial results have appeared in the literature. According to Perry[47], the critical moisture content increases with drying rate and the thickness of the layer being dried. However, according to Bell[48], the critical moisture content is more dependent on the amount of moisture water absorbed. Its dependence on the drying rate and the structure of the material is much weaker and may often be ignored, though this dependence has been illustrated repeatedly. It seems the critical moisture content really depends on the specific material. In general, it can be said that the critical moisture content of a hygroscopic material is greater than a similar nonhygroscopic material with similar construction and saturation of absorbed water.

Table 6.1 summarizes the critical moisture content values for the three different tile products, each at three different temperatures. It is noteworthy that these critical moisture content values are remarkably in a narrow range (0.50-0.55). The fact that the critical moisture content changes negligibly with temperature should be largely expected. As stated above, the critical moisture content should only be a function of the microstructure of the Nylon fibers, primary backing, and the type and the amount of latex. In the case of three different products used in this study, the latex and primary backing remain the same. However, the major difference for the Grand Plaza product is that it is a cut pile product; it has almost twice the Nylon weight; and the fiber cross-section is a bit different (Figure 5.3). Even so, one should not take this constant value of critical moisture content for grated, and it should be evaluated experimentally for a given product.

Figures 6.4-6.6 show the drying rates as a function of moisture content for RR, MS, and GP at different temperatures. These curves were constructed after fitting the raw data (shown in Figures 6.1-6.3). As anticipated, the drying rate remains constant even as the moisture content of the carpet moisture content decreases from 200% to 50%. Below 50%, the drying rate decreases almost by a factor of 2.5~3.0, as the moisture content decreases from 50% to ~0%. Another observation is that during the constant rate drying period, the drying rate increases roughly by a factor of 2 as the gas-phase temperature was increased from 212 F to 284 F. Some of this increase is due to increased convective heat transfer coefficient, but a majority of increase should be attributed to increased driving force (Ta-T).

Table 6.1 Critical moisture contents of the three different types of carpet at different temperatures

T / Products	212 F	248 F	284 F
Roadrunner	50.6%	51.2%	49.8%
Midnight sparkle	51.6%	51.3%	49.3%
Grand plaza	55.5%	53.1%	53.4%

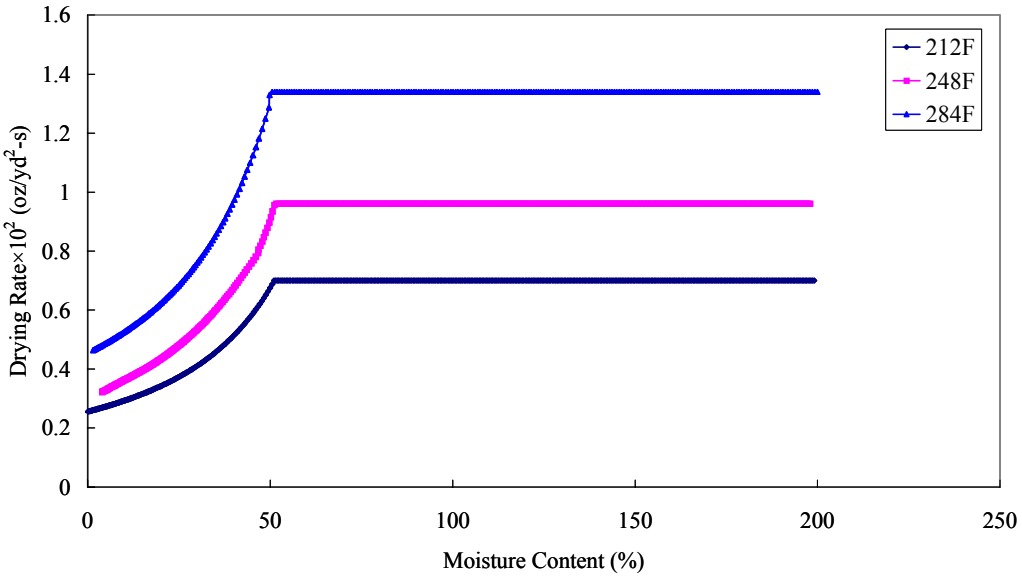

Figure 6.4 Drying rate as a function of moisture content for RR at different temperatures

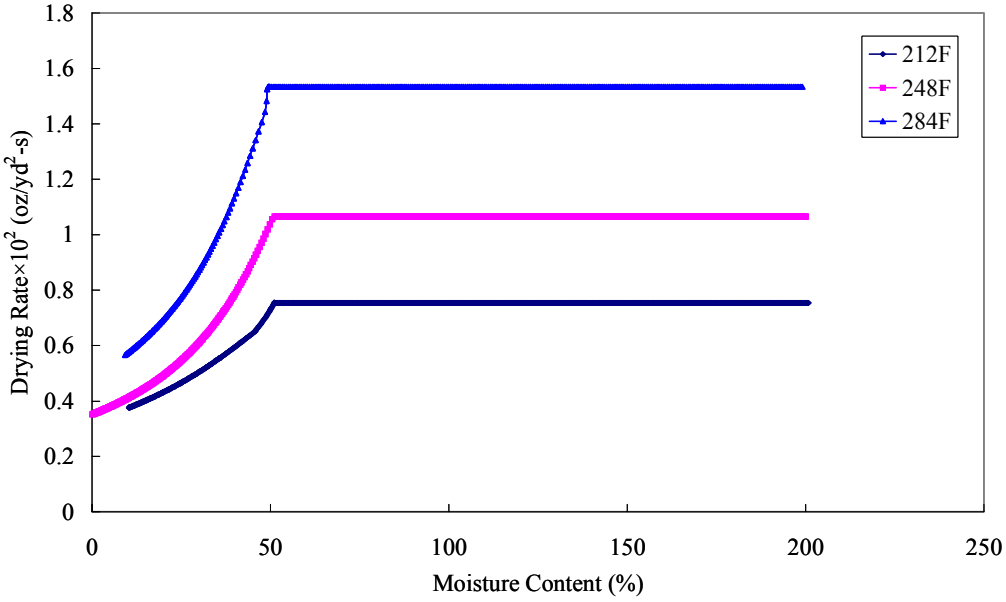

Figure 6.5 Drying rate as a function of moisture content for MS at different temperatures

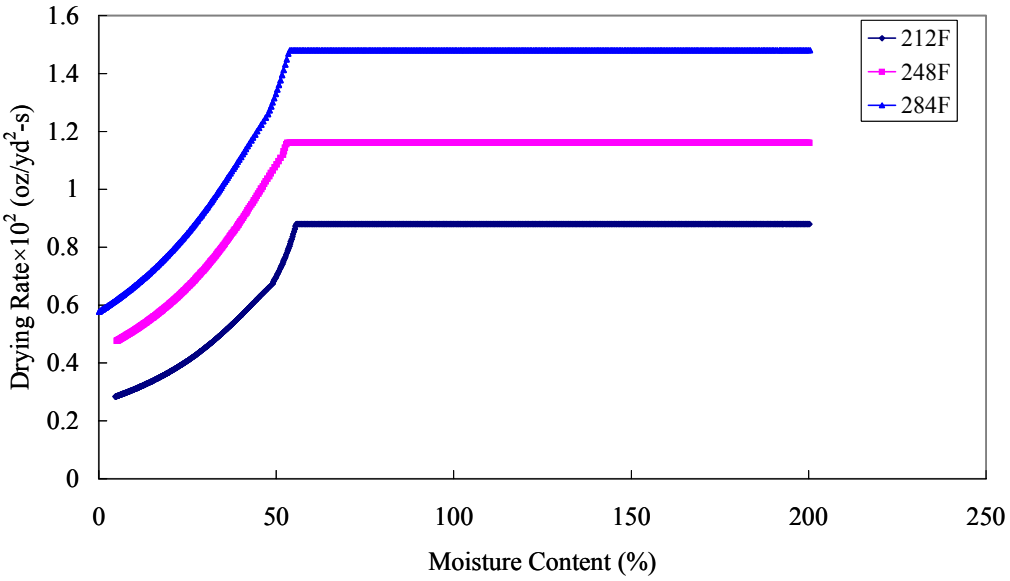

Figure 6.6 Drying rate as a function of moisture content for GP at different temperatures

6.3 Determination of Heat Transfer and Mass Transfer Coefficients

The convective heat transfer and mass transfer coefficients are two important parameters for studying this drying process. The mass transfer coefficient is related to the heat transfer coefficient by Chilton-Colburn analogy. Under the condition of forced convection, the heat transfer coefficient depends mainly on the system geometry, thermal and flow properties of the fluid. The general relationship between the convective heat transfer coefficient, h, and the dimensionless Nusselt number, Nu, is expressed by the following equation[49]:

$$Nu = \frac{hL}{K} = \Phi(\mathrm{Re}, \mathrm{Pr}) \qquad (6.1)$$

Where k is the thermal conductivity of the fluid; L is the characteristic length; Re is the Reynolds number; and Pr is the Prandtl number.

Since a detailed analysis of flow conditions is needed to utilize the empirical expression for heat transfer coefficients in terms of Reynolds and Prandtl numbers, it is far more convenient to calculate heat transfer value from the experimental data. This approach is also justified by the fact that the laboratory flow conditions were vastly different from those in the industrial dryer. The mass transfer coefficient is obtained from its correlation to the heat transfer coefficient through the Chilton-Colburn analogy.

Figure 6.7 shows the heat transfer coefficient determined for the three types of carpet (RR, MS, and GP) at three different temperatures 212 F, 248 F, and 284 F. The values obtained for different types of carpet at the same temperature match each other fairly well. There is a general trend that the heat transfer coefficient increases slightly with increasing temperature. This is expected. Also one should not expect heat transfer values to be different for the three different products, since heat transfer value is only dependent on the surface geometry and the flow conditions.

6.4 Diffusion Coefficient

As stated earlier, during the falling drying rate period, the drying process is determined by the moisture migration rate. When the moisture content at the Nylon fiber surface approaches the critical moisture content, the evaporation front begins to recede from the Nylon pile surface into the interior, which is called the moving evaporation front. In the dry region, the moisture content is assumed to be zero. When the evaporation occurs at the evaporation front, the water vapor diffuses through the wet region to the Nylon fiber surface.

The value of the diffusion coefficient can be determined from the best fit of the analytical model to the experimental data. Details are given in Appendix A. Figure 6.8 shows the diffusion coefficient of the three different types of carpet (RR, MS, and GP) under three different temperatures 212 F, 248 F, and 284 F. It can be seen that the values of the diffusion coefficients of different carpet tiles at the same temperature are

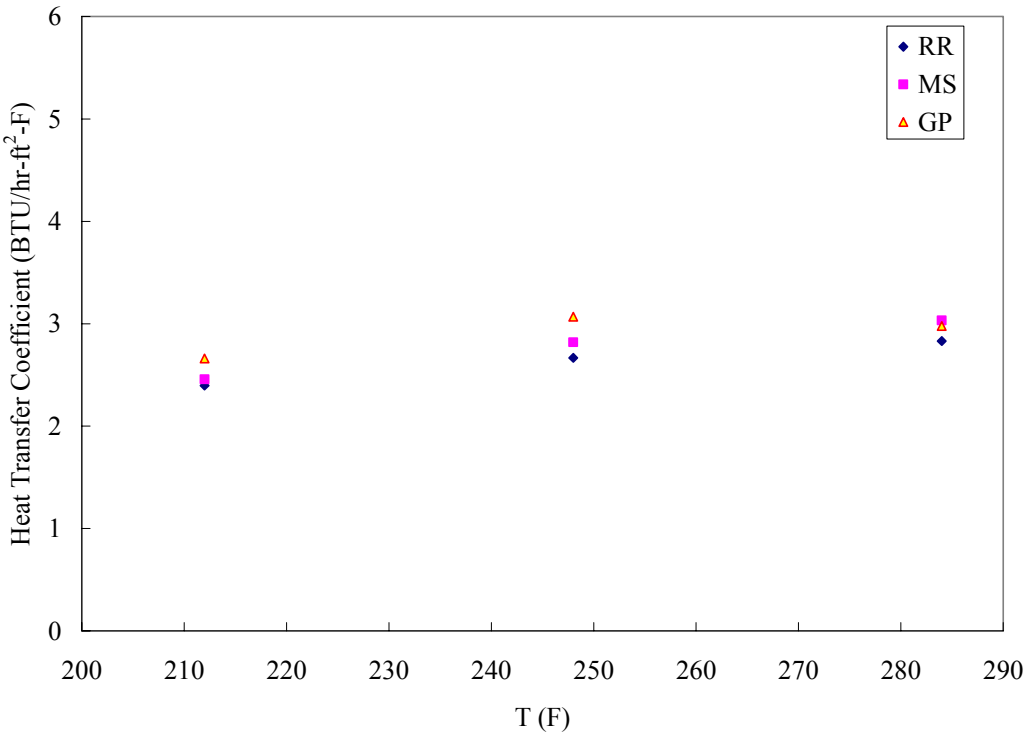

Figure 6.7 Experimental values of the heat transfer coefficient for RR, MS, and GP at different temperatures

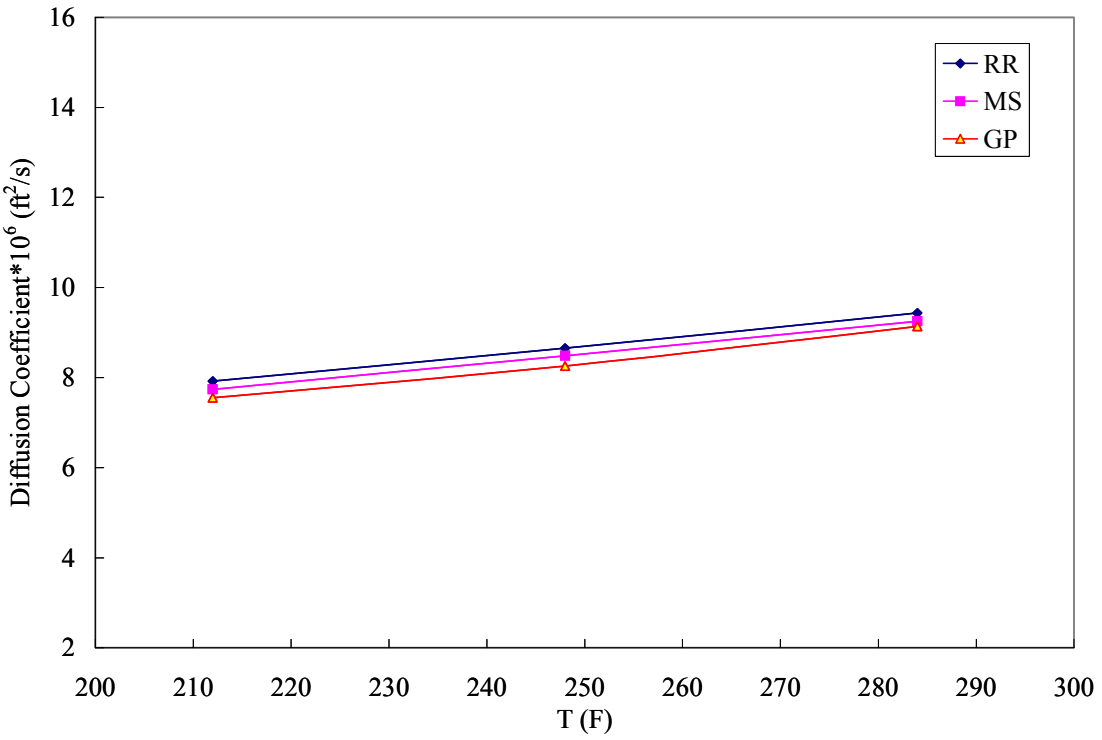

Figure 6.8 Diffusion coefficients as a function of temperature for RR, MS, and GP

consistent with each other. It indicates that, for the three different types of carpet in this study, the diffusion coefficient is only dependent on the temperature, not the specific type of carpet. Just like the critical moisture content, the diffusivity values for the Grand Plaza tiles are similar to those for the Roadrunner and Midnight Sparkle tiles. It also shows that the diffusion coefficient increases with temperature. The diffusivity can be described as a power function of the temperature, and this could be verified from literature[50]. From the consistent diffusivity values determined at the three different temperatures, this unique relationship between the diffusion coefficient and the temperature can be extrapolated to a wider temperature range, which would serve a basis for determination of the diffusion coefficient at higher temperatures in the industrial drying operations.

6.5 Effect of Drying Air Temperature

The laboratory drying experiments were conducted at three different temperatures, so the effect of air temperature on the drying process will be elaborated here. Figures 6.9-6.11 show how the drying rates change with time for the three carpet tiles at each temperature. Drying time for each region decreases significantly with increasing temperature, which is as expected. In the constant drying rate region, heat and mass transfers occur simultaneously via convection mechanism. The drying rate in this region is governed by the heat transfer rate because of evaporation. For a given amount of evaporation (or mass transport), large amount of heat transport is needed. Increased air temperature would increase the driving force for heat transfer, which

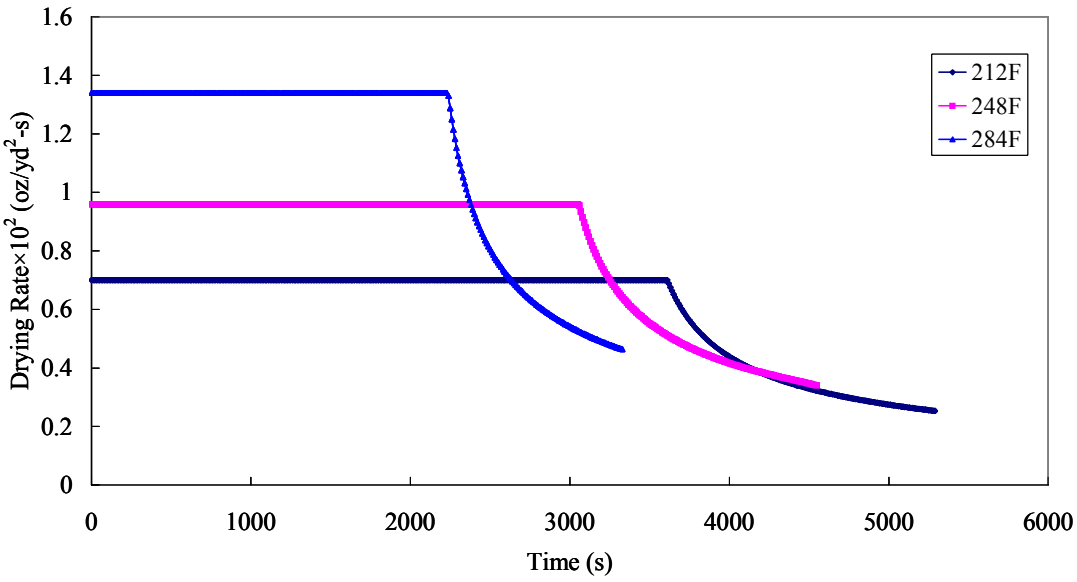

Figure 6.9 Drying rate as a function of time for RR at different temperatures

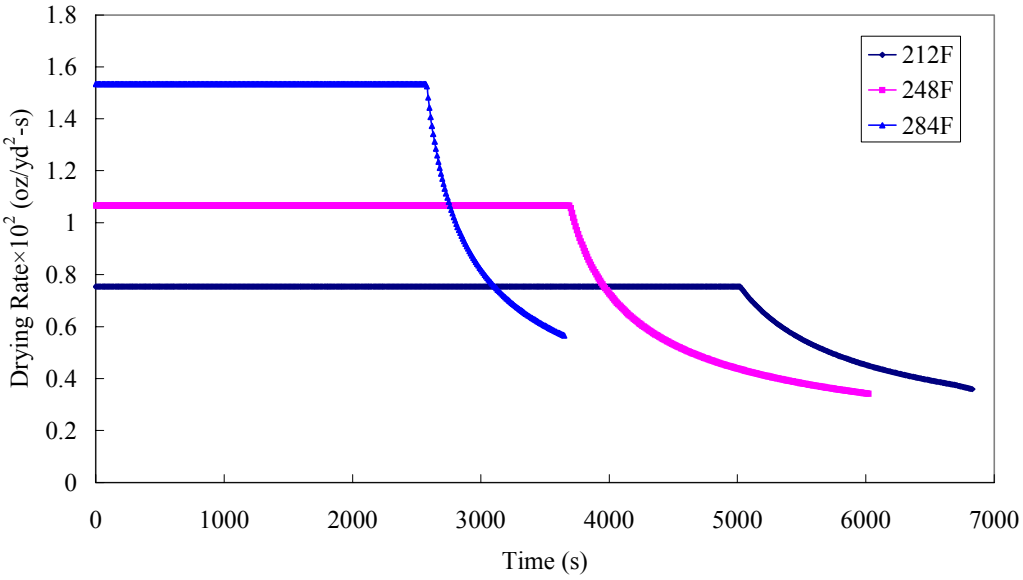

Figure 6.10 Drying rate as a function of time for MS at different temperatures

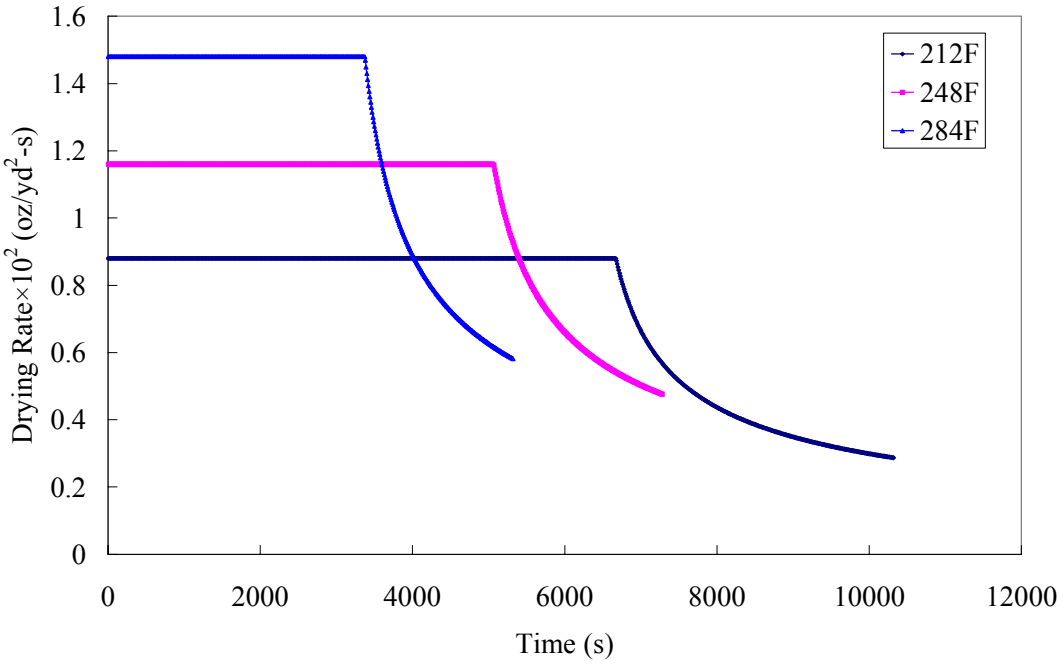

Figure 6.11 Drying rate as a function of time for GP at different temperatures

results in a significant increase in the drying rate. It may seem that since in the constant drying rate region, the drying rate is governed by the rate of heat transfer, there is no need to use excess air (for increased driving force for mass transfer). Model calculations clearly show this not to be the case. The fabric temperature is dependent on the y_a (air moisture content) and thus would be a function of excess air. Figure 6.12 shows the fabric temperature as function of y_a. This is obtained by the simultaneous solution of Equations (5.2) and (5.21). Figure 6.13 shows the drying rates obtained at a constant gas-phase temperature, but with varying y_a values. The heat transfer values used in Figure 6.13 were those obtained from laboratory data.

During the falling drying rate period, however, the drying rate is limited by the diffusion of the moisture inside the Nylon fiber. Increasing temperature will result in higher diffusivity as well as the vapor pressure at the evaporation front would increase with increasing Nylon temperature. Thus higher gas phase temperatures would lead to higher drying rate and shorter drying time. As a result, the increase of drying rate in both regions would reduce the drying time significantly for the whole drying process.

From Figure 6.9, it is observed that, when the temperature increases from 212 F to 248 F, the rate in the constant drying rate period increased by 37%. When the temperature is increased by the same amount from 248 F to 284 F, the drying rate also increases by 37%. Similar trends can be observed with the other tile products as shown in Figures 6.10 and 6.11. The change in drying rates (in the constant drying rate region) with temperature is shown in Figure 6.14. Thus, to maximize the drying rate, the drying

air temperature should be as high as possible, without causing negative effect on the carpet tile quality.

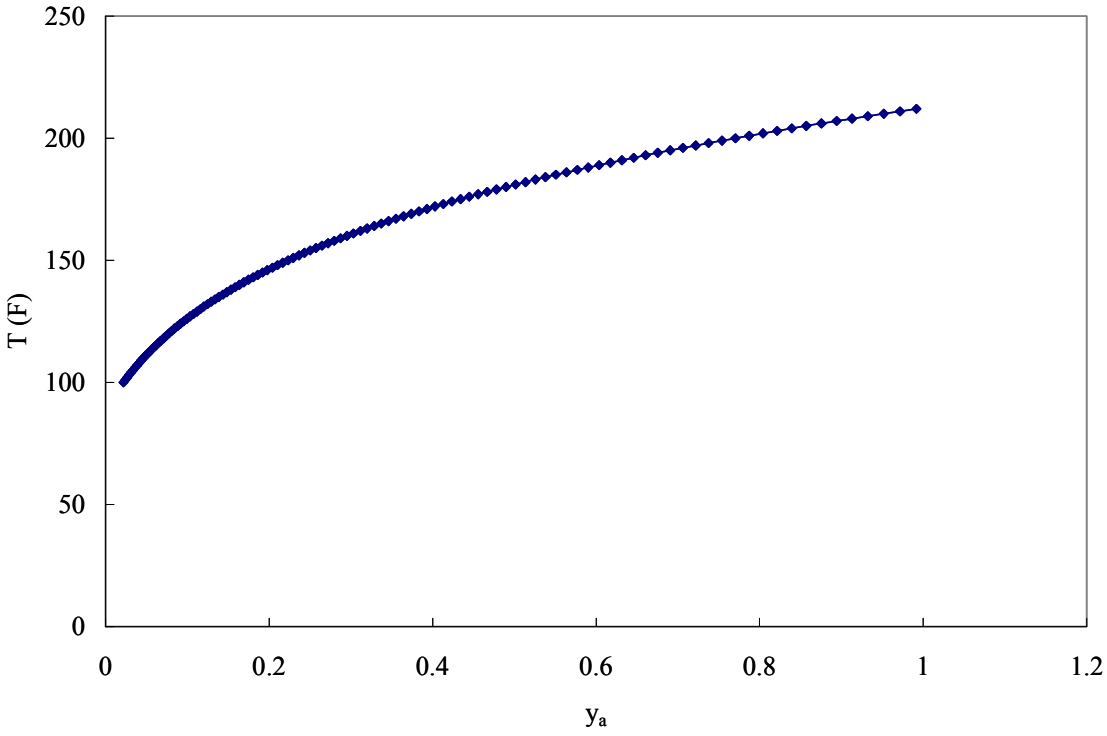

Figure 6.12 The carpet temperature as a function of the drying air humidity

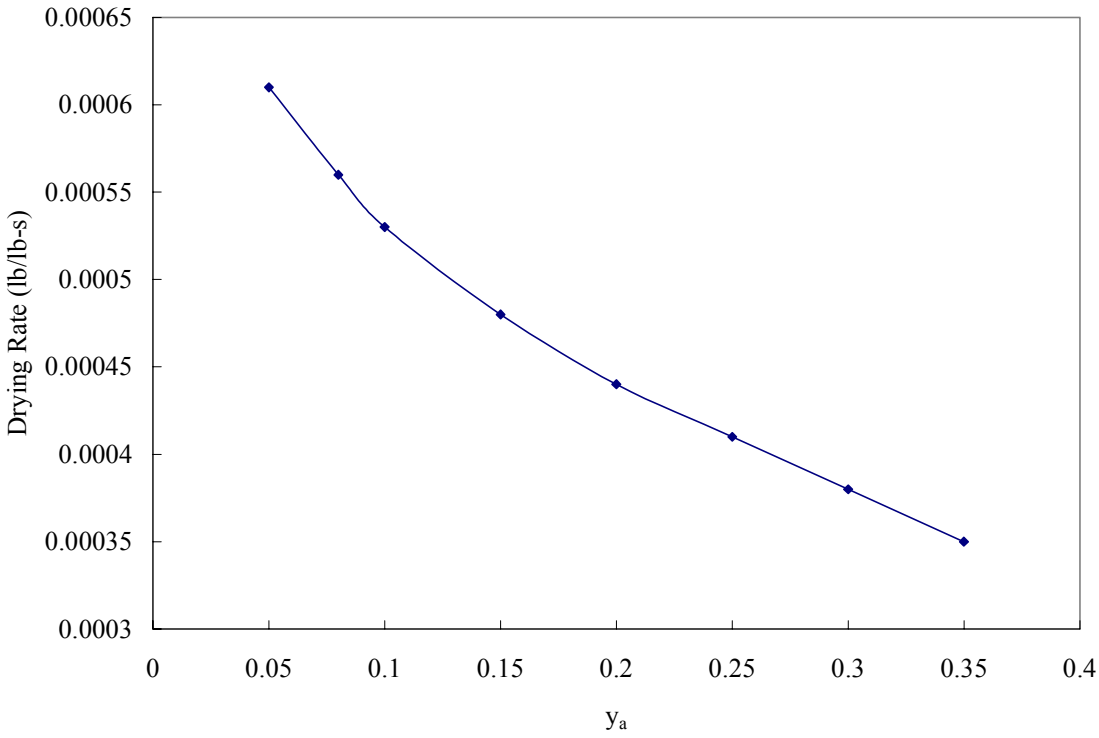

Figure 6.13 Drying rate as a function of air humidity at 248 F

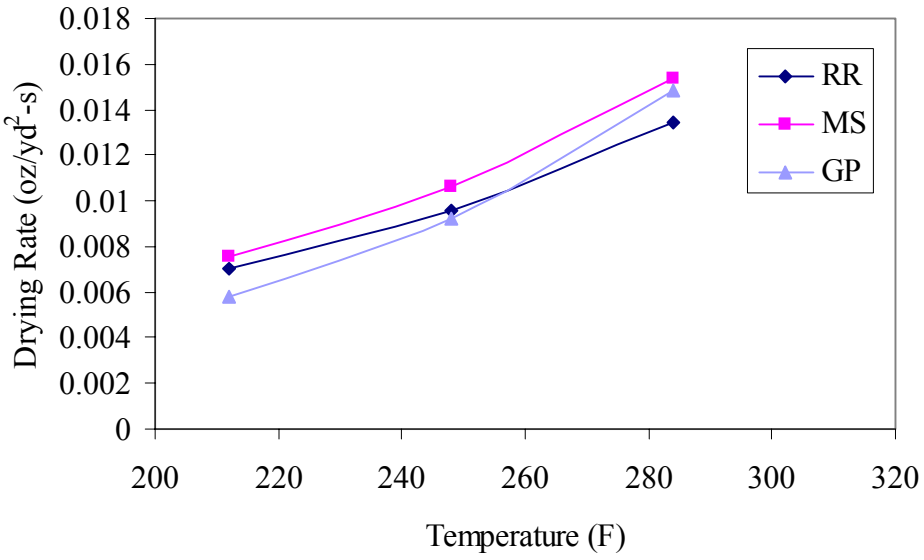

Figure 6.14 Drying rates of RR, MS, and GP at different temperatures

CHAPTER VII

MODEL APPLICATION TO INDUSTRIAL DRYING

It was shown in Chapter VI that the model fits the experimental data from laboratory scale drying process very well. Key model parameters such as critical moisture content, diffusion coefficient, and heat and mass transfer coefficients were obtained from independent study under laboratory oven drying conditions. Laboratory results also show that increasing temperature leads to higher tile drying rates. However, the real usefulness of a model can only be realized if it can be shown to provide guidance for industrial continuous drying process. Therefore, the thrust of this chapter is on utilizing the model to predict the industrial drying process and to suggest ways to improve on the existing operation.

The values of critical moisture content (w_c), diffusion coefficient (D), and heat transfer coefficient (h) at three different temperatures (212 F, 248 F, and 284 F) were presented in Chapter VI. Since critical moisture content (w_c) and diffusion coefficient (D) can be considered to be dependent on the microstructure of the Nylon pile as well as that of the region near the primary backing, latex coating, and Nylon tufts, it is safe to assume that these values are also applicable under industrial drying conditions. One should note with caution that any change in the Nylon fiber microstructure or in the

amount or composition of latex layer in the future would likely lead to changes in the critical moisture content value and/or diffusion coefficient.

The convective heat transfer coefficient (h) obtained in the laboratory drying condition is likely to be very different from that in the industrial dryer. This parameter depends on the flow conditions as well as the flow geometry. Impinging flow creates very high gas velocities (32.8 ~ 328 ft/s) at the Nylon pile surface, which cannot be duplicated or matched in the laboratory dryer. Therefore, this parameter would have to be adjusted to fit the industrial dryer data.

7.1 Determination of the Convective Heat Transfer Coefficient

Before transforming laboratory modeling results to the industrial drying operations, the heat transfer coefficient needs to be evaluated. The heat transfer coefficient under industrial carpet tile drying conditions was determined through the model fitting to the temperature profile of the drying process.

Figure 7.1 shows a typical temperature profile for the Roadrunner tile product (RR) during the industrial drying process. The nylon fiber temperature increases quickly from ~70 F to a relatively constant temperature indicating the constant drying rate period. In this period, the nylon layer temperature remains constant, while energy being supplied is used up as the latent heat of water evaporation. Only when all the unbound moisture is removed, does the carpet tile temperature increase, indicating the beginning of the falling drying rate period. Figure 7.1 shows that the constant rate

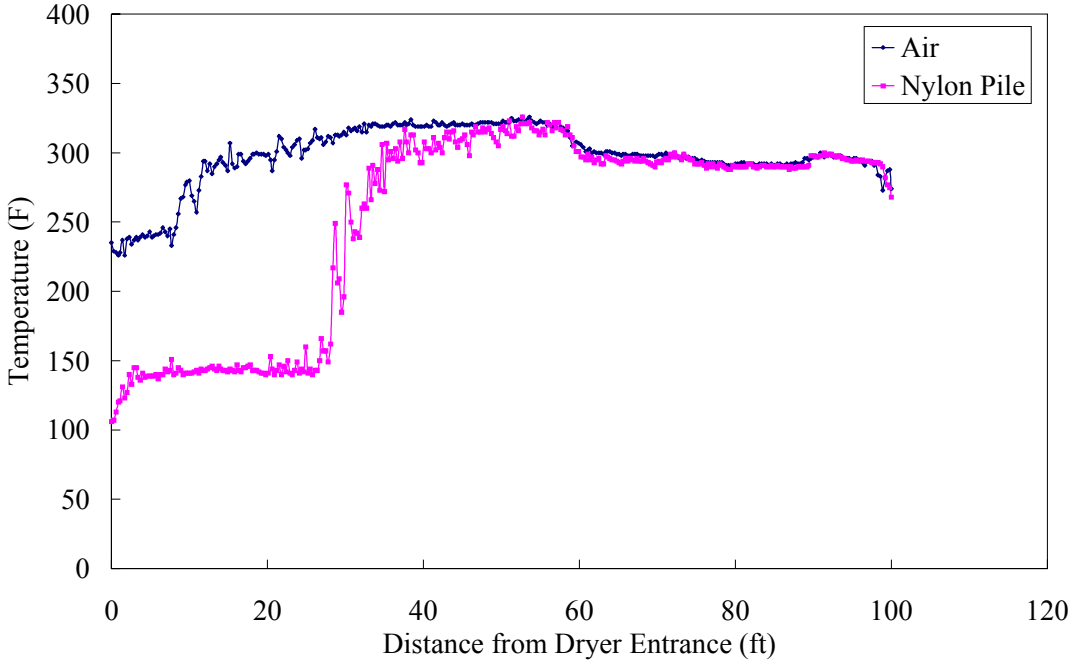

Zone	1	2	3	4	5	6	7	8	9	10
T(F)	330	330	330	330	330	330	300	300	300	300

Figure 7.1 Temperature profile for carpet Roadrunner during the industrial drying process

(Temperature settings of the ten sequential temperature zones of the dryer are listed in the above table)

drying region lasted in the first three zones. The temperature of the nylon pile remained constant (~140 F) in this region. It is important to note that the industrial dryer consisted of ten zones, each zone being 10ft long. Figure 7.1 also shows the temperature settings of these zones (listed in the table). The first six zones and the last four zones are maintained at 330F and 300F, respectively. As was discussed in Chapter VI and in the Appendix A, the heat transfer coefficient would be determined from this constant drying rate period data where the gas-phase temperature is 330 F. It should be noted from Figure 7.1 that the total drying time would be in the range of 5~6 minutes. The industrial dryer is 100 ft long (each zone 10 ft) and carpet runs at a speed of 15~20 fpm. This drying time (5~6 min) is more than an order of magnitude lower than the typical drying times observed in the laboratory drying conditions (4,000~6,000 sec). This clearly suggests much higher values of convective heat transfer coefficient. For Roadrunner tile products, the values of convective heat transfer coefficients ranged between 36~40 BTU/hr-ft^2-F. The small variations can be attributed to fitting data over a very large time span (more than 1 year) as well as different dryer ranges. In any case, these values of heat transfer coefficient are 10~15 fold higher than those found in the laboratory studies.

7.2 Model Validation by Industrial Drying Conditions

Having all the model parameters for simulation of industrial dryer operation, testing the model validity is the next logical step. Figure 7.2 shows the transient

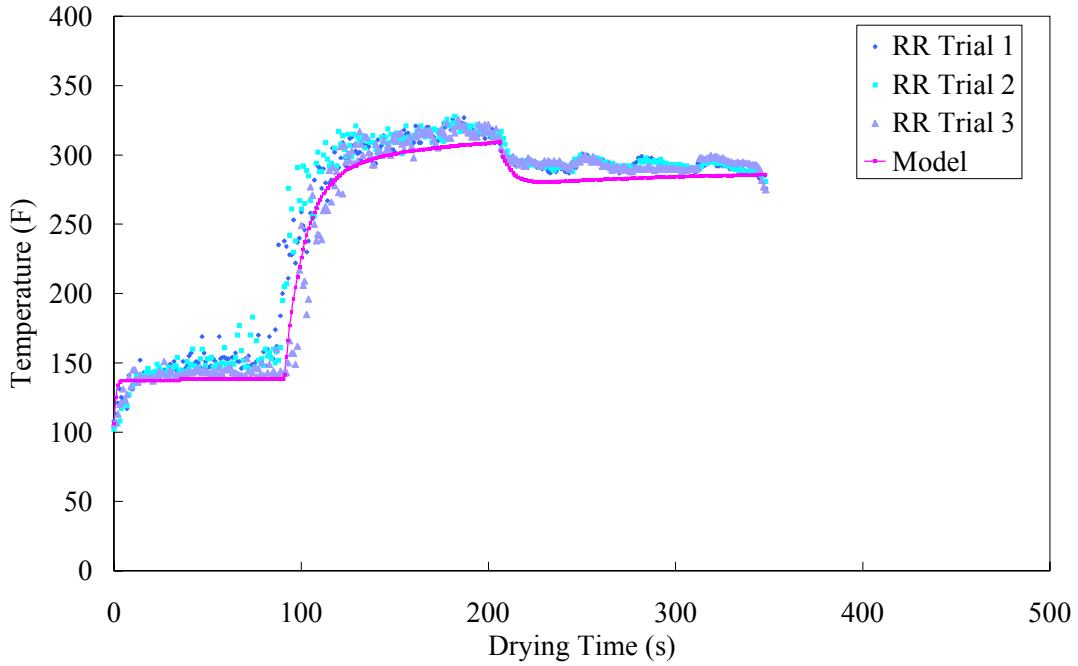

Zone	1	2	3	4	5	6	7	8	9	10
T(F)	330	330	330	330	330	330	300	300	300	300

Figure 7.2 Model fitting of the Nylon pile temperature profiles of carpet Roadrunner

(Temperature settings of the ten sequential temperature zones of the dryer are listed in the above table)

temperature data for the nylon pile from three different runs for the Roadrunner tile product. These three profiles were obtained on three different Roadrunner tiles and on three different days. Thus, the scatter in Figure 7.2 represents a good measure of product and process variability. The table shown in Figure 7.2 lists the temperatures in each of the ten zones. From the constant rate drying period data, an h value of 40 BTU/hr-ft^2-F is obtained. This value of h, together with the values of D and w_c was used to develop mathematical model predictions. It should be noted that the mathematical model was solved for each zone, one by one. This is necessary because the gas phase temperature varied from zone to zone. The value of D was adjusted for temperature in each zone.

The model prediction is shown by the solid line in Figure 7.2. The agreement between the model prediction and the data is remarkable. The fact that there is a good fit in the constant drying rate region is not as surprising since the h value was obtained by fitting the rate equations. What is particularly noteworthy is the model prediction after the tile has moved beyond the constant drying rate region, because moisture diffusion controls the drying rate here. The diffusion parameter (D) and the critical moisture content (w_c) were obtained from the laboratory scale drying experiments, and the time scale of these experiments was at least an order of magnitude higher than the industrial drying conditions. The excellent fit (both qualitative as well as quantitative) provides a good validation of the model. Most likely, it also reflects the fact that the model is developed based on a physical description of the drying process. This sets the stage for using the model's abilities to predict and improve the performance of the

industrial dryer. A successful outcome here would provide additional support for model validity.

An opportunity was presented by our industrial partner, Milliken & Company. The vacuum slot just before the tile dryer was mal-functioning, leading to higher initial wet pick-up (WPU=317%). The temperatures employed in the ten zones were as follows:

Zone	Temperature(F)	Zone number	Temperature(F)
1	310	6	330
2	330	7	300
3	330	8	280
4	330	9	280
5	330	10	280

The dryer speed had to be lowered to 14 fpm to ensure a dry carpet (< 4% WPU in tile is considered a dry carpet tile). The challenge was to suggest a way to increase the dryer speed. The first step was to see what drying time would be predicted by the mathematical model.

When applying the model, each individual heating zone in a dryer has to be considered separately. And the residence time of the carpet tile in each zone needs to be known. So knowledge of drying speed and time are very important given a set of temperature zones. The calculation of the drying time in this study is mainly based on a trial and error approach. First, the residence time of the carpet or the drying speed is

assumed from industrial running experience. Then, the actual drying speed under a known dryer temperature setting is calculated and determined by comparing with the assumed value. If these two numbers are far apart, go back to step 1 and repeat the trial and error process. Figure 7.3 shows the drying rate and temperature profiles of the Roadrunner tile with an initial water pickup of 317%. The model predicted that the total drying time to be 433 sec, which is very close to the actual drying time 428 sec in manufacturing.

Yet further validation of the mathematical model was achieved with another simulation of the drying of Roadrunner tile product. Figure 7.4 shows the results of model simulation. The total drying time was predicted to be 402 sec vs 400 sec observed in the industrial dryer. The temperature profiles used in Figure 7.4 data is slightly different than that used in Figure 7.3. Also, a different dryer was employed for the data of Figure 7.4.

This excellent agreement between model prediction and industrial operation is very encouraging and allows one to suggest modifications with certain confidence.

7.3 Model Predictions from Parametric Study

Before applying the model to the industrial drying, parametric study was carried out to investigate the effects of key operating parameters on the drying characteristics of the carpet tile under the industrial drying conditions. Some basic results have been derived and their implications to the drying operations will be discussed below. The

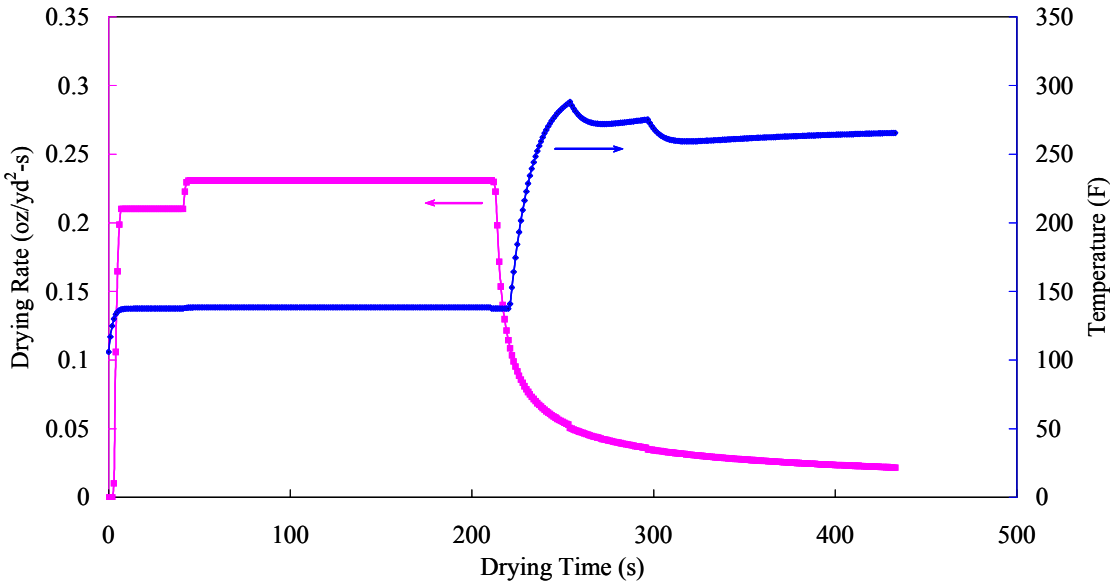

Zone	1	2	3	4	5	6	7	8	9	10
T(F)	310	330	330	330	330	330	300	280	280	280

Figure 7.3 Drying rate and temperature profiles for carpet Roadrunner drying

(Temperature settings of the ten sequential temperature zones of the dryer are listed in the above table)

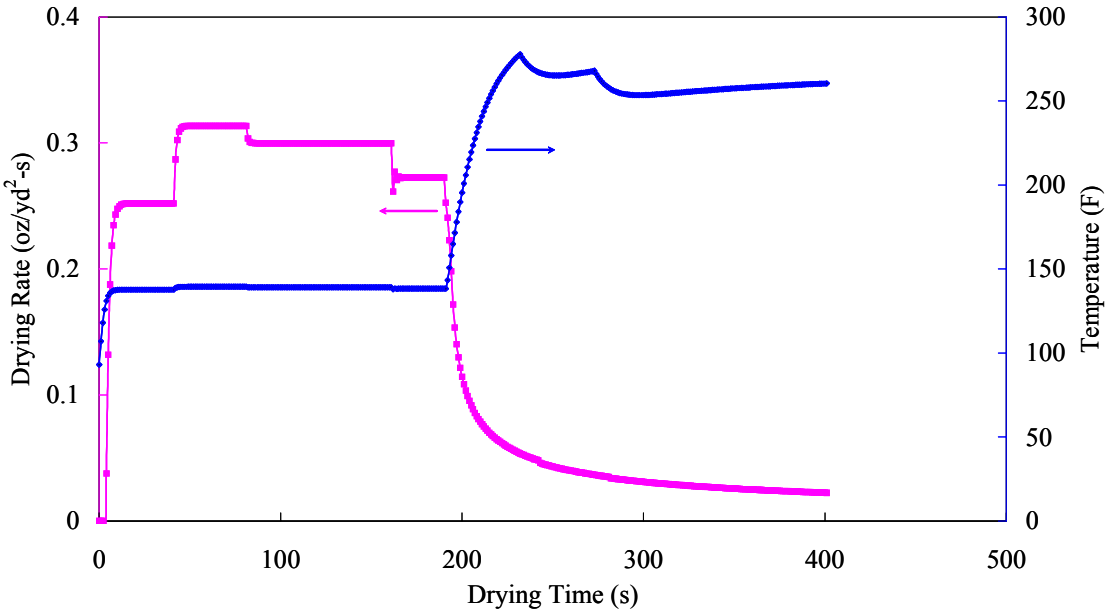

Zone	1	2	3	4	5	6	7	8	9	10
T(F)	310	360	350	350	330	330	300	280	280	280

Figure 7.4 Drying rate and temperature profiles for carpet Roadrunner drying

(Temperature settings of the ten sequential temperature zones of the dryer are listed in the above table)

study has been focused on the effects the temperature settings in each of the ten heating zones. As shown in Table 7.1 and Figure 7.5, cases one through four consider the effects of different temperature settings in each of the ten zones on the drying time with an initial moisture content of 317%. In Case 1, the temperature in each of the first seven zones is 330 F, whereas for Case 2, all the temperatures are set at 310 F, it shows that the drying time decreases from 433 sec (Case 1)to 389 sec (Case 2), and the dryer speed from 14 fpm (Case 1) to 15.4 fpm (Case 2). Case 3 represents a constant temperature of 330 F in all the ten zones, and it leads to a further reduction in the drying time to 360 sec (or an increase in the dryer speed to 16.7 fpm).

Once can conclude that the dryer speed can be improved by optimizing temperature settings in each dryer zone. Especially, increasing the temperature in the last several dryer zones can increase the drying rate significantly. In addition, in the constant drying rate period, the drying process is dominated by the heat transport, so increasing the temperature in the first several zones can increase the driving force thus leading to higher drying rate. This is illustrated in Case 4. When the temperature in the first several zones is increased to 350 F, the total drying time is reduced to 340 sec. In summary, the model predicts that the temperature should be set as high as the sensitive temperature of the carpet tile in order to obtain the highest drying rate. The increased temperatures in the dryer should be balanced against the potential adverse effects on tile quality, e.g., high temperature may lead to delamination problems and/or shade variability.

Table 7.1 Dryer temperature profiles for four different cases in Figure 7.5

T(F) / case	zone 1	zone 2	zone 3	zone 4	zone 5	zone 6	zone 7	zone 8	zone 9	zone 10
1	310	330	330	330	330	330	300	280	280	280
2	310	310	310	310	310	310	310	310	310	310
3	330	330	330	330	330	330	330	330	330	330
4	350	350	350	350	350	330	330	330	330	330

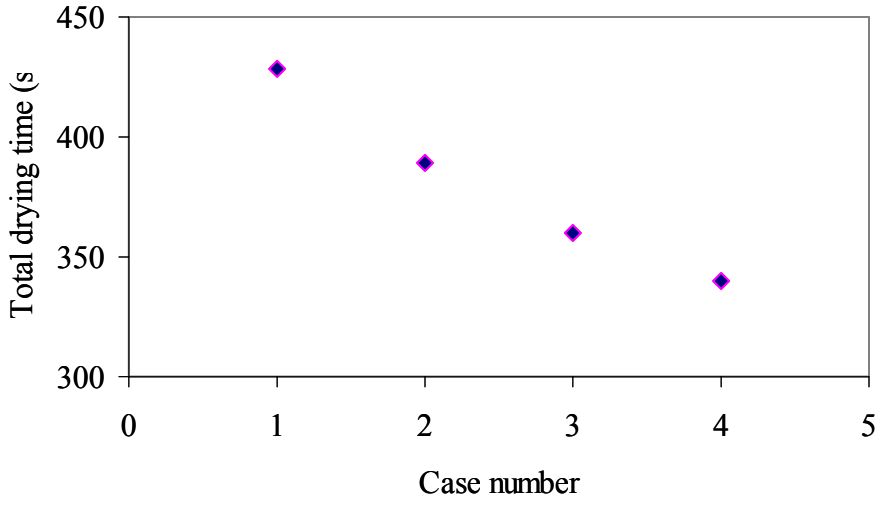

(a)

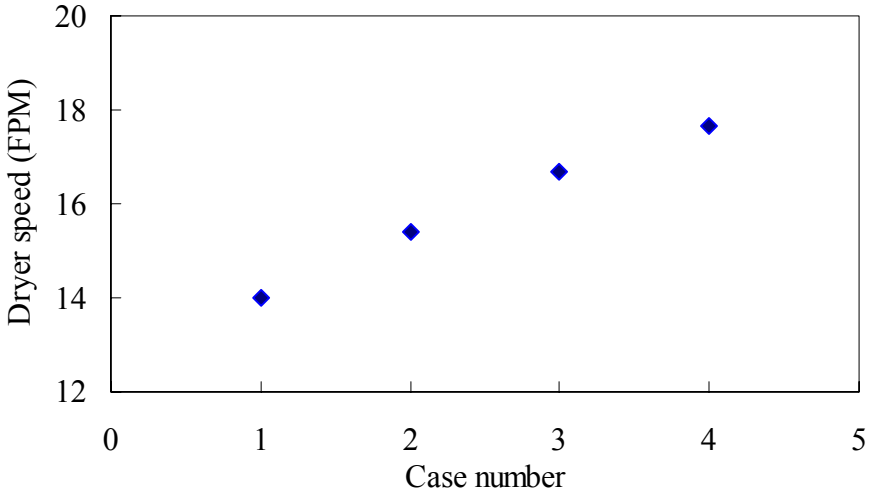

(b)

Figure 7.5 Simulation of carpet Roadrunner drying with an initial WPU of 317% for the four cases: (a) the total drying time, and (b) dryer speed

7.4 Model Application for Improving Dryer Speed in Milliken & Company

From the previous section, the model predicts that increasing the drying temperature in general will improve the drying rate. In particular, the temperature setting in the last several heating zones should be set at a higher temperature than the current industrial settings in general. Another way of reducing the drying time is to lower the initial wet pick-up of the carpet tile. Because the cost of removing the moisture by mechanical means (squeezing or vacuum) is much lower than that for the thermal means. Under the situation in this study, the vacuum slots should be operated more efficiently to reduce the initial wet pick-up of the carpet tile to increase the dryer speed.

By these principles the modeling work is applied to provide guidance to improve the dryer operation in Milliken and Company. Table 7.2 shows the temperature settings for four different cases (initial moisture content is changing as well). Figures 7.6 and 7.7 show the Nylon temperature profiles and the drying rate profiles for these four cases, respectively. Case 1 represents the baseline case (the same as shown in Figure 7.3). Here the initial moisture content was 317 F, and the temperature profile in the dryer zones is shown in Table 7.2. The drying time predicted by model was 433 sec (actual drying time 428 Sec). Figure 7.6 shows that more than half of the total drying time is spent in the constant rate drying region. Case 2 represents the situation when the vacuum slot mal-function was taken care of and the initial moisture content was 176.7%. With slightly higher temperature in the first four zones, the drying time was reduced from 428 sec to 358 sec. Figure 7.7 shows that increased temperatures in the

first 4 zones raised the drying rate by ~10%, but as is clear from Figure 7.6, the time spent in the constant rate drying region was decreased a lot (as compared to Case 1). Thus the most significant effect is from reduction in the initial moisture content.

Case 3 depicts a more aggressive temperature profiles in the dryer (as compared to Case 2). This is particularly true for the last four zones (Table 7.2). Not surprisingly, Figure 7.6 shows that it takes about the same time (~110 sec) for Cases 2 and 3 to reach the critical moisture level. However, the time to remove the bound moisture from the tile is significantly lowered in Case 3, due to using higher temperatures in the last four zones. The total drying time is ~330 sec. (versus 358 sec for Case 2).

Case 4 (versus case 3) shows the effect of decreased inlet moisture (more efficient vacuum slot operation). Same temperature profiles are maintained in Cases 3 and 4. As shown in Figures 7.6 and 7.7, the major effect is a reduction in time spent in the constant drying rate region. Here the total drying time is 288 sec. Figure7.8 summarizes the results of simulations for these four cases. By using a combination of reduced initial moisture content and higher temperatures in the dryer zones, it is possible to decrease the drying time from 428 sec to 288 sec. This directly results in improved productivity, since dryer is the bottleneck on the production range, and the ranges speed can be increases from 14 fpm to 20.9 fpm (a 49% increase).

Table 7.2 Dryer temperature profiles and initial WPU for the four different cases in Figures 7.6-7.8

case	WPU (%)	zone1 T(F)	2 T(F)	3 T(F)	4 T(F)	5 T(F)	6 T(F)	7 T(F)	8 T(F)	9 T(F)	10 T(F)
1	317	310	330	330	330	330	330	300	280	280	280
2	176.7	315	360	360	350	330	330	300	280	280	280
3	176.7	350	350	350	350	350	330	330	330	330	330
4	152	350	350	350	350	350	330	330	330	330	330

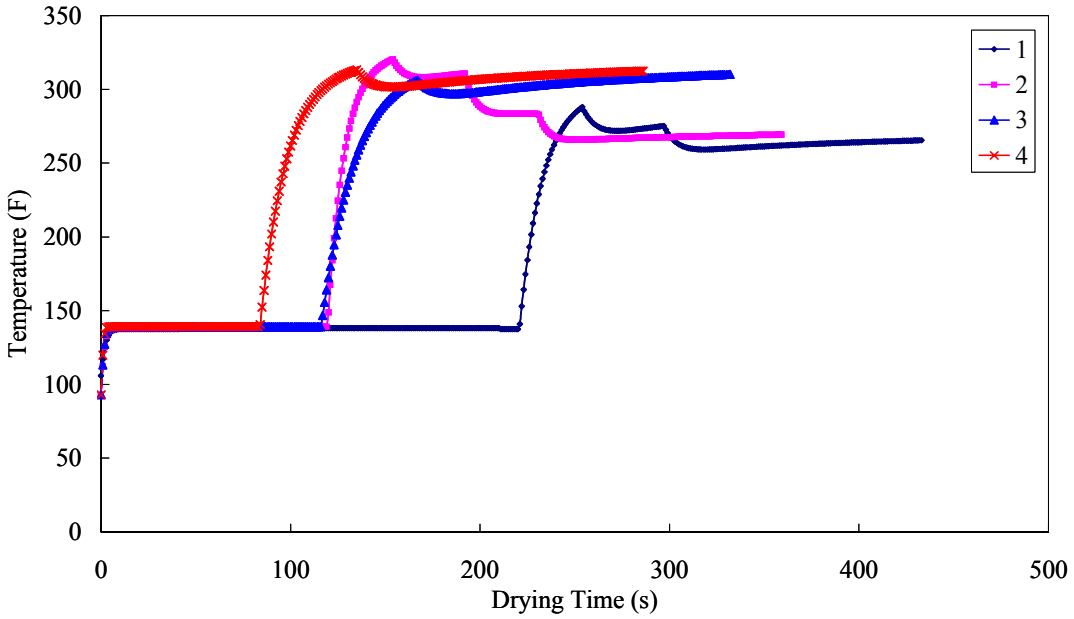

Figure 7.6 Temperature profiles for carpet Roadrunner drying process for the four cases

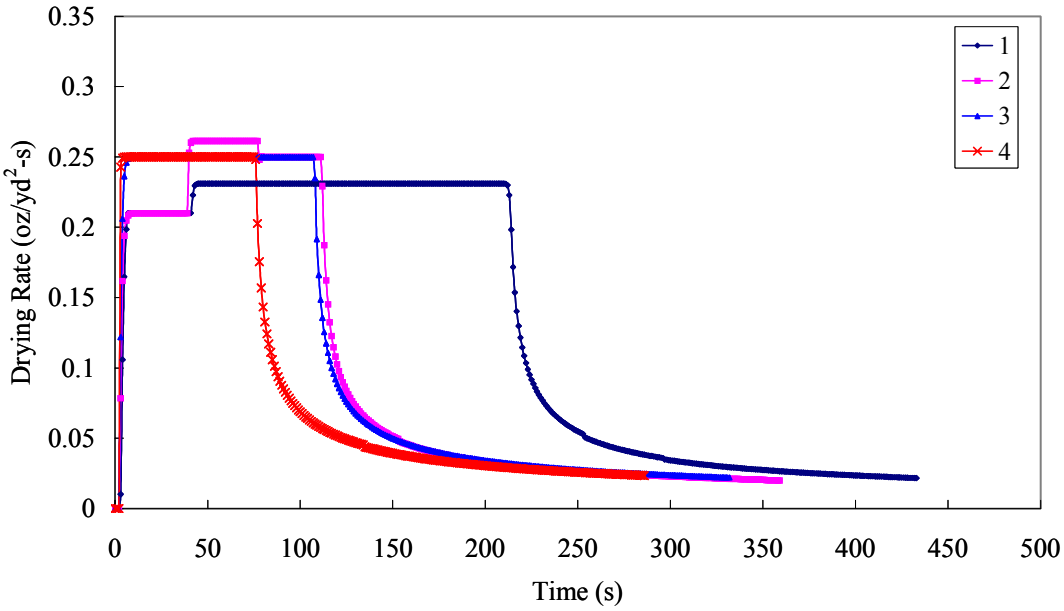

Figure 7.7 Drying rate curves as a function of time for carpet Roadrunner for the four cases

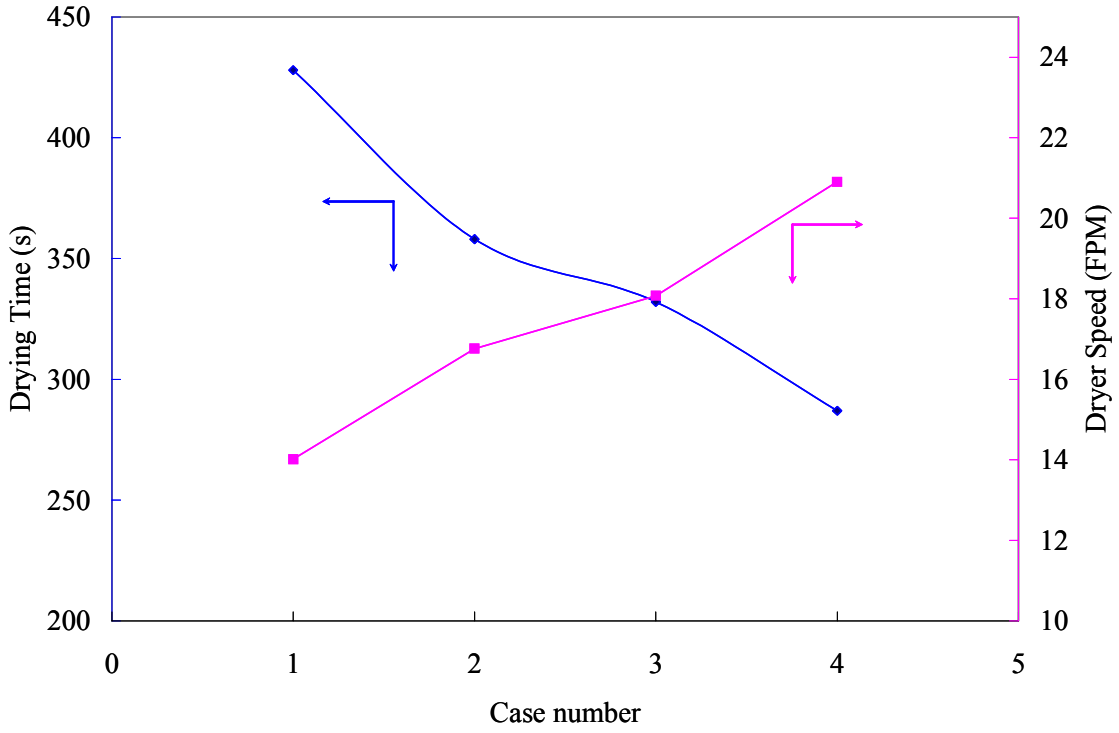

Figure 7.8 The total drying time and the dryer speed for Roadrunner tile drying for the four cases

CHAPTER VIII

CONCLUSIONS AND RECOMMENDATIONS

8.1 Conclusions

Analysis of exhaust gas composition of the dryer exhaust shows a large amount of excess air used in the dryer operations. For the heat setting of fabrics in Duncan Stewart Plant, the excess air usage is up to 2400%, as a result, up to 95% of the energy is wasted. This large amount of excess air is justified on the basis of the smoke/volatilization being generated due to heat setting. A more efficient flow system is needed. Energy savings could be realized by reducing the excess air. For the demanding application in Live Oak/Milstar Plant, large amount of excess air appears needed to accommodate the dryer operation. Ranges L5 and L6 represent the most demanding applications, followed by Ranges L3 and L4, and finally, Ranges L1 and L2 represent relatively low demanding applications. For these demanding situations (L5 and L6), excess air seems necessary to keep low moisture level in the drying air in order to maintain a high driving force. However, better quantitative understanding of the drying rate curves is still needed to justify this.

A two-step drying process that incorporates physical characteristics observed in the industrial tile drying process was used to develop a mathematical model. The first step in the drying process involves simultaneous convective heat and mass transfer processes which can be described by the Chilton-Colburn analogy. During this first step, free moisture is readily available at the Nylon pile surface. The second step involves diffusion of moisture vapor from the interior of the Nylon pile to the surface. As carpet becomes increasingly dry, the evaporation front recedes into the interior. In this region, the drying rate continually decreases, approaching 20~25% of the rate in the constant rate drying region (first step).

The mathematical model is validated in several ways: (1) the model parameters obtained from laboratory experiments offer a picture consistent with the physical aspects as expected, i.e., heat transfer coefficient values vary only slightly with temperature, and diffusion coefficient is a power function of temperature. These also remain relatively unchanged between different tile products, indicating similar microstructure; (2) with only one adjustable parameter (convective heat transfer coefficient h), the model applies to the industrial dryer operation quantitatively. This adjustable parameter h remains constant for various runs and different dryers; (3) the model was used to develop improved temperature profiles in the dryer to increase the dryer speed, and the model predictions were verified in industrial dryer trials and were incorporated into the dryer operation on a regular basis.

8.2 Recommendations

Heat-setting of textile fabrics is a non-demanding application which should not use much excess air. Better flow system should be implemented to accommodate the release of volatiles generated during the heat-setting process. A large exhaust fan speed should not be used to make up for inefficient flow patterns within the dryer. This problem is exacerbated by the auxiliary flow through open windows.

In the initial 4~5 zones of the industrial dryer, constant drying rate conditions prevail. It would be of help to use excess air and open exhaust vents for these zones. On the other hand, not much is to be gained by using excess air in the falling rate period. Thus the exhaust vents in the last 5 zones can be set at a low opening.

The data for flow-through drying of broadloom carpets should be collected and analyzed to optimize the dryer operation or to reduce energy waste.

The effect of latex composition and quantity on the critical moisture content should be investigated in detail.

APPENDIX A

DETERMINATION OF THE MODEL PARAMETERS

The methods used to determine the key parameters are demonstrated using the drying results for carpet Roadrunner at 248F.

A.1 Heat Transfer Coefficient

The convective heat transfer coefficient is determined by fitting the mathematical model to the experimental data in the constant drying rate period. Using OriginLab software, the fitting result is shown in Figure A.1 The parameter P2 is the slope of this curve, which equals the evaporation rate dw/dt.

Based on the energy analogy in the constant drying rate period, the following equation can be derived:

$$m_f \frac{dw}{dt} = \frac{h(T_a - T_f)}{H_v} \qquad (A.1)$$

where m_f = 21 oz/yd^2 =0.1458 lb/ft^2

dw/dt =P1=0.00048 lb water/lb fiber-s = 1.728 lb water/lb fiber –hr

T_a =248 F

T_f = 134 F

H_v=1164 BTU/lb

From Equation (A.1), the heat transfer coefficient h can be calculated:

h= (0.1458 * 1.728* 1164)/(248 – 134)

= 2.573 BTU/hr-lb-F

A.2 Critical Moisture Content and Diffusion Coefficient

The diffusion coefficient is determined by fitting the mathematical model to the experimental data in the falling drying rate period. The curve fitting result in the falling drying rate period is shown in Figure A.2.

The parameter P1 in Figure A.2 is the critical moisture content w_c. From the fitting results, w_c equals 0.51223.

The parameter P2 in Figure A.2 equals the following:

$$P_2 = \frac{2DM_w C(y_{x^*} - y_a)}{m_f L} \qquad (A.2)$$

Where P_2 = 0.00035 s^{-1}

M_w =18 lb /lb mol

C = P/RT = 1 / (0.7302*707) = 0.001936 lbmol/ft^3

m_f =0.1458 lb/ft^2

L = 0.64 cm = 0.02097 ft

$y_{x^*} = P^*/760$

where P* is in mmHg, it is calculated from Antoine equation:

$$\lg P^* = 7.96681 - (1668.210/(120 + 228))$$

the value of P* = 1489 mmHg

$y_{x^*} = 1.96$

$y_a = 0.15$

From Equation (A.2), the diffusion coefficient D can be calculated as following:

D = (0.00035*0.1458*0.02097)/((2*18*0.001936*(1.96-0.15))

$= 8.483 * 10^{-6}$ ft^2/s

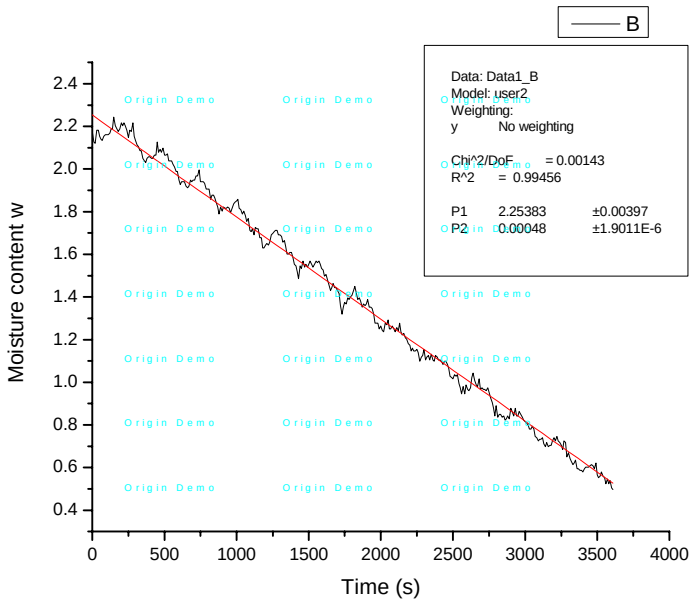

Figure A.1 The result of fitting the mathematical model to the experimental data in the constant drying rate period

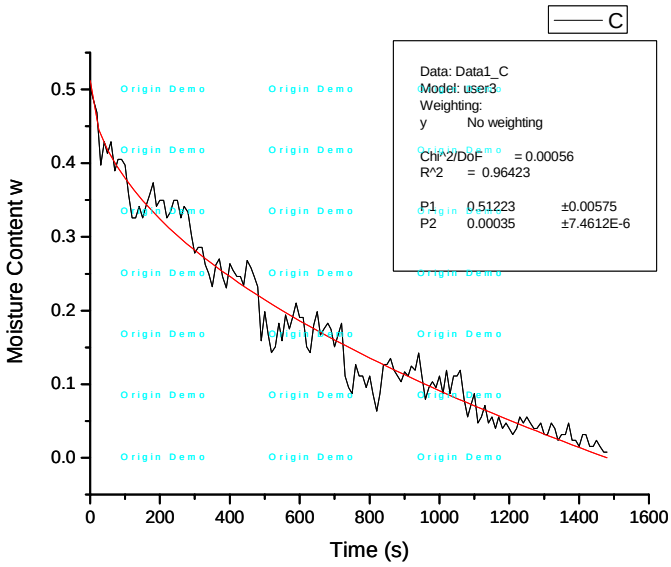

Figure A.2 The result of fitting the mathematical model to the experimental data in the falling drying rate period

REFERENCES

[1] W. F. Beckwith and J. N. Beard, "Scheme to assist in the evaluation of tenter frame dryer performance", *Journal of Engineering for Industry-Transactions of the ASME*, 101 (1), 80-84, 1979.

[2] P. K. Agrawal, CCACTI project proposal, Dalton, GA, June, 2002.

[3] C. J. Geankoplis, *Transport Processes and Unit Operations*, 3rd edition, Prentice Hall, 1993.

[4] W. L. McCabe, J. C. Smith, P. Harriott, *Unit Operations of Chemical Engineering*, 6th edition, MaGraw Hill, 2001.

[5] K. M. Waananen, J. B. Litchfield, and M. R. Okos, "Classification of drying models for porous solids", *Drying Technol.*, 11(1), 1-40, 1993.

[6] A. S. Foust, *Principles of Unit Operations*, 2nd edition, John Wiley & Sons, 1980.

[7] F. Thurner and E. U. Schlunder, "Convective drying of porous materials containing binary mixtures", *Proceedings of 4th international drying symposium*, 1, 133-141, 1984.

[8] A. S. Mujumdar, *Handbook of Industrial Drying*, NY Marcel Dekker, 1985.

[9] P. Chen and D. C. T. Pei, "A mathematical model of drying processes", *International Journal of heat and Mass Transfer* 32(2), 297-310, 1989.

[10] R. M. Perkin, "The drying of porous materials with electromagnetic energy generated at radio and microwave frequencies", *Prog. Filtration Separation*, 3, 205-266, 1983.

[11] M. A. Roques and A. R. H. Cornish, "Phenomenological coefficients for heat and mass transfer equations in wet porous media", *Drying 1980*, 2, 36-42, 1980.

[12] J. V. Brakel, "Mass transfer in convective drying", *Adv. Drying*, 1, 217-267, 1980.

[13] R. Toei, "Drying mechanism of capillary porous bodies", *Adv. Drying*, 2, 269-297, 1983.

[14] P. Chen and P. S. Schmidt, "An integral model for drying of hygroscopic and non-hygroscopic materials with dielectric heating", *Drying Technol.*, 8(5), 907-930, 1990.

[15] S. Whitaker, "Simultaneous heat, mass and momentum transfer in porous media: a theory of drying", *Adv. Heat Transfer*, 13, 119-203, 1977.

[16] S. Bories, "Recent advances in modelisation of coupled heat and mass transfer in capillary bodies", *Drying*, 46-62, 1989.

[17] C. Moyne and P. Perre, "Processes related to drying I – Theoretical model", *Drying Technol.*, 9 (5), 1135-1152, 1991.

[18] S. B. Nasrallah and P. Perre, "Detailed study of a model of heat and mass transfer during convective drying of porous media", *Int. J. Heat Mass Transfer*, 31(5), 957-967, 1988.

[19] J. D. Brock and C. W. Gorton, "Through-flow drying of tufted textiles materials", *Textile Research Journal*, 34, 1-13, 1964.

[20] J. D. Brock, *Through-Flow Drying of Tufted Textiles Materials*, M.S. Thesis, Georgia Institute of Technology, 1963.

[21] H. S. Lee, W. W. Carr, J. Leisen, et al., "Through-air drying of unbacked tufted carpets", *Textile Research Journal*, 71 (7), 613-620, 2001.

[22] H. S. Lee, W. W. Carr, H. W. Beckham, et al., "A model of through-air drying of tufted textile materials", *Int. J. Heat Mass Transfer*, 45 (2), 357-366, 2002.

[23] H. S. Lee, W. W. Carr, J. K. LaRoche, "Improving carpet through-air drying by means of increased air permeability", *Text. Res. J.*, 72 (8), 681-685, 2002.

[24] N. D. Francis, "Heat and mass-transfer in a semi-porous textile composite", *Drying Technol*., 13 (4), 1027-1028, 1995.

[25] N. D. Francis, *Heat and Mass Transfer in a Semi-Porous Textiles Composite*, Ph.D. Thesis, Georgia Institute of Technology, 1994.

[26] N. D. Francis and W. J. Wepfer, "Jet Impingement Drying of a Moist Porous Solid", *Int. J. Heat and Mass Transfer*, 39 (9), 1911-1923, 1996.

[27] H. Martin, "Heat and mass transfer between impingement gas jets and solid surfaces", *Adv. Heat Transfer*, 13, 1-60, 1977.

[28] N. D Francis, W. J. Wepfer, "Experimental and numerical analysis of the drying characteristics of modular carpet tiles", *Text. Res. J.*, 63 (1), 1-13, 1993.

[29] N. D. Francis, *Experimental and Analytical study of the Drying Characteristics of Carpet Tiles*, M.S. Thesis, Georgia Institute of Technology, 1991.

[30] C. F. Solis and W.J. Wepfer, "Analytical determination of the drying characteristics of carpet tiles", *Text. Res. J.*, 68 (5), 342-350, 1998.

[31] C. F. Solis, *The Determination of the Drying Characteristics of Foam-backed Carpet Tiles*, M.S. Thesis, Georgia Institute of Technology, 1996.

[32] C. Moyne. and A. Degiovanni., "Importance of Gas Phase Momentum Equation in Drying Above The Boiling Point of Water", edited by A. S. Mujumdar, and R. Toei, *Drying '85*, 109-115, 1985.

[33] D. R. O'Dell, *The Drying Behavior of Carpet tiles in a Medium of Superheated Steam*, M.S. Thesis, Georgia Institute of Technology, 1994.

[34] G. H. Crapiste, S. Whitaker, E. Rotsten, "Drying of cellular material II. Experimental and numerical results", *Chemical Engineering Science*, 43, 2929-2936, 1988.

[35] C. Ratti and G.H. Crapiste, "A generalized drying curve for shrinking food material", *Drying '92*, Part A, edited by A. S. Mujumdar, 864-873, 1992.

[36] A. A. Almubarak and C. J. Mumford, "Characteristics of the receding evaporation front in convective drying", *Drying '94*, edited by Mujumdar, 231-238, 1994.

[37] P. M. Heertjes and H. E. Tuinder, "Some Observations on Heat and Water Transfer in a Drying Consolidated Mass", *Ingenious*, 74 (28), 45-64, 1962.

[38] S. K. Chou, M. N. A. Hawlader, and K. J. Chua, "Identification of the receding evaporation front in convective food drying", *Drying Technol*., 15(5), 1353-1367, 1997.

[39] C. F. Solis, *The Determination of the Drying Characteristics of Foam-backed Carpet Tiles*, M.S. Thesis, Georgia Institute of Technology, 1996.

[40] H. W. Beckham, W. W. Carr, H. W. Spiess, and B. Blumich, "Nuclear-magnetic-resonance Imaging of Water Distributions in Loop-pile Nylon Carpet Tiles", *J. Text. Inst*., 89 Part I, 2, 1998.

[41] R. H. Perry, *Perry's Chemical Engineer's Handbook*, McGraw Hill, 1984.

[42] R. E. Treybal, *Mass Transfer Operations*, McGraw Hill, 1980.

[43] J. R. Welty, C. E. Wicks, R. E. Wilson, and G. Rorrer, *Fundamentals of Momentum, Heat, and Mass Transfer*, 4th edition, Wiley, 2000.

[44] I. S. Sandler, *Chemical and Engineering Thermodynamics*, New York: Wiley, c1999.

[45] S. B. Warner, *Fiber Science*, Prentice-Hall, Inc., Englewood Cliffs, NJ, 1995.

[46] P. W. Gibson and M. Charmchi, "Modeling Convection/Diffusion Process in Porous Textiles with Inclusion of Humidity-Dependent Air Permeability", *Int. Comm. Heat Mass Transfer*, 24 (5), 709-724, 1997.

[47] R. H. Perry, Perry's Chemical Engineer's Handbook, McGraw Hill, 1950.

[48] J. R. Bell and P. Grosberg, "The movement of Vapor and Moisture During the Falling Rate Period of Drying of Thick Textile Materials", *Journal of the Textile Institute*, 53 (5), p.250, 1982.

[49] J. R. Welty, C. E. Wicks, R. E. Wilson and G. Rorrer, *Fundamentals of Momentum, Heat, and Mass Transfer*, 4th edition, Wiley, 2000.

[50] P. W. Gibson and M. Charmchi, "Modeling Convection/Diffusion Process in Porous Textiles with Inclusion of Humidity-Dependent Air Permeability", *Int. Comm. Heat Mass Transfer*, 24 (5), 709-724, 1997.